International Ocean Discovery Program
Expedition 352 Preliminary Report

Izu-Bonin-Mariana Fore Arc

Testing subduction initiation and ophiolite models by drilling the outer Izu-Bonin-Mariana fore arc

30 July–29 September 2014

Expedition 352 Scientists

Published by
International Ocean Discovery Program

Publisher's notes

This publication was prepared by the *JOIDES Resolution* Science Operator (JRSO) at Texas A&M University as an account of work performed under the International Ocean Discovery Program (IODP). Funding for the program is provided by the following agencies:

National Science Foundation (NSF), United States

Ministry of Education, Culture, Sports, Science and Technology (MEXT), Japan

European Consortium for Ocean Research Drilling (ECORD)

Ministry of Science and Technology (MOST), People's Republic of China

Korea Institute of Geoscience and Mineral Resources (KIGAM)

Australian Research Council (ARC) and GNS Science (New Zealand), Australian/New Zealand Consortium

Ministry of Earth Sciences (MoES), India

Coordination for Improvement of Higher Education Personnel, Brazil

Disclaimer

Copyright

Citation:
Expedition 352 Scientists, 2015. Izu-Bonin-Mariana fore arc: Testing subduction initiation and ophiolite models by drilling the outer Izu-Bonin-Mariana fore arc. *International Ocean Discovery Program Preliminary Report,* 352. http://dx.doi.org/10.14379/iodp.pr.352.2015

ISSN

World Wide Web: 2372-9562

February 2015

Expedition 352 participants

Expedition 352 scientists

Julian A. Pearce
Co-Chief Scientist
School of Earth & Ocean Sciences
Cardiff University
Main Building, Park Place
Cardiff CF10 3AT
United Kingdom
pearceja@cardiff.ac.uk

Mark K. Reagan
Co-Chief Scientist
Department of Earth & Environmental Sciences
The University of Iowa
121 Trowbridge Hall
Iowa City IA 52242
USA
mark-reagan@uiowa.edu

Katerina Petronotis
Expedition Project Manager/ Staff Scientist
International Ocean Discovery Program
Texas A&M University
1000 Discovery Drive
College Station TX 77845-9547
USA
petronotis@iodp.tamu.edu

Sally Morgan
Logging Staff Scientist
Department of Geology
University of Leicester
University Road
Leicester
LE1 7RH
United Kingdom
sm509@le.ac.uk

Renat Almeev
Physical Properties Specialist
Institut für Mineralogie
Leibniz University of Hannover
Callinstrasse 3
30167 Hannover
Germany
r.almeev@mineralogie.uni-hannover.de

Aaron J. Avery
Paleontologist (nannofossils)
Earth, Ocean and Atmospheric Sciences
Florida State University
909 Antarctic Way
Tallahassee FL 32306
USA
aja12b@my.fsu.edu

Claire Carvallo
Paleomagnetist
Institut de Minéralogie et de Physique des Milieux Condensés (IMPMC)
Université Pierre et Marie Curie
4 Place Jussieu
75005 Paris
France
carvallo@impmc.upmc.fr

Timothy Chapman
Petrologist
School of Geosciences, F05
University of Sydney
46 Brook Road
Glenbrook NSW 2773
Australia
t.chapman@sydney.edu.au

Gail L. Christeson
Physical Properties Specialist
University of Texas Institute for Geophysics
JJ Pickle Research Campus Building 196
10100 Burnet Road
Austin TX 78758-4445
USA
gail@ig.utexas.edu

Eric C. Ferré
Structural Geologist
Department of Geology
Southern Illinois University at Carbondale
1259 Lincoln Drive, Parkinson Lab
Carbondale IL 62901-4234
USA
eferre@geo.siu.edu

Marguerite Godard
Inorganic Geochemist
Geosciences Montpellier- UMR 5243
Université Montpellier II
CC 60, Place Eugene Bataillon
34095 Montpellier
France
mgodard@univ-montp2.fr

Daniel E. Heaton
Petrologist
College of Earth, Ocean and Atmospheric Sciences
Oregon State University
104 CEOAS Administration Building
Corvalis OR 97331-5503
USA
dheaton@coas.oregonstate.edu

Maria Kirchenbaur
Inorganic Geochemist
Geologisches Institut
Universität Kõln
Zulpicher Strasse 49
50674 Koln
Germany
mkirchen@uni-koeln.de

Walter Kurz
Structural Geologist
Institute of Earth Sciences
University of Graz
Heinrichstrasse 26
A-8010 Graz
Austria
walter.kurz@uni-graz.at

Steffen Kutterolf
Sedimentologist
GEOMAR Helmholtz Centre for Ocean Research Kiel
Wischhofstrasse 1-3
24148 Kiel
Germany
skutterolf@geomar.de

Hongyan Li
Petrologist
State Key Laboratory of Isotope Geochemistry
Guangzhou Institute of Geochemistry, Chinese Academy of Sciences
511 Kehua Street, Wushan
Guangzhou 510640
P.R. China
hongyanli@gig.ac.cn

Yibing Li
Inorganic Geochemist
Institute of Geology
Chinese Academy of Geological Science
Baiwanzhuang Road 26
Beijing 100037
P.R. China
yibing007@gmail.com
tansei007@aliyun.com

Katsuyoshi Michibayashi
Physical Properties Specialist
Institute of Geosciences
Shizuoka University
836 Ohya, Suruga-ku
Shizuoka 422-8529
Japan
sekmich@ipc.shizuoka.ac.jp

Wendy R. Nelson
Petrologist
Earth & Atmospheric Sciences
University of Houston
312 Science & Research Building 1
Houston TX 77204
USA
wrnelson2@uh.edu

Julie Prytulak
Petrologist
Department of Earth Science & Engineering
Imperial College London
South Kensington Campus Prince Consort Road
London SW7 2AZ
United Kingdom
j.prytulak@imperial.ac.uk

Marie Python
Alteration Petrologist
Department of Earth and Planetary Sciences
Hokkaido University
Kita-ku, Kita 10, Nishi 8
Hokkaido Sapporo 060-0810
Japan
marie@sci.hokudai.ac.jp

Alastair H.F. Robertson
Sedimentologist
School of Geosciences
University of Edinburgh
West Mains Road
Edinburgh EH9 3JW
United Kingdom
alastair.robertson@ed.ac.uk

Jeffrey G. Ryan
Inorganic Geochemist
Department of Geology
University of South Florida, Tampa
4202 East Fowler Avenue SCA 528
Tampa FL 33620
USA
ryan@mail.usf.edu

William W. Sager
Paleomagnetist
Earth & Atmospheric Sciences
University of Houston
127B Science and Research Building 1
Houston TX 77204
USA
wwsager@uh.edu

Tetsuya Sakuyama
Physical Properties Specialist
Institute for Research on Earth Evolution (IFREE)
Japan Agency for Marine-Earth Science and Technology (JAMSTEC)
2-15 Natsushima-cho
Yokosuka Kanagawa 237-0061
Japan
sakuyama@jamstec.go.jp

Present address (1 October 2014):
Department of Science
Osaka University
3-3-138 Sugimoto
Sumiyoshi-ku Osaka 558-8585
Japan

John W. Shervais
Petrologist
Department of Geology
Utah State University
4505 Old Main Hill
Logan UT 84322-4505
USA
john.shervais@usu.edu

Kenji Shimizu
Petrologist
Institute for Research on Earth Evolution (IFREE)
Japan Agency for Marine-Earth Science and Technology (JAMSTEC)
2-15 Natsushima-cho
Yokosuka 237-0061
Japan
shimmy@jamstec.go.jp

Scott A. Whattam
Petrologist
Department of Earth and Environmental Sciences
Korea University
Seoul 136-701
Republic of Korea
whattam@korea.ac.kr

Siem Offshore AS officials

Steve Bradley
Master of the Drilling Vessel

Wayne Malone
Offshore Installation Manager

Education and outreach

Elizabeth A. Christiansen
Education Officer
H.H. Dow High School
Midland MI 48640
USA
christiansenEA@gmail.com

Amy E. West
Education Officer
San Luis Obispo CA
USA
amy@amyewest.com

Technical support

Lisa Brandt
Chemistry Laboratory

Timothy Bronk
Assistant Laboratory Officer

Chad Broyles
Curatorial Specialist

Lisa Crowder
Assistant Laboratory Officer

Keith Dupuis
Publications Specialist

Emily Fisher
Thin Section Laboratory

Seth Frank
X-ray/Microbiology Laboratory

Timothy Fulton
Imaging Specialist

Clayton Furman
Schlumberger Logging Engineer

Randy Gjesvold
Marine Instrumentation Specialist

Rachael Gray
Chemistry Laboratory

Margaret Hastedt
Core Laboratory

Michael Hodge
Marine Computer Specialist

Stephen Midgley
Operations Superintendent

William Mills
Laboratory Officer

Algie Morgan
Applications Developer

Zenon Mateo
Underway Geophysics Laboratory

Beth Novak
Paleomagnetism Laboratory

Garrick Van Rensburg
Marine Instrumentation Specialist

Thomas Wick
Marine Computer Specialist

Abstract

The objectives for Expedition 352 were to drill through the entire volcanic sequence of the Bonin fore arc to

1. Obtain a high-fidelity record of magmatic evolution during subduction initiation and early arc development,
2. Test the hypothesis that fore-arc basalt lies beneath boninite and understand chemical gradients within these units and across the transition,
3. Use drilling results to understand how mantle melting processes evolve during and after subduction initiation, and
4. Test the hypothesis that the fore-arc lithosphere created during subduction initiation is the birthplace of suprasubduction zone (SSZ) ophiolites.

Expedition 352 successfully cored 1.22 km of igneous basement and 0.46 km of overlying sediment, providing diverse, stratigraphically controlled suites of fore-arc basalts (FAB) and boninite related to seafloor spreading and earliest arc development. FAB were recovered at the two deeper water sites (U1440 and U1441) and boninites at the two sites (U1439 and U1442) drilled upslope to the west. FAB lavas and dikes are depleted in high-field strength trace elements such as Ti and Zr relative to mid-ocean-ridge basalt but have relatively diverse concentrations of trace elements bezcause of variation in degrees of melting and amount of subducted fluids involved in their genesis. All FAB magmas underwent significant crystal fractionation in a persistent magma chamber system. Holes U1439C and U1442A yielded entirely boninitic lavas. We defined three boninite differentiation series based on variations in MgO, SiO_2, and TiO_2 concentrations of the parental magmas. Lavas in both pairs of holes have compositions that generally become more primitive and have lower TiO_2 concentrations upward. The presence of dikes at the base of the sections at Sites U1439 and U1440 provides evidence that boninitic and FAB lavas are both underlain by their own conduit systems and that FAB and boninite group lavas are likely offset more horizontally than vertically. We thus propose that seafloor spreading related to subduction initiation migrated from east to west after subduction initiation and during early arc development. Initial spreading was likely rapid, and an axial magma chamber was present. Melting was largely decompressional during this period, but subducted fluids affected some melting. As subduction continued and spreading migrated to the west, the embryonic mantle wedge became more depleted, and the influence of subducted constituents dramatically increased, causing the oceanic crust to be built of boninitic rather than tholeiitic magma. The general decrease in fractionation upward

reflects the eventual disappearance of persistent magma chambers, either because spreading rate was decreasing with distance from the trench or because spreading was succeeded by off-axis magmatism trenchward of the ridge. The extreme depletion of the sources for all boninitic lavas was likely related to the incorporation of mantle residues from FAB generation. This mantle depletion continued during generation of lower silica boninitic magmas, exhausting clinopyroxene from the mantle such that the capping high-Si, low-Ti boninites were generated from harzburgite.

Additional results of the cruise include recovery of Eocene to recent deep-sea sediment that records variation in sedimentation rates with time resulting from variations in climate, the position of the carbonate compensation depth, and local structural control. Three phases of highly explosive volcanism (latest Pliocene to Pleistocene, late Miocene to earliest Pliocene, and Oligocene) were identified, represented by 132 graded air fall tephra layers. Structures found in the cores and reflected in seismic profiles show that this area had periods of normal, reverse, and strike-slip faulting. Finally, basement rock *P*-wave velocities were shown to be slower than those observed during logging of normal ocean crust sites.

Background

Izu-Bonin-Mariana system

The Izu-Bonin-Mariana (IBM) system is the type locality for studying oceanic crustal accretion immediately following subduction initiation. It is sufficiently old that it carries a full record of the evolution of crustal accretion from the start of subduction to the start of normal arc volcanism and sufficiently young that the key features have not been excessively disturbed by subsequent erosion or deformation. Intraoceanic arcs are built on oceanic crust and are sites of formation of juvenile continental crust (Rudnick, 1995; Tatsumi and Stern, 2006). Most active intraoceanic arcs are located in the western Pacific. Among these, the IBM system stands out as a natural scientific target. This predominantly submarine convergent plate boundary is the result of ~52 My of subduction (Ishizuka et al., 2011; Reagan et al., 2013) of the Pacific plate beneath the eastern margin of the Philippine Sea plate. Stretching for 2800 km from the Izu Peninsula, Japan, to Guam, USA (Figure **F1**), the IBM system (summarized in Stern et al., 2003) has been extensively surveyed and has become an important natural laboratory for International Ocean Discovery Program (IODP) expeditions aimed at understanding subduction initiation, arc evolution, and continental crust formation.

A scientific advantage of studying the IBM system is its broad background of scientific investigation resulting from its designation as a focus site by the U.S. National Science Foundation MARGINS-Subduction Factory experiment and similar efforts in Japan. We know when subduction and arc construction began, even if the precise paleogeography is controversial, and there is a good time-space record of crustal development.

Petrologic evolution

The petrologic evolution of early stage magmatism in the IBM arc has been reconstructed mainly based on volcanic sections that are exposed on the fore-arc islands (Bonin Islands and Mariana Islands) and that have been recovered from Deep Sea Drilling Project (DSDP) and Ocean Drilling Program (ODP) fore-arc drill sites. Recent dredging and submersible studies have provided additional information. Consequently, we were able to predict the sequence of magmas likely to characterize the drill site and its surrounding region, which developed after subduction initiation and prior to establishment of a stable magmatic arc to the west by the late Eocene. The physical evolution of the fore arc and its associated lavas reflects the reorganization of mantle convection and slab-derived fluid flow in response to the changing behavior of the sinking Pacific plate. This evolution, from initial seafloor spreading and eruption of mid-ocean-ridge basalt (MORB)-like tholeiites to eruption of boninites to fixing of the magmatic arc ~150 km west of the trench (separated by a broad, dead fore arc), took 7–8 My (Ishizuka et al., 2011). The process is reflected in the succession of igneous rocks of the Bonin Ridge, which is described in greater detail below and depicted in the time-space diagram (Figure **F2**).

Early subduction-related volcanism

Diving and dredging on the fore-arc slope east of the Bonin Ridge and south of Guam recovered basaltic rocks from stratigraphic levels below boninite. These basalts have chemical compositions that are similar to those of normal MORB (N-MORB). However, they are not identical, and hence the term “fore-arc basalt (FAB)” was coined by Reagan et al. (2010) to highlight their distinctive setting and to emphasize that, in detail, FAB is a different magma type from MORB. Most of the reliable $^{40}Ar/^{39}Ar$ ages and U-Pb zircon ages of FAB are identical within error in both locations and indicate that FAB magmatism occurred from ~51 to 52 Ma, preceding boninite eruption by 2–4 My (Ishizuka et al., 2011; Reagan et al., 2013). Lavas with compositions transitional between FAB and boninites from DSDP Site 458 were dated at 49 Ma (Cosca et al.,

1998). FAB and related gabbros are thought to relate to the first magmas produced as the IBM subduction zone began to form (Reagan et al., 2010).

Geochemical data show that FAB magmas have light rare earth element–depleted rare earth element (REE) patterns, indicating derivation from a moderately depleted lherzolitic upper mantle, similar to that responsible for generating MORB (Figure **F3**). FAB in the IBM, however, has low Ti/V (14–16), a diagnostic ratio (Shervais, 1982) that distinguishes FAB from subducting Pacific MORB (26–32) and from Philippine Sea back-arc lavas (17–25) (Figure **F4**). Chemically and petrographically, Bonin Ridge FAB are indistinguishable from Mariana FAB. This strongly implies that FAB tholeiitic magmatism was associated with fore-arc spreading along the length of the IBM arc. Low concentrations of incompatible elements and low trace element ratios such as Ti/V imply that FAB magmas were derived from more depleted mantle and/or were larger degree mantle melts than typical Philippine Sea MORB (Reagan et al., 2010).

Pb isotopic compositions of FAB from the Bonin fore arc show that they are, like other IBM arc and back-arc magmas, derived from a mantle with Indian Ocean characteristics, as demonstrated by high Δ8/4 Pb compared to Pacific MORB (Ishizuka et al., 2011). Isotopic characteristics indicate some differences between the mantle sources of Philippine Sea MORB and FAB, including distinctly higher $^{87}Sr/^{86}Sr$ and $^{206}Pb/^{204}Pb$ (Figure **F5**), which may imply the presence of lithospheric mantle with inherited enrichment (Parkinson et al., 1998). Most significantly, incompatible trace elements derived from subducted crust do not unambiguously affect the source region of most FAB, although some FAB lavas from the Mariana fore arc have Pb isotopic compositions consistent with a weak influence of subducted Pacific crust (Reagan et al., 2010). Differences in isotopic and trace element characteristics between IBM FAB and MORB including that from the Philippine plate strongly imply that FAB does not represent preexisting ocean basin or back-arc basin crust trapped prior to subduction initiation, as originally concluded by Johnson and Fryer (1990) and DeBari et al. (1999) for MORB-like tholeiites recovered from the Mariana and Izu inner trench walls.

Lavas with compositions that transition upward between FAB and boninite were recovered at DSDP Leg 60 Sites 458 and 459 (the alternate site) and illustrate that FAB and boninite are genetically linked (Reagan et al., 2010). The oldest of these lavas have REE patterns similar to those of MORB but are more enriched in silica and have higher concentrations of "fluid-soluble" elements such as K, Rb, U, and Pb than FAB. These lavas also have Pb isotopic compositions that are more similar to lavas from the Pacific than to those from the Indian plate, supporting the contention that subducted

fluids were involved in their genesis. The youngest lavas at Site 458 are strongly depleted in REE, somewhat resembling boninites but less magnesian and more calcic.

Boninite volcanism follows FAB volcanism as an integral part of the evolution of the nascent subduction zone. The type locality of boninite is in the Bonin (Ogasawara) Islands, an uplifted segment of the IBM fore arc. Boninites are better exposed on the Bonin Islands than anywhere else in the world, particularly on the island of Chichijima. $^{40}Ar/^{39}Ar$ dating indicates that boninitic volcanism on Chichijima took place briefly during the Eocene, between 46 and 48 Ma (Ishizuka et al., 2006). A slightly younger volcanic succession is exposed along the Bonin Ridge, including 44.74 ± 0.23 Ma high-Mg andesites (HMA) from the Mikazukiyama Formation, the youngest volcanic sequence on Chichijima, and 44.0 ± 0.3 Ma tholeiitic to calc-alkaline andesite from Hahajima. Four submersible *Shinkai* 6500 dives on the Bonin Ridge Escarpment mapped an elongate constructional volcanic ridge atop the escarpment and recovered fresh andesitic clasts from debris flows along the northern segment of the ridge; they also recovered HMA lava blocks from the escarpment northwest of Chichijima. Three samples of andesite collected from the Bonin Ridge Escarpment range in age from 41.84 ± 0.14 to 43.88 ± 0.21 Ma (Ishizuka et al., 2006).

Boninites from the Bonin Islands are characterized by high MgO at given SiO_2 concentrations, low high-field-strength elements, low Sm/Zr, low REE, and a U-shaped REE pattern (Figure **F3**). These are "low-Ca boninites" (Crawford et al., 1989) and can be explained by low-pressure melting of depleted harzburgite that was strongly affected by slab flux. These boninites are isotopically characterized by high Δ7/4 Pb, high $^{87}Sr/^{86}Sr$, and low $^{143}Nd/^{144}Nd$ relative to local MORB and FAB sources (Figure **F5**). In contrast to the FAB mantle source, which was not much affected by subduction-related fluids or melts, the boninite magma source manifests a major contribution from subducted pelagic sediment and oceanic crust. The boninites are also distinct from ~44 Ma lavas exposed on Hahajima Island and recovered by *Shinkai* 6500 diving on the Bonin Ridge Escarpment (Ishizuka et al., 2006). HMA from Chichijima and the Bonin Ridge Escarpment are more similar to relatively enriched boninitic lavas from ODP Site 786 (Pearce et al., 1992) and Guam, including having higher Sm/Zr at a given Zr content and higher REE and Ti concentrations compared to Chichijima boninites (cf. Taylor and Nesbitt, 1994). The HMA are isotopically distinct from the boninites (Figure **F5**) and were derived from a source mantle that was less affected by fluids or melts derived from the subducted plate.

Post-45 Ma, tholeiitic to calc-alkaline andesites from the Bonin Ridge and ~45 Ma rhyolites from Saipan (Reagan et al., 2008) exhibit strong characteristics of arc magmas: they are depleted in Nb and enriched in fluid-mobile elements such as Sr, Ba, U, and Pb. These characteristics indicate that, by 45 Ma, near-normal configurations of mantle flow and melting, as well as subduction-related fluid formation and metasomatism, were established for this part of the IBM arc. The Bonin Ridge Escarpment, Mikazukiyama Formation, and Hahajima andesites thus represent a transitional stage from the waning stages of fore-arc spreading (represented by FAB and perhaps boninites) and the stable, mature arc that developed in the late Eocene. These orthopyroxene-bearing, high-Mg, tholeiitic to calc-alkaline andesites erupted along the Bonin Ridge Escarpment as the arc magmatic axis localized and retreated from the trench. Post-45 Ma andesites (and basalts) do not show the influence of pelagic sediment melt from the slab (Figure **F5**). Instead, the mantle source seems to have only been affected by hydrous fluid derived mainly from subducted altered oceanic crust.

Overall, the geochemical and isotopic characteristics of the IBM arc along its entire length appear to have evolved in tandem with the formation of a new subduction zone and a new mantle flow regime by

1. Initial decompression melting with little to no slab flux, producing MORB-like basalt and fore-arc spreading (51–52 Ma),
2. Mixing of fluids or melts from subducted sediments and oceanic crust into an extremely depleted (harzburgitic) mantle to generate boninites (49–45 Ma), and
3. Continued influx of hydrous fluid input into increasingly fertile lherzolitic mantle to generate tholeiitic and calc-alkaline magma (post-45 Ma), marking the time when a mature, stable arc magmatic system was finally established (Ishizuka et al., 2006, 2011).

Note however that although we have established a general volcanic stratigraphy, it is a composite stratigraphy based on dredging, submersible grab sampling, and coring at widely spaced localities. There is no reference stratigraphic section to check this subduction initiation stratigraphy and, in particular, to identify the nature of the boundaries between the units and demonstrate that units have not been missed. Defining this stratigraphic section is the aim of this expedition.

Tectonic evolution

It has been generally accepted (Bloomer et al., 1995; Pearce et al., 1999; Stern, 2004; Hall et al., 2003) that the IBM subduction zone began as part of a hemispheric-scale foundering of old, dense lithosphere in the western Pacific (Figure **F6**). The beginning of large-scale lithospheric subsidence, not true subduction but its precursor, is constrained to predate the 51–52 Ma age of igneous basement of the IBM fore arc (Bloomer et al., 1995; Cosca et al., 1998; Ishizuka et al., 2006). The sequence of initial magmatic products is similar everywhere the forearc has been sampled, implying a dramatic episode of asthenospheric upwelling and melting associated with magmatism and seafloor spreading over a zone that was perhaps hundreds of kilometers broad and thousands of kilometers long. It is clear from the extensive geochronology for IBM fore-arc rocks that this episode took place ~52 My ago, and was followed by a period of shallow hydrous melting through about 44-45 My ago (Figure **F2**). Expedition 352 drilling intends to sample these parts of the tectonic history of the IBM arc.

Interestingly, these time-space trends in IBM fore-arc composition can be found in many ophiolite terranes. The world's largest ophiolite, the Semail ophiolite of Oman/United Arab Emirates has long been known to exhibit a stratigraphy of FAB-like tholeiites overlain by depleted arc tholeiites (e.g., Alabaster et al., 1982), and recent discoveries of boninites in the upper part of the sequence (Ishikawa et al., 2002) confirm the full trend from tholeiite to boninites. Other large, complete ophiolites with complex fore-arc-type stratigraphies involving tholeiites and boninites include the Troodos Massif of Cyprus, the Pindos Mountains in Greece, the Bay of Islands ophiolite in Newfoundland (Canada), and numerous others distributed through most of the world's mountain belts (e.g., Pearce et al., 1984; Dilek and Flower, 2003). Many of these stratigraphies are economically significant, with associated volcanogenic massive deposits and/or podiform chromite mineralization.

The presence of boninites is in itself an important tectonic indicator, requiring a combination of shallow melting, high water content, and depleted mantle. Boninites are defined by the International Union of Geological Sciences (IUGS) to have >52 wt% silica, <0.5 wt% TiO_2, and >8 wt% MgO and can usefully be distinguished from basalts on a diagram of Ti8 versus Si8, where Ti8 and Si8 refer to the oxide concentrations at 8 wt% MgO (Pearce and Robinson, 2010). On this projection (Figure **F7**), the earliest lavas are basalts (FAB) that plot in the MORB field. Later lavas (~48–44 Ma) plot as boninites before compositions eventually become basaltic again with eruptions at, for example, Hahajima. This appears to be a characteristic of subduction initiation, but to

properly interpret its tectonic significance we need the full lava stratigraphy to know whether the basalt–boninite transition is gradational or episodic or has both magma sources available simultaneously. Drill core would also enhance the opportunity to obtain glass samples that can be analyzed for volatile and fluid-mobile element concentrations.

After a brief period of spreading, lavas began to build atop the newly formed crust and retreat from the trench, at the same time changing composition, perhaps first from FAB to boninite and then from boninite to calc-alkaline and tholeiitic arc magmas. The timing and rate of the migration of the magmatic locus away from the trench remains uncertain, but it is clear that the locus of magmatism reached the location of the first magmatic arc on Guam and the edge of the Ogasawara escarpment within ~8 My. This left vast tracts of infant arc crust "stranded" to form the IBM fore arc, which cooled and remained "frozen" in its primitive state. Understanding the formation of fore-arc crust is clearly critical for understanding the formation of subduction zones (and the magmatic responses), growth of arcs, evolution of continental crust, and origins of ophiolite.

Structure and thickness of fore-arc crust

The most detailed trench-orthogonal published images of IBM fore-arc crustal structure in the region of interest come from a seismic refraction/reflection study by Kamimura et al. (2002) in a region some distance north of the section from Sites U1439–U1442. While recognizing that the actual crustal structure for the drill sites might be slightly different than that shown, we infer from the study of Kamimura et al. (2002) that the crust beneath the drill sites is 6–8 km thick—slightly thicker than normal oceanic crust. In detail, the crust beneath this part of the fore arc can be divided into 5 identifiable layers. The first layer (V_P = 1.8–2.0 km/s) is mostly composed of thin sediment; this layer is actually very variable and Sites U1439–U1442 were originally chosen to have at least 100 m of sediment in order to facilitate drilling and casing operations of the uppermost part of the holes. The second layer (V_P = 2.6–3.3 km/s) is 1–2 km thick and probably consists of fractured volcanic rocks and dikes; this information contributed to our precruise estimate of 1.25 ± 0.25 km as the likely lava thickness that we needed to drill in order to reach the sheeted dikes.

Choice of drill sites

The Bonin fore arc was chosen because it had the advantage of being in the same region as Chichijima (Bonin Island), the type locality for the key boninite rock type. It is part of a complete ophiolite section that has been sampled by dredging and diving (Ishizuka et al., 2011) and has full site survey data (Kodaira et al., 2010, pers. comm., 2013).

Two important hypotheses to be tested by drilling have been (1) that subduction initiation produces a consistent volcanic stratigraphy (from oldest to youngest): FAB, transitional lavas, low-Ca boninites, enriched HMA and related rocks, and normal arc volcanic rocks (Reagan et al., 2010), and (2) that this sequence was originally stacked vertically before erosion and therefore represents an in situ analog for sections through many SSZ ophiolites. Sites U1439–U1442 (Figure **F8**) were chosen to maximize the likelihood of testing these hypothesis because the sheeted dike/FAB contact was approximately located during *Shinkai* 6500 diving in 2009 along the inner wall of the Bonin Trench, near a location where the drill could spud into a sediment pond and sample the lower part of the fore-arc volcanic succession.

Figure **F9** summarizes the distribution of rocks sampled during three expeditions: YK04-05, the first manned submersible (*Shinkai* 6500) diving survey of the western escarpment of the Bonin Ridge (Ishizuka et al., 2006); R/V *Hakuho-maru* KH07-2, which dredged 19 stations along the length of Bonin Ridge; and YK09-06 in the proposed Site U1439–U1442 area (Ishizuka et al., 2011). They show that, in particular,

1. Overall, there is an ophiolite-like sequence in the inner trench wall of lavas, dikes, gabbros, and peridotites;
2. Of the lavas and dikes, MORB-like tholeiites occupy the deepest part of the trench-side slope of the ridge (i.e., the easternmost part of the ridge). These are chemically indistinguishable from FAB as defined by Reagan et al. (2010) from the Mariana fore arc;
3. Boninites crop out to the west and upslope of the FAB/MORB outcrops; and
4. Younger tholeiitic/calc-alkaline basalt to rhyolite crop out on the western Bonin Ridge and are especially well exposed on the western escarpment.

The 2009 diving survey using the *Shinkai* 6500 examined and better established the igneous fore-arc stratigraphy exposed on the trench-side slope of the Bonin Ridge (YK09-06 cruise: 24 May–10 June 2009; Ishizuka et al., 2011). The northernmost dive

area near 28°25′N for this survey (Dives 1149, 1150, 1153, and 1154) was located near the drill sites (Figure **F8**).

The deepest dive (1149) sampled gabbro and basalt/dolerite and appears to have traversed the boundary between the two units. The lower slope traversed during Dive 1149 is composed of fractured gabbro, whereas pillow lavas were observed in the uppermost part of this dive at ~6000 m water depth. Dives 1153 and 1154 surveyed upslope of Dive 1149 between 6000 and 5200 m water depth. These two dives found outcrops of gabbro and dolerite, as well as fractured basalt lava cut by dikes. The contact between basalt and dolerite was thought to be ~5400 m based on these results, and Site U1440 was chosen to drill through this contact (Figure **F10**). The shallowest dive (1150; 4600 to 3700 m) recovered volcanic breccia and conglomerate with boninite. Thus, the boundary between boninite and basalt was estimated to lie at ~4000 m water depth. Site U1439 was chosen to drill through the transition zone from boninite to basalt. The resulting drilling has shown that this boundary might be geographically limited and lie to the east.

Scientific objectives

1. *Obtain a high-fidelity record of magmatic evolution during subduction initiation by coring volcanic rocks down to underlying intrusive rocks, including radiometric and biostratigraphic ages.*

Recent advances in studying the IBM fore arc document important vertical compositional variations within the volcanic sections. We know that the IBM fore arc exposes rocks that formed when this subduction zone began at ~52 Ma (Stern and Bloomer, 1992; Ishizuka et al., 2011). Reagan et al. (2010) documented that the volcanic succession exposed in the inner trench wall of the southernmost Mariana fore arc comprises a volcanic succession that changes from MORB-like tholeiites at the base (FAB) through increasingly arc-like basalts to boninites near the top. They inferred that the 450–700 m sections cored at Sites 458 and 459 in the Mariana fore arc sampled the transition between the FAB and boninite successions. Similar successions are common in ophiolites, many of which are increasingly recognized as fossil fore arcs (Stern et al., 2012; see below). The significance of this simple succession has not hitherto been appreciated because of a lack of direct information on fore-arc volcanic stratigraphy, mainly because this was not a priority for dredging and diving. The results of Reagan et al. (2010) provide the first reconstruction of this stratigraphy, and this dredging and diving in the Bonin fore arc was undertaken to see whether a similar

magmatic stratigraphy was present there. In the area, the results of Ishizuka et al. (2011) support the conclusions of Reagan et al. (2010). Drilling and coring of the volcanic succession at or near Sites U1439–U1442 will provide a crucial test of this hypothesis by providing a more continuous section. It is also important to further constrain the rates at which the fore-arc magmatic succession was emplaced. Evidence so far available indicates that this sequence takes 7–8 My to form during subduction initiation, after which magmatic activity retreats ~200 km to the ultimate position of the arc magmatic front. Recovered cores should provide more material for U-Pb zircon, $^{40}Ar/^{39}Ar$, and biostratigraphic age determinations.

2. *Use the results of Objective 1 to test the hypothesis that fore-arc basalt lies beneath boninites and to understand chemical gradients within these units and across their transitions.*

We expect to find a thick section of FAB at the base of the Bonin fore-arc volcanic succession and a thinner sequence of arc-like and boninitic lavas at the top. To understand the significance of these vertical variations, we need to know how the transition from one magma type to the next takes place: is it a step-function, or is there a slow transition from one magma type to the next? If it is a transition, we need to know whether it is continuous, gradual, and progressive or whether it is accomplished by alternations of one magma type with another. Within the main FAB sequence, we need to know whether there is any evidence that the subduction component increases with stratigraphic height and thus time. A key related question is whether the boninites vary in any systematic way upsection, for example from high-Ca boninite at the base to low-Ca boninite near the top. The nature of these transitions and variations provide important constraints for how mantle and subducted sources and processes changed with time as subduction initiation progressed.

3. *Use drilling results to understand how mantle melting processes evolve during and after subduction initiation.*

Assuming that we are able to accomplish Objectives 1 and 2, we will use the results to better understand how the mantle responds to subduction initiation. For example, a thick basal FAB succession indicates that adiabatic decompression is the most important process at the very beginning of subduction initiation in the IBM system, and an upper section of boninites indicates that flux melting was important just before the transition into normal arc magmatism. Whatever information is obtained from the cores will be used to construct geodynamic and petrologic models of this transition.

4. *Test the hypothesis that the fore-arc lithosphere created during subduction initiation is the birthplace of supra-subduction zone ophiolites.*

Much has rightly been made of the highly successful efforts of IODP and its precursors in establishing the architecture and crustal accretion processes associated with mid-ocean ridges of varying spreading rates and linking these to ophiolites. As discussed earlier, however, it now appears that most ophiolites form when subduction begins and are preserved as fore-arc crust until they are obducted. One testable hypothesis is that ophiolites that formed during subduction initiation can be recognized by a volcanic stratigraphy that varies from MORB-like at the base to arc-like or boninitic near the top, similar to the sequence that we expect to recover from the IBM fore arc. Most ophiolites are not well enough preserved or studied to infer volcanic chemostratigraphies, but some are (e.g., Mesozoic ophiolites such as Pindos, Mirdita, Semail, and Troodos and Ordovician ophiolites of the northeast Appalachians and Norwegian Caledonides). Some of these have volcanic stratigraphies that are similar to those of the IBM fore arc. Results from Bonin fore-arc drilling will allow us to prepare a more detailed volcanic chemostratigraphy expected for subduction initiation, which will in turn allow more detailed comparisons with these ophiolites and encourage geoscientists to try to reconstruct the magmatic stratigraphies of other ophiolites.

Principal results

Site U1439 summary

Operations

After a 457 nmi transit from Yokohama, Japan, the vessel arrived at Site U1439 (proposed Site BON-2A; Figure **F8**). The vessel stabilized over the site at 0324 h (all times reported are ship local time, UTC + 9 h) on 6 August 2014. Because of the short initial period planned at this site, no seafloor-positioning beacon was deployed, and GPS was used for positioning the ship. A seafloor beacon was subsequently deployed once the vessel returned to Site U1439 on 26 August.

Site U1439 consists of three holes. Hole U1439A was cored using the advanced piston corer (APC)/extended core barrel (XCB) system to 199.4 m below seafloor (mbsf) (Table **T1**). Nonmagnetic core barrels were used for Cores 352-U1439A-1H to 10H. Core orientation was performed using the FlexIT tool on Cores 2H through 9H. Temperature measurements were taken with the advanced piston corer temperature tool

(APCT-3) on Cores 4H, 6H, 8H, and 10H. Basement was tagged with the XCB system for the purpose of identifying where in the volcanic stratigraphy this section belongs. Ten APC cores were taken over a 92.3 m interval and recovered 84.3 m (91%). Thirteen XCB cores were taken over a 107.1 m interval and recovered 86.4 m (81%). Overall recovery in Hole U1439A was 86%. The total time spent on Hole U1439A was 59.75 h.

The vessel was offset 20 m east on 8 August, and Hole U1439B was drilled without coring to 42.2 mbsf for a jet-in test in advance of deploying casing beneath a reentry cone in Hole U1439C. After the completion of the jet-in test, the drill string was raised to 100 m above the seafloor, and at 2030 h on 8 August the vessel started the move to Site U1440 using the dynamic positioning system.

After completion of operations at Site U1440, the vessel moved back to Site U1439 on 26 August. A reentry system was prepared, and 178.5 m of 10.75 inch casing was assembled and landed in the reentry cone in the moonpool. A drilling bottom-hole assembly (BHA), including a mud motor, underreamer, and bit, was picked up and installed. The casing with the reentry system attached was lowered to the bottom, drilled into the seafloor, and released on 27 August. Hole U1439C was cored with the rotary core barrel (RCB) system to 544.3 mbsf (Table **T1**). Coring was terminated on 8 September as a result of poor hole conditions. A total of 45 rotary cores were taken over a 362.3 m interval and recovered 107.8 m (30%). An additional 1.5 m of material was recovered during hole cleaning operations. The hole was logged to ~400 mbsf with the triple combination–Magnetic Susceptibility Sonde (MSS) and Formation MicroScanner (FMS)-sonic tool strings. The total time spent in Hole U1439C was 382.75 h. The total time spent at Site U1439 was 447.75 h, or 18.66 days. The vessel moved to Site U1441 on 11 September.

Sedimentology

Sediment and sedimentary rocks were recovered from the seafloor to 176.47 mbsf in Hole U1439A, beneath which a thin interval of basic volcanic and volcaniclastic rocks was recovered within the igneous basement. The sediment represents the late Eocene–recent deep-sea sedimentary cover of the Izu-Bonin fore-arc basement. The underlying volcanogenic rocks are interpreted as the fore-arc basement. The sedimentary succession is divided into 5 lithologically distinct units (Figure **F11**). Lithologic Units I and II are each further divided into 2 subunits. The main criteria for the recognition of the lithologic units and subunits are a combination of primary lithology, grain size, color, and diagenesis. Within the overall succession, 44 ash or tuff layers were observed.

- Unit I (0–50.43 mbsf) is recognized mainly on the basis of a relatively high abundance of calcareous nannofossils compared to the sediment beneath. Unit I is divided into an upper, relatively nannofossil-poor subunit (0–5.54 mbsf) and a lower, relatively nannofossil-rich subunit (5.54–50.43 mbsf).
- Unit II (50.43–100.50 mbsf) is recognized on the basis of a downward change to silty mud and fine to coarse sand, in which the upper subunit (50.43–82.80) is relatively fine grained and the lower subunit (82.80–100.50 mbsf) relatively coarse grained.
- Unit III (100.50–110.93 mbsf) is easily recognizable because of a predominance of pale nannofossil ooze.
- Unit IV (110.93–129.76 mbsf) is marked by a distinct downward change to more clastic sediment dominated by clay, with minor silt, sand, and nannofossil-bearing sediment.
- Unit V (129.76–178.50 mbsf) is characterized by a diverse mixture of fine- to coarse-grained clastic sediment interbedded with fine-grained, nannofossil-rich sediment and sedimentary rock. The base of Unit V is defined as a thin (<3 cm) layer of dark gray to black, weakly consolidated manganese oxide–rich sediment.

Biostratigraphy

Calcareous nannofossils were present in 19 of 22 Hole U1439A core catcher samples and Sample 352-U1439A-20X-2, 0–2 cm. Preservation of calcareous nannofossils is variable, ranging from "good" in the most recent samples to "poor" in certain taxa and intervals. The oldest samples in the hole exhibit more diagenesis than younger samples. Reworking may be common throughout the section, making initial age constraints somewhat difficult. Close examination reveals somewhat continuous recovery from the Upper Pleistocene to the upper Eocene with a few gaps, especially in Miocene-aged sediment (Figure **F11**). The youngest age obtained was Late Pleistocene (Subzone CN14a; ~0.44–1.04 Ma), whereas the oldest age was late Eocene/early Oligocene (Zones NP19/20 or NP21; ~34.44–35.92 Ma).

Fluid geochemistry

Twenty-one samples were collected in Hole U1439A for headspace hydrocarbon gas analysis as part of the standard shipboard safety monitoring procedure; 1 sample per core was collected from Cores 352-U1439A-1H through 23X, except for Cores 21X and 22X in which no sediment was recovered. Thirteen whole-round samples were collected for interstitial water analyses in Hole U1439A; 1 sample per core from Cores

1H through 10H and 1 sample every 3 cores from Cores 13X through 19X. No headspace gas or interstitial water samples were collected from the basement rocks in Hole U1439C. All interstitial water samples were analyzed for salinity, alkalinity, pH, Cl^-, Br^-, SO_4^{2-}, Na^+, K^+, Ca^{2+}, Mg^{2+}, and PO_4^{3-}.

Methane concentrations range from 2.49 to 12.44 ppmv in Hole U1439A, with the highest methane concentration measured in Core 1H at 5.9 mbsf. This high value is attributed to decomposition of organic matter in the uppermost layers of the sedimentary column. No ethane or propane was detected in Hole U1439A samples. The major result of the interstitial water analyzes from Hole U1439A is a broad correlation with the described lithologic units, with the exception of Mg^{2+} and Ca^{2+}. The distribution of these elements in the sedimentary column is invariant of lithology and shows a downhole increase in Ca^{2+} to 40.5 mM and a decrease in Mg^{2+} to 39.2 mM. These variations can probably be attributed to metasomatism by interaction with fluids released from the basaltic basement.

Petrology

Igneous rocks were recovered in Holes U1439A and U1439C. Hole U1439A tagged basement during XCB coring (Cores 352-U1439A-20X through 23X; 3.7 m recovery), whereas Hole U1439C penetrated 362.3 m of igneous basement (Cores 352-U1439C-2R through 45R; 108.5 m recovery). The uppermost part of the section comprises heterolithic breccia, which represents seafloor colluvium. The lowermost part of the section is composed of mafic dikes or sills. The volcanic rocks in between are dominated by pillow lava with intercalations of massive sheet flows, igneous breccias especially hyaloclastites, and subaqueous pyroclastic flow deposits. This site is notable for the variety of boninites cored and for the intercalation of more and less differentiated boninites at several levels throughout the section. In one unit, these magmas appear to have erupted simultaneously, forming complex magma mingling textures. Phenocrysts are common in the basement boninitic rocks throughout Holes U1439A and U1439C. However, the variations in phase assemblages and abundances are not always diagnostic. As a result, chemical distinctions based on portable X-ray fluorescence (pXRF) spectrometry were also used to assess changes in rock composition and to track the occurrence of different magma series.

Ten igneous units were identified in the basement at Site U1439 (Figure **F12**). Unit boundaries represent an abrupt change in chemical characteristics, phenocrysts, and groundmass assemblages. Subunits typically represent changes in the eruptive nature of a unit (e.g., from hyaloclastite to pillow lava or massive lava), although minor

changes in chemical composition occur at some subunit boundaries. Unit 10 is doleritic and was interpreted to represent sheeted shallow dikes or sills.

Fresh igneous rocks at Site U1439 are dominantly boninites characterized by phenocrysts of olivine and orthopyroxene and are typically set in a groundmass of pale glass and acicular to tabular pyroxene prisms. Acicular plagioclase is commonly present in the groundmasses of lower-silica boninites, but is only in the groundmasses of the most highly differentiated high-Si boninite series lavas. Phenocryst and groundmass assemblages document a range in boninite compositions:

1. Orthopyroxene > olivine phenocrysts with an orthopyroxene-dominated groundmass (Units 1–4),
2. Olivine + augite ± orthopyroxene phenocrysts with an augite ± plagioclase–bearing groundmass (Unit 5), and
3. Olivine > orthopyroxene ± augite phenocrysts with augite ± orthopyroxene ± plagioclase in the groundmass (Units 6–9).

Based on using Niton handheld pXRF analyses, these units are also distinguished by their Ti/Zr ratios (see **"Preliminary scientific assessment"**): 1 has very low Ti/Zr (<60), 2 has significantly higher Ti/Zr (90–120), and 3 has intermediate Ti/Zr (65–90).

Boninites in the first group are canonical boninites, whereas those in the second and third groups have lower silica concentrations and were assigned a shipboard classification of "basaltic boninites" and "low-Si boninites," respectively (see discussion of nomenclature under **"Preliminary scientific assessment"**).

The basaltic boninites in Hole U1439 have abundant modal plagioclase in the groundmass and high magnetic susceptibilities. These basaltic boninites also are notable, however, for their low TiO_2 contents and Ti/Zr compared with those of the fore-arc basalts of Site U1440.

Alteration in Hole U1439C basement units is highly variable. Fresh boninite glass is relatively common, but most samples have calcite, zeolite, and/or smectite clays partially to replacing groundmass, olivine and more rarely, orthopyroxene phenocrysts. Palagonite, clays, and more rarely, zeolites replace glass. Calcite and zeolite-filled veins and vesicles are common throughout the core, rarely associated with pyrite. Quartz is a rare component in some veins. The alteration generally becomes more intense with depth. Talc is present from Core 350-U1439C-22R to 26R. A green secondary phyllosilicate, perhaps chlorite, first appears in Core 26R and becomes common

below Core 29R. In fresh glass from Cores 28R to 33R, biogenic microtubes are common. Veins, principally of calcite, zeolite, and smectite, are abundant in Hole U1439C downhole to the boundary between boninite pillow lavas and dolerites.

Rock geochemistry

Whole-rock chemical analyzes were performed on 48 igneous rocks and 22 sediment samples representative of the different lithologic units recovered from Site U1439. The 22 sediment samples were collected in Hole U1439A (1 per core) and analyzed for major and trace element concentrations and volatile contents. Hole U1439A sediments show a broad range of compositions, mainly marking the downhole changes in lithology from the carbonate-rich calcareous ooze (CaO > 50 wt%, Sr up to 2000 ppm, total C up to 11wt%, and Zr of ~30–40 ppm) to the clay- and volcaniclastic-rich silty muds (CaO < 2 wt%, Sr up to ~200 ppm, and Zr up to 150 ppm). The downhole transition to igneous basement is marked by a thin, muddy, manganese-rich layer (MnO = 2–5 wt%) and enrichments in Cu (>500 ppm), V (>200 ppm), and Zr (>150 ppm).

At the bottom of Hole U1439A, 1 orthopyroxene-phyric volcanic rock and 1 volcanic glass were sampled. In addition, 46 igneous rocks were selected by the Shipboard Science Party as representative of the different lithologies recovered from Hole U1439C. The rocks were grouped as olivine-pyroxene-phyric or plagioclase-bearing volcanic rocks, the latter being observed mainly at the bottom of the hole. The 48 igneous rocks were analyzed for major and trace element concentrations by inductively coupled plasma–atomic emission spectroscopy (ICP-AES) and for CO_2 and H_2O contents by gas chromatography for samples with loss on ignition (LOI) >2 wt%. An aliquot of the powder used for ICP-AES analyzes was subsequently used for XRF analyses, which were carried out with the pXRF. In addition, pXRF "chemostratigraphic" analyses were conducted on 350 archive-half pieces from Hole U1439C cores. The results of these chemical analyses, in conjunction with observations on core material and thin sections carried out by the petrology team, contributed to the lithologic division of the lavas into different units.

Site U1439 igneous rocks range from slightly to highly altered with LOI values from 2.5 to 16.2 wt%. LOI values primarily vary with H_2O contents (0.5–8.8 wt%) and, thus, the amount and type of secondary hydrous minerals. However, several samples from the upper Units 1–8 also show high CO_2 values (up to 6.4 wt%) together with higher Ca content, the result mostly of late carbonate addition. This shows that the primary compositions of several samples were modified significantly by alteration. For this reason, the igneous rocks of Hole U1439C were screened for alteration based

on petrology and selected chemical criteria before further description and interpretation of their primary geochemical signature.

Igneous samples recovered from Hole U1439C are boninites with SiO_2 concentrations ranging from 50.5 to 60.2 wt% at total alkali contents of 1.60–4.70 wt%. Olivine-pyroxene-bearing igneous rocks are characterized by high Cr concentrations (221–1562 ppm), high Mg# (cationic Mg/[Mg + Fe], with all Fe as Fe^{2+}) of 64–80, and CaO/Al_2O_3 ratios of 0.49–0.93. The lowermost lavas and dolerites (Units 9 and 10) have lower Cr concentrations (51–750 ppm) and Mg# (59–76) than overlying units.

A characteristic feature of Site U1439 samples is the progressive decrease in TiO_2 concentrations that characterize the transition from the plagioclase-bearing igneous rocks sampled deep in Hole U1439C to the shallower, higher Si boninite samples. Another characteristic feature is the enrichments in highly incompatible and mobile elements (e.g., Ba) in igneous rocks sampled at Site U1439 compared to those from Site U1440. These enrichments are not correlated with indices of alteration and appear to be of magmatic origin.

Structural geology

Structures observed in Site U1439 cores originated from drilling-induced, sedimentary, igneous, and tectonic processes. Drilling-induced deformation in the sediment, including dragging-down, rotational shear, and postretrieval core dilation, prevented observation of sedimentary structures between ~92 and 155 mbsf. Sedimentary structures, such as bedding planes, stylolites, dewatering structures, and cross-bedding, point to an overall nearly horizontal bedding attitude. Igneous structures, although rarely observed, consist of local magmatic foliation marked by alignment of primary minerals, and a few centimeter-long enclaves in zones of magmatic mingling.

Tectonic structures, present mostly in igneous rocks, comprise tension fractures (veins), shear fractures, breccias, cataclasites, and fault zones. Veins are generally filled with (Mg-) calcite, zeolite, and clay. These veins typically dip steeply and do not correlate with the presence of faults. Vein thickness varies with depth and decreases from 350 to 500 mbsf. Three major fault zones occur at 348–401, 420–446, and 475–535 mbsf. The dominant sense of slip determined on slickensides is normal. Calcite microstructures in the deepest intervals include Type I and II twins, as well as subgrain boundaries, which suggests a relatively high differential stress.

Physical properties

Many of the physical property measurements display variability at similar depths, suggesting a few major boundaries. There is a distinct increase in natural gamma ray (NGR) values at 100–130 mbsf in lithologic Units III–IV. At 135–180 mbsf in Unit V, magnetic susceptibility and *P*-wave velocity increases. The reflectance parameters L*, a*, and b* decrease with depth from 0 to 130 mbsf in Units I–IV and display an abrupt increase in values at 128–130 mbsf at the boundary between Units IV and V. Bulk, dry, and grain densities show no systematic variation with depth. Porosity increases with depth from 0 to 130 mbsf in Units I–IV and decreases in Unit V.

Magnetic susceptibility distinctly increases and density distinctly decreases at 478–540 mbsf in igneous Units 9–10. NGR values decrease with depth from 180 to 390 mbsf in Units 1–6 and are low from 390 to 540 mbsf in Units 8–10, with some peaks correlated to magnetic susceptibility peaks. At 200–240 mbsf in Subunit 3a, density and *P*-wave velocity increase and porosity decreases. The reflectance parameters a* and b* have a small peak at 330 mbsf in Unit 3.

Paleomagnetism

Sediment cored in Hole U1439A is relatively strongly magnetic and has low coercivities, so it acquired a strong drill string overprint. This overprint was easily removed by alternating field demagnetization, revealing a Pliocene–Pleistocene magnetic stratigraphy in Cores 352-U1439A-1H through 10H (0–85 mbsf). Magnetic chrons downhole to the Gilbert Chron (~4.5 Ma) were clearly identified. The identification of older chrons downhole to Chron 3B is less certain. Cores 15X through 19X show clear magnetic polarity zones tentatively correlated with Chrons 8 through 13 (~25–34 Ma).

Igneous rock samples from Hole U1439C have mostly low inclinations with absolute values less than ~30° and an average of ~5°. This is consistent with the hypothesis that the Izu-Bonin arc formed near the paleoequator. Several zones of outlier paleoinclinations occur near observed fault zones. These anomalous values may be explained by remagnetization or tectonic rotation.

Downhole logging

A ~220 m interval of basement rocks in Hole U1439C was logged over a ~18 h period with 2 tool strings, the triple combo-MSS and FMS-sonic tool strings. Borehole conditions were relatively stable during logging operations, but weather conditions and sea state deteriorated. NGR, density, resistivity, magnetic susceptibility, sonic velocity,

and microresistivity images were successfully acquired. Changes in the character and trend of these logs are used to define 7 logging units in this hole.

Logging Unit 1 (~180–189 mbsf) is characterized by increasing values in NGR, resistivity, density, and velocity, in combination with decreasing magnetic susceptibility downhole. Unit 2 (~189–202 mbsf) shows decreases in density, resistivity, and magnetic susceptibility, whereas NGR is high relative to the units above and below. Unit 3 (~202–213 mbsf) exhibits overall decreases in resistivity, magnetic susceptibility, and NGR values with coincident discrete peaks in NGR and density. High-frequency variations in both resistivity and magnetic susceptibility, in combination with anticorrelated profiles of density and NGR, characterize logging Unit 4 (~213–246 mbsf). Unit 5 (~246–314 mbsf), the thickest of the logging units, is characterized by a wide range in magnetic susceptibility values, with a significant high in the uppermost 6 m of the unit. Unit 6 (~314–365 mbsf) is delineated from Unit 5 by a major washed-out zone. The resistivity, magnetic susceptibility, and velocity profiles through this interval are very variable, which can, in part, be attributed to increased borehole rugosity. The deepest unit, Unit 7 (~365–402 mbsf, the bottom of the logged interval), has limited data available, but is differentiated from the overlying unit by higher values of resistivity, magnetic susceptibility, and NGR. Overall, density, velocity, and resistivity increase with depth. NGR and magnetic susceptibility values do not show such systematic changes with depth. The oriented microresistivity images show a wide range of features and textures in the walls of the borehole, including fracture networks, vesicles, and through-going planar features.

Although the logging unit boundaries do not correspond perfectly with the petrologic unit boundaries, there are clear relationships between the logging data and the physical properties and geochemistry of the core. Ongoing integration of the core and logging data sets will be essential in filling in some of the gaps in core recovery in the volcanic extrusive sequence of this hole.

Site U1440 summary

Operations

After an 8.2 nmi transit from Site U1439, the vessel arrived at Site U1440 (proposed Site BON-1A; Figure **F8**) and a positioning beacon was deployed at 0548 h on 9 August 2014. Site U1440 consists of 2 holes. Hole U1440A was cored with the APC to 103.5 mbsf and then cored with the XCB to a final depth of 106.1 mbsf (Table **T1**). Nonmagnetic core barrels were used with all APC cores. Cores 352-U1440A-1H through 6H were

oriented using the FlexIT tool, which was removed with Core 7H as a result of the high heave conditions experienced by the vessel. APCT-3 temperature measurements were taken with Cores 4H, 6H, 8H, and 11H. Basement contact was recorded at ~101 mbsf. The APC coring system was deployed 12 times, with 103.5 m cored and 96.4 m recovered (93%). The XCB coring system was deployed twice, with 2.6 m cored and 0.2 m recovered (8%). The total time spent in Hole U1440A was 49.25 h.

A reentry system with a reentry cone and 99 m of 10.75 inch casing was drilled into the seafloor in Hole U1440B using a mud motor, underreamer, and drilling bit assembly. Coring with the RCB began at 102.3 mbsf in Hole U1440B and was terminated after bit failure at a final depth of 383.6 mbsf (Table **T1**). Basement contact was estimated at ~125 mbsf. The RCB coring system was deployed 36 times, with 281.3 m cored and 34.7 m recovered (12%). Following coring, 2 logging runs were made with the triple combo–Ultrasonic Borehole Imager (UBI) and FMS-sonic tool strings. As a result of deteriorating hole conditions, the triple combo-UBI tool string collected data downhole to 254 mbsf, and the FMS-sonic tool string collected data to ~243 mbsf. The total time spent in Hole U1440B was 364.75 h. The acoustic beacon was recovered at 0612 h on 26 August, and the vessel returned to Site U1439. The total time spent at Site U1440 was 414 h or 17.25 days.

Sedimentology

Sediment and sedimentary rocks were recovered from the seafloor to 103.5 mbsf in Hole U1440A, beneath which a thin interval of basic volcanic rocks was recovered. The sediment represents a section through the early Oligocene to recent deep-sea sedimentary cover of the IBM fore-arc basement. The underlying basaltic rocks recovered here are interpreted as representing the fore-arc basement. The sedimentary succession in Hole U1440A is divided into 3 lithologically distinct units (Figure **F13**). Unit I is further divided into 3 subunits, and Unit II is divided into 2 subunits. The main criteria used to define the lithologic units and subunits are a combination of primary lithology, grain size, color, and diagenesis.

- Unit I (0–32.98 mbsf) is recognized mainly on the basis of a relatively high abundance of poorly consolidated brown mud. Subunit IA (0–13.33 mbsf) is composed of mud with calcareous nannofossil and ash layers. Subunit IB (13.33–21.61 mbsf) is composed of mud with foraminifers and minor ash layers. Subunit IC contains mud with diatoms, together with minor tuffaceous sandstone and ash layers (21.61–32.98 mbsf).

- Unit II (32.98–77.50 mbsf) is recognized on the basis of a downward increase in grain size to more clastic and volcanogenic sediment. Subunit IIA (32.98–58.50 mbsf) is relatively coarse grained and volcanogenic. Subunit IIB (58.50–77.50 mbsf) is even coarser grained and includes muddy volcanogenic breccia/conglomerate with gravel.
- Unit III (77.50–103.52 mbsf) exhibits a return to finer grained silty mud with subordinate volcanogenic gravel. The basalt beneath forms the top of the basement.

The proportions of the main sediment types recovered are

- Ash/tuff = 2.89 m or 2.9% of the total recovered sediments,
- Coarse-grained sediment (sand to conglomerate) = 16.5 m or 17.1%,
- Fine-grained mud, silt/mudstone, and siltstone = 75.51 m or 78.5%, and
- Nannofossil ooze = 1.24 m or 1.2%.

In addition, sediment was recovered in 3 cores immediately below the drilled interval in Hole U1440B (Cores 2R through 4R; 102.3 to ~115.3 mbsf). These cores correspond to Unit III in Hole U1440A.

Biostratigraphy

Calcareous nannofossils were recovered intermittently in Hole U1440A, where productive intervals are interspersed with barren intervals dominated by siliceous microfossils (especially radiolarians) and volcaniclastic material. There is a long barren interval from Sample 352-U1440A-6H-CC to 10H-CC. The youngest age obtained is Late Pleistocene (Subzone CN14a; ~0.44–1.04 Ma), and the oldest age obtained is early Oligocene (Zone NP23; ~29.62–32.02 Ma) (Figure **F13**). Three samples were examined from Hole U1440B. Samples 352-U1440B-2R-CC and 4R-1, 14–15 cm, contained calcareous nannofossils sufficient for age diagnostics, whereas Sample 3R-CC was barren. Preservation was moderate to poor in each sample with many taxa showing strong dissolution and overgrowth. Both of the Hole U1440B samples have an early Oligocene age (Zones NP22 and NP21, respectively), with a range that is difficult to constrain better than ~32.02–34.44 Ma given the lack of reliable marker taxa for the equatorial Pacific. Absolute age determinations were more difficult to make at Site U1440 compared to Site U1439 as a result of increased dissolution and a number of barren intervals.

Fluid geochemistry

Twelve samples (1 per core) were collected in Hole U1440A for headspace hydrocarbon gas analysis as part of the standard shipboard safety monitoring procedure, and 12 whole-round samples were collected for interstitial water analyses (1 per core). No headspace gas or interstitial water samples were collected in Hole U1440B. All interstitial water samples were analyzed for salinity, alkalinity, pH, Cl^-, Br^-, SO_4^{2-}, Na^+, K^+, Ca^{2+}, Mg^{2+}, and PO_4^{3-}.

Only minor methane was detected in the headspace gas samples. The highest methane concentration (5.84 ppmv) was measured in Core 352-U1440A-1H at 1.5 mbsf and may be attributed to the decomposition of organic matter in the uppermost layers of the sediment.

The major result of the interstitial water analyses from Hole U1440A is the distinctive behavior of Mg^{2+} and Ca^{2+}. Both elements have seawater concentrations at the top of the hole, but Ca^{2+} concentrations then decrease with depth to 41.2 mM at the bottom of the hole, whereas Mg^{2+} concentrations increase to 36.6 mM. These variations are independent of lithologic units and are attributed to pervasive fluid input from the underlying hydrothermally altered basaltic basement and alteration of volcanic ash in the sediment.

Petrology

Igneous rocks were recovered in both Holes U1440A and U1440B. Hole U1440A tagged basement during XCB coring with low recovery (Cores 352-U1440A-13X and 14X; 0.2 m recovered), whereas Hole U1440B penetrated 268.3 m of igneous basement, again with low recovery (Cores 352-U1440B-4R through 36R; 33.9 m recovered). The basement/sediment contact is marked in both holes by a Mn-rich sediment layer or coating. The uppermost igneous unit in both holes comprises a mixture of volcanic rock fragments in a sediment matrix and likely represents talus or volcaniclastic breccia. This unit is ~35 cm thick and underlain by over 175 m of volcanic rock, which transitions over ~70 m into dikes at 329.0 mbsf. The dikes are interpreted as part of a sheeted dike complex. The igneous basement is divided into 15 igneous units numbered in order of increasing depth (including the uppermost breccia) based largely on the physical nature of recovered lithologies, which were interpreted to be hyaloclastites, pillow lavas, sheet flows, and dikes (Fig. **F14**). The lowermost unit (15) is a dike complex further divided into 5 chemically distinct subunits (15a–15e).

Igneous rocks at Site U1440 are typically aphyric to sparsely phyric, plagioclase-pyroxene-magnetite phyric basalts with intergranular to intersertal textures. The coarser grained units in the dike complex and transition zone are dolerites with subophitic textures. All of the igneous rocks are petrographically similar to IBM FAB collected elsewhere and have chemical compositions consistent with this classification. They are distinct petrographically and chemically from the boninite-suite lavas, which are typically orthopyroxene and olivine phyric.

The degree of alteration of the igneous rocks at Site U1440 is low in the volcanic section where the secondary mineralogy is dominated by calcite, smectite-group clays, and zeolites including phillipsite. These minerals form abundant veins in Cores 352-U1440B-12R through 24R, some of which are associated with pyrite and native copper. Alteration becomes more intense in the transition zone and dike complex where the secondary mineralogy includes chlorite. Secondary minerals typically only replace the groundmass phases, leaving the silicate framework minerals (plagioclase and pyroxene) unaffected, except in the lower part of the dike complex where pyroxene and plagioclase may be partially replaced. Glass is commonly devitrified and, less commonly, replaced by palagonite, clays, and zeolite.

Rock geochemistry

Whole-rock ICP-AES chemical analyses were performed on 33 igneous rocks and 16 sediment samples representative of the different lithologic units recovered at Site U1440. Twelve sediment samples were collected from Hole U1440A (1 per core), and 3 samples were collected in the deepest part of the sediment sequence in Hole U1440B from 104.4 to 115.1 mbsf. Additionally, 1 sandstone piece was recovered within the igneous sequence in Section 352-U1440B-15R-1 (192.8 mbsf). One aphyric basalt sample was collected at the bottom of Hole U1440A, and 32 samples, mostly basaltic, were collected in Hole U1440B. The 16 sediment samples were analyzed for major and trace element concentrations and volatile contents. The 33 igneous rocks were analyzed for major and trace element concentrations. An aliquot of the powder used for ICP-AES analyses was subsequently used for pXRF analyses.

The sediment sampled at Site U1440 is dominantly silty mud, and its compositional variations reflect sedimentary unit changes. The range of compositions is more restricted than in the sediment in Hole U1439A. The sediment has, on average, low CaO contents (<2 wt%), high SiO_2 contents (>55 wt%), and variable Cu concentrations (120–240 ppm). A few samples contain slightly higher carbonate contents with total C contents >0.9 wt%, CaO of 5–22 wt%, and lower Cu concentrations (70–90 ppm).

Hole U1440B sediment has the same composition as that of lithologic Unit III sediment in Hole U1440A. Similarly, the sandstone recovered within igneous Unit 4 rocks overlaps in composition with lithologic Unit III sediment. This sandstone could represent an accidental fragment displaced by drilling or an accumulation of sand in an open fracture.

Site U1440 igneous rocks are mostly basalts with one andesite unit (igneous Unit 6). SiO_2 ranges from 48 to 57 wt%, and total alkali ($Na_2O + K_2O$) contents vary from 2.1 to 3.2 wt%. These rocks are relatively depleted in incompatible trace elements (e.g., TiO_2 = 0.6–1.4 wt%) and have highly variable Cr concentrations (15–380 ppm), indicating different degrees of differentiation. Downhole profiles of major element compositions exhibit a distinct increase in SiO_2 concentrations and Mg# at ~260 mbsf. This depth marks the transition between igneous Units 7 and 8, which is interpreted as the boundary between the volcanic series and the lava/dike transition. The sampled igneous rocks have major element compositions similar to those of FAB collected by diving in the Bonin forearc (cf. Ishizuka et al., 2011).

XRF chemostratigraphic analyses were conducted on archive-half pieces of cores and on thin section billets and powders. The results of these chemical analyses, in conjunction with observations on core material and thin sections carried out by the petrology team, contributed to the 15 unit lithologic division of the lavas and dikes, and are discussed in the **"Preliminary scientific assessment"** section below. Briefly, TiO_2 and Zr concentrations in basalts generally decrease downhole from Unit 4. Although there is some cyclicity, Cr concentrations and Sr/Zr ratios increase over the same interval. Above Unit 4, the basalts have low Zr, TiO_2, and Cr concentrations, and relatively high Sr/Zr ratios. Unit 6 andesites are characterized by low TiO_2 and Sr concentrations, and the highest Zr concentrations of any lavas from Sites U1440 and U1441.

Structural geology

Bedding planes in the sediment are marked by dark pyroclastic beds and thin sandy layers and are generally subhorizontal. Drilling-induced deformation of core features precluded meaningful structural measurements in the sediment between ~57 and 102 mbsf. In the igneous rocks, magmatic fabrics are rare and limited to a few centimeter-wide domains of grain alignment. Steep, metamorphic, chlorite-based foliation overprints primary fabrics at ~145–146, 281–291, and 358–369 mbsf. Tension veins filled with (Mg-) calcite, zeolite, chlorite, and clays are common at ~164–166, 202–264, and 319–369 mbsf. These veins typically form two sets at a high angle from each

other with average dips of ~40° ± 10° and 80° ± 10°. The basalts and dolerites are overall free of plastic and cataclastic deformation features such as slickensides.

Physical properties

Changes in the trends of physical properties are encountered at similar depths, and these changes tend to be associated with different units. At ~10 mbsf in lithologic Unit I, there is a positive spike in *P*-wave velocity and NGR accompanied by a slight increase of gamma ray attenuation (GRA) density. This is an interval rich in tephra layers. At 35–40 mbsf in Unit II, *P*-wave velocity and GRA density increase sharply, whereas NGR decreases. Color reflectance parameters L*, a*, and b* decrease in the same interval. Physical properties show significant variability in Unit III. At 83–87 mbsf, magnetic susceptibility increases suddenly and color reflectance parameter L* decreases. At ~87–100 mbsf, *P*-wave velocity increases; magnetic susceptibility and NGR are variable but generally decrease with depth; color reflectance parameters decrease with depth; GRA, dry, and bulk density increase with depth; and porosity decreases with depth. At 100–102 mbsf, *P*-wave velocity, magnetic susceptibility, NGR and GRA, and dry and bulk density suddenly decrease accompanied by a sudden increase in porosity. Physical property parameters change in igneous Units 7 and 8. At ~230 mbsf in Unit 7, porosity decreases sharply, *P*-wave velocity increases, and bulk and dry density increase. At 270–280 mbsf in Unit 8, NGR decreases and magnetic susceptibility increases, with high values observed between 280 mbsf and the bottom of the hole.

Paleomagnetism

Remanent magnetization measurements reveal that sediment cored at Site U1440 is highly magnetic (~0.1–2 A/m natural remanent magnetization [NRM]), apparently as a result of input of volcaniclastic material from nearby sources. A normal Pliocene–Pleistocene magnetic stratigraphy has been established for the upper sedimentary section and includes the period from the upper Gilbert Chron (~4 Ma) to the Brunhes Chron at the surface. Paleomagnetic samples from the igneous basement section reveal a probable magnetic reversal sequence. The upper ~50 and lower ~120 m of the section have normal polarity, whereas the intervening ~70 m has reversed polarity. Until radiometric dates are available for the basement section, the pattern cannot be correlated with the geomagnetic polarity timescale.

Downhole logging

A ~130 m open hole interval of Hole U1440B was logged over a ~24 h period with 2 tool strings, the triple combo-UBI and the FMS-sonic. Although borehole conditions deteriorated while downhole logging was in progress, NGR, density, resistivity, sonic velocity, and microresistivity images were successfully acquired.

Seven logging units are defined on the basis of the character and trend of the various logs. Logging Unit 1 (~99–116 mbsf) is characterized by relatively consistent resistivity and velocity with depth whereas the underlying Unit 2 (~116–122 mbsf) shows sharp increases in NGR, resistivity, and density downhole. Units 3 (~122–164 mbsf) and 5 (~170–211 mbsf) exhibit similarities in their log responses, steadily increasing in resistivity with depth and with no net change in NGR. However, Unit 3 does show much greater variability in bulk density compared to the range of densities measured in Unit 5. Units 4 (~164–170 mbsf) and 6 (~211–222 mbsf) are relatively thin by comparison to Units 3 and 5, and are characterized by high resistivity, high velocity, and increasing density with depth. Unit 7 has limited data available but is differentiated from the overlying unit by a marked changed in the character of the resistivity log. Overall, there are downward increases in density, resistivity, and sonic velocity, whereas NGR and porosity (as derived from resistivity) exhibit decreasing downhole trends. Microresistivity images overall echo the increasing resistivity with depth and also elucidate a range of textures and features through the logged interval.

Preliminary analysis of the data shows a reasonable agreement between the logging unit boundaries and the lithologic unit boundaries that were defined on the basis of core description and geochemical analyses. It is anticipated that the logging data, although only available for the lowermost sedimentary interval and upper volcanic extrusive section, will be useful in filling in some of the gaps in core recovery.

Site U1441 summary

Operations

The *JOIDES Resolution* completed the 6.2 nmi transit from Site U1439 in dynamic positioning mode while the drill string was being lowered to the seafloor. The vessel arrived at Site U1441 (proposed Site BON-6A) at 1512 h on 11 September 2014, and a seafloor positioning beacon was deployed.

Site U1441 consists of one hole. An RCB BHA was assembled with a C-4 bit. Hole U1440A was spudded at 2245 h on 11 September. The RCB coring system with nonmagnetic core barrels was deployed 22 times (Cores 352-U1441A-1R through 22R) and the hole was advanced to 205.7 mbsf (Table **T1**). Cores 11R and 12R had no recovery as a result of a plugged bit. Hole U1441A was terminated as a result of poor core recovery, the rubbly nature of the formation, and high risk of getting stuck. The RCB cores recovered 50.7 m over the 205.7 m cored interval (25%). The total time spent in Hole U1441A was 75.75 h. The seafloor positioning beacon was recovered at 0914 h on 14 September, and the vessel started the slow transit to Site U1442 while continuing to pull the drill string to the surface.

Sedimentology

Pelagic and volcaniclastic sediment was recovered from the seafloor to 83.00 mbsf, beneath which igneous rocks were recovered. The sedimentary succession is divided into five lithologically distinct units (Fig. **F15**). Lithologic Unit I is further divided into 2 subunits. The volcanic rocks beneath are interpreted as the fore-arc basement. The main criterion for the recognition of the lithologic units and subunits is a combination of primary lithology, grain size, color, and diagenesis. Within the overall succession, 16 ash or tuff layers were observed. The bedding planes are generally oriented subhorizontally, with dip angles <10°.

- Unit I (0–15.02 mbsf) is divided into 2 subunits. Subunit IA (0–0.17 mbsf) is recognized by the occurrence of brownish mud with medium to coarse sand. Subunit IB (0.17–15.02 mbsf) is a relatively nannofossil-rich interval of silty calcareous ooze with nannofossils and sparse planktonic foraminifers.
- Unit II (15.02–24.50 mbsf) is recognized on the basis of a downward change to more clastic-rich sediment composed of muddy volcanic breccia/conglomerate and volcaniclastic sand layers.
- Unit III (24.50–58.64 mbsf) is characterized by a return to finer grained silty mud with relatively abundant radiolarians.
- Unit IV (58.64–70.38 mbsf) is distinguished by a distinct downward change to greener, relatively fine-grained sediment dominated by greenish gray silty clay.
- Unit V (70.38–83.00 mbsf) is a much coarser, mud-supported conglomerate with sandy and silty clay and also clay.

Biostratigraphy

Calcareous nannofossils were present in 3 of 10 core catcher samples. Samples 352-U1441A-1R-CC and 2R-CC are nannofossil oozes, whereas siliceous fossils dominate Sample 5R-CC. Preservation was "moderate" to "good" in each sample. Samples 1R-CC and 2R-CC yield an approximately Late Pleistocene age, whereas Sample 5R-CC yields an approximately late Miocene age (5.59–8.12 Ma). The widespread presence of radiolarians in the lower part of the sediments will help us improve the biostratigraphy postcruise.

Fluid geochemistry

Ten samples were collected from Hole U1441A for headspace hydrocarbon gas analysis as part of the standard shipboard safety monitoring procedure. Methane concentrations range from 1.08 to 1.29 ppmv, and neither ethane nor propane were detected.

Petrology

All of the igneous rocks at Site U1441 are FAB similar to those drilled at Site U1440. These basalts are also similar texturally and chemically to FAB recovered in diving expeditions in the region. They are dominated by modal plagioclase, clinopyroxene, and magnetite in the groundmass, and most are aphyric. Four units were identified based on hand specimen and thin section description and XRF data (Figure **F16**). Microphenocrysts of plagioclase are rare, but igneous Unit 3 contains 2%–3% clinopyroxene phenocrysts. Not surprisingly, Unit 3 is also the unit with the highest CaO content. Three chemical varieties of basalt were found. The upper basalts (Units 1 and 2) are depleted in TiO_2 and Zr and have low Cr concentrations. The lowest basalts, which comprise Unit 4, are normal FAB very close in composition to those at Site U1440. In contrast, the Unit 3 basalts, which lie stratigraphically between these types, are among the most depleted basalts found along the IBM fore arc, with very low TiO_2 and Zr concentrations and high Ti/Zr ratios. With the exception of Unit 3, TiO_2, Zr, and Cr all show subtle increases steadily downhole.

Rock geochemistry

Seven igneous rocks from Cores 352-U1441A-10R to 22R were analyzed by ICP-AES for major and trace elements and by CHNS for CO_2 and H_2O contents. The igneous rocks recovered have LOIs of 2.0–4.6 wt%. They have higher H_2O contents in the upper part of the basement (Unit 1) and relatively uniform H_2O contents of 2.0–2.5 wt% in the lower units.

The igneous rocks recovered from Hole U1441A are all basalts, with SiO_2 concentrations of 49–51 wt% and total alkali contents of 2–4 wt%. Overall, the major element composition of Site U1441 basalts is relatively homogeneous with MgO of 6.4–8.4 wt%, CaO of 10.7–11.6 wt%, and Fe_2O_3 of 10.8–12 wt%. Site U1441 basalts are very similar in composition with the IBM FABs previously recovered by drilling at Site U1440 and by diving. The single sample analyzed from Unit 3 has high Cr and CaO concentrations, a high Mg#, and low concentrations of TiO_2, Zr, and Y. This sample plots as a magnesian end-member composition on trace element variation diagrams but, despite its lower Ti contents, is both geochemically and petrographically distinct from Site U1439 boninites.

Structural geology

In the igneous units, viscous-plastic fabrics related to magmatic flow are rare and limited to millimeter- to centimeter-wide domains, defined primarily at the microscale. These domains are relatively common in the lower parts of Hole U1441A (e.g., in Sections 352-U1441A-19R-1 and 22R-1). The magmatic foliation is mainly defined by the shape-preferred orientation of acicular feldspar crystals embedded within a glassy or microcrystalline matrix.

Extensional fractures without mineral fillings are subvertical and are observed at 85.15 and 180.45 mbsf. Subvertical to inclined, whitish, crystalline, millimeter-thick veins are abundant at 122.22–141.43 and 190.2–190.6 mbsf. In the lower interval the veins form steeply inclined conjugate sets. The vein-filling material consists of (Mg-) calcite and/or zeolite and/or chlorite.

Slickensides are abundant at 84.00–88.25 mbsf and dip steeply to subvertically. The general sense of shear is left-lateral strike-slip to oblique reverse including a left-lateral component as well. One subhorizontal slickenside shows a normal sense of shear. In the lowermost sections of Hole U1441A (interval 20R-1, 15–27 cm), a semiductile to brittle, low-angle shear zone was observed within a highly altered domain. The shear zone was recovered as a single piece with an oblong shape, without a preserved contact with the wall rock. Its position within the lithostratigraphic sequence cannot be defined exactly because of the poor core recovery. The recovered basalt pieces below and above do not show any indication of comparable alteration or deformation. Within the shear zone, shear bands form subparallel sets, indicating a top-down sense of shear.

Physical properties

Many of the physical properties display similar downhole trends in the sedimentary section. *P*-wave velocities have peaks as high as 1580 m/s at 22–24 mbsf (lithologic Unit II) and 1540 m/s at 56–58 mbsf (Unit III). Magnetic susceptibility values also have peaks to 250–300 IU at the same depths. These peaks in *P*-wave velocities and magnetic susceptibility values correspond to tephra layers. GRA densities are 1.4–1.5 g/cm^3, and NGR values are 10–20 counts/s from 0 to 69 mbsf. All of these parameters have a high peak at 70 mbsf at the bottom of Unit IV. Porosities are 65%–85% from 0 to 78 mbsf. Porosities are higher than 80% in Unit II and have the lowest value of 70% in Unit III.

Physical properties typically exhibit stepwise increases between Units 1 and 2. Magnetic susceptibility values start at >1000 IU at the top of the basement, at ~85 mbsf in Unit 1, and decrease to 500 IU in Units 2–4. GRA density values are 2–2.5 g/cm^3 with a peak of 2.7 g/cm^3 at 171 mbsf in Unit 3. NGR values increase from 9 to 20 counts/s in Unit 1 and decrease to 5 counts/s in Units 2–4. Although the values of reflectance parameter L* remain steady at 50–55 in Units 1–4, both a* and b* values are high (>10) in Unit 1 and low (<5) in Units 2–4. Bulk densities of the discrete samples are 2.4 g/cm^3 in Unit 1 and increase to ~2.8 g/cm^3 in Units 2–4. Porosities are ~30% in Unit 1 and decrease to 10% in Units 2–4. *P*-wave velocities of discrete samples are 3000–4000 m/s in Unit 1 and increase to 5500 m/s in Units 2–4.

Paleomagnetism

The remanent magnetization of archive-half sediment sections from sediment Cores 352-U1441A-3R to 9R was measured with the cryogenic magnetometer. The magnetic inclinations of the sediments define normal and reversed polarity zones. The inclinations are steep, typically >60°, which is probably the result of sediment disturbance by rotary coring. However, there are significant gaps in core recovery that hinder interpretation. In addition, the reversal pattern shows a small number of polarity zones, whereas there should be several on the basis of the biostratigraphic ages and the geomagnetic polarity time scale. Thus, we are unable to interpret the polarity record of the sediments in Hole U1441A.

The remanent magnetization was measured on 14 igneous rock samples from Cores 352-U1441A-10R to 22R. These samples have both normal and reversed polarities with two normal polarity zones at the top and bottom of the section bracketing a reversed polarity zone. The magnetic inclinations are close to that of the current field,

implying that these rocks may have been remagnetized in the near geologic past. Most of the samples are from igneous Unit 1, which is thought to consist of talus, so the coherent inclinations are surprising. Therefore, remagnetization could explain the coherency of the jumbled pile of rocks.

Site U1442 summary

Operations

The *JOIDES Resolution* completed the 5.5 nmi transit from Site U1441 in dynamic positioning mode while the drill string was being raised from the seafloor. The vessel arrived at Site U1442 (proposed Site BON-5A) at 1630 h on 14 September 2014, and a seafloor positioning beacon was deployed. The vessel then offset 500 m at an azimuth of 81°.

A RCB BHA was assembled with a C-4 bit and then lowered to the seafloor. Hole U1442A was spudded at 2320 h on 14 September (28°24.5784′N, 142°37.3368′E; 3162 m water depth). The RCB coring system with nonmagnetic core barrels was deployed 57 times (Cores 352-U1442A-1R through 57R), with 529.8 m cored and 100.7 m recovered (19%) (Table **T1**). The basement contact was at ~82 mbsf. A free-fall funnel was deployed on 19 September so that the RCB bit could be changed. The bit change occurred at 46.1 h of coring time. Hole U1442A was terminated when the time available for coring expired. The hole was then logged with the triple combo-MSS tool string (to 371 mbsf on the first pass and 305 mbsf on the second pass) and the FMS-sonic (to 287 mbsf on both passes) tool string. The total time spent in Hole U1442A was 235.75 h. The seafloor positioning beacon was recovered at 0940 h on 24 September. After the thrusters were raised at 1030 h on 24 September, the vessel started the transit to Keelung, Taiwan.

Sedimentology

Pelagic and volcaniclastic sediment was recovered from the seafloor to 83.1 mbsf, beneath which igneous rocks were drilled. The sediment represents part of the late Oligocene to recent deep-sea sedimentary cover of the Izu-Bonin fore arc, which is stratigraphically condensed because of its position on a basement high.

The recovered sedimentary succession is divided into 4 lithologically distinct units (Figure **F17**). Lithologic Unit III is divided into 2 subunits. The main criterion for the recognition of the lithologic units and subunits is a combination of primary lithology,

grain size, color, and diagenesis. Within the overall succession, 21 ash or tuff layers were observed.

- Unit I (0–2.59 mbsf) is mostly silty to sandy nannofossil mud and nannofossil ooze, with additional dark gray "blotches" rich in volcanic glass that probably represent the remains of thin ash-rich layers.
- Unit II (2.59–33.00 mbsf) is dominantly silty nannofossil ooze with slight color banding (off-white to pale brown), reflecting the presence of muddy and silty/sandy layers. The silty and sandy material is volcaniclastic in origin and is accompanied by several thin, discrete, ash layers, which are dispersed over tens of centimeter–thick intervals within the background sediment.
- Unit III (33.00–62.40 mbsf) is divided into 2 subunits. Subunit IIIA (33.0–52.60 mbsf) is recognized by the presence of brownish mud and nannofossil-rich mud. Subunit IIIB (52.60–62.40 mbsf) is relatively pure clay with some manganese-stained horizons and also nannofossil ooze intervals.
- Unit IV (62.40–83.12 mbsf) is distinguished by nannofossil-rich sediment, which becomes more lithified downward, and transition to nannofossil chalk. This sediment contains variable amounts of clay, volcaniclastic silt/siltstone, and volcaniclastic fine sand/sandstone. The most clastic-rich sediment can be classified as nannofossil-bearing fine sand/sandstone. The sedimentary succession is terminated downwards by a thin manganese layer, followed by a profound change to brownish red, noncalcareous volcanogenic sandy and silty clay, interspersed with clasts of mafic extrusive igneous rocks.

Biostratigraphy

Calcareous nannofossils were examined in core catcher Samples 352-U1442A-1R-CC to 9R-CC. An additional sample was taken from Section 10R-2, 22–23 cm, just above the layer containing igneous rocks. Preservation was "moderate" to "good" in each sample. A fairly continuous condensed section was recovered comprising sediments from the Eocene/Oligocene boundary up to as recent as the Late Pleistocene.

Fluid geochemistry

Ten samples were collected from sediment in Hole U1442A for headspace hydrocarbon gas analysis as part of the standard shipboard safety monitoring procedure. Only minor methane was detected (1.08–1.29 ppmv), and the relatively low and uniform methane concentrations imply negligible concentrations of organic matter. No ethane or propane was detected.

Petrology

Igneous rocks were recovered in Hole U1442A, which penetrated more than 440 m of igneous basement (Figure **F18**). The top of the igneous basement is defined by a Mn-rich sediment layer. The uppermost part of the section comprises breccia that may represent seafloor colluvium. This is underlain by boninitic lavas and hyaloclastites. Hole U1442A contains multiple zones of faulting.

Coring in Hole U1442A recovered igneous units similar to those in Hole U1439C, which lies ~1.3 km away. Nevertheless, there are notable differences between the two holes. Hole U1442A recovered low- and high-silica boninites together with evolved low-silica boninites. However, no dikes and no units dominated by basaltic boninites were encountered. Given the proximity of the 2 sites and the wealth of pXRF data, we correlated like units between the sites (see **"Preliminary scientific assessment"**). However, faults were encountered in Holes U1439C and U1442A, most indicating normal slip and some with evidence for reverse and oblique strike-slip motion. These faults raise the possibility that their stratigraphic records were disturbed and that the 2 sites were originally further apart. However, with the exception of the igneous Unit 1/2 boundary discussed below, units continued across fault surfaces at both holes suggesting that the stratigraphic record disturbance was minimal. We have no evidence for significant strike-slip motion between the sites, but such motion cannot be ruled out based on present knowledge.

Unit 1 (83–250 mbsf) consists mostly of hyaloclastites and lava flows of high-Si boninitic affinity. Unit 1 in Hole U1439C compositionally correlates with this unit but contains significantly less hyaloclastite. The most distinctive chemical feature of the upper section of Hole U1442A is the variable Cr content, which reaches values in excess of 1000 ppm. Below a fault zone at 240–270 mbsf, which separates Subunit 1e from Subunit 2a, Cr contents drop significantly and, with a few exceptions, remain below 500 ppm. Units 2–4 contain textural and compositional evidence of magma mingling, in which evolved boninite magma was intruded by less-evolved boninite magma. The subtle petrographic and chemical differences seen below Unit 1 were used to define subunits.

Finally, a striking feature of Hole U1442A is its excellent preservation in comparison to Site U1439, which is located only ~1.3 km away. Fresh glass is pervasive throughout the entire igneous interval in Hole U1442A, making it an invaluable resource for post-cruise research requiring fresh material.

Rock geochemistry

Seven sediment samples were analyzed from Hole U1442A (1 per core from Cores 352-U1442A-1R through 4R, 7R, 8R, and 10R) for carbonate contents. Carbonate contents range from 50 to 78 wt%, except for 1 sample (interval 7R-5, 49–50 cm) with ~0.6 wt% carbonate.

We selected 21 representative igneous rock samples from Sections 352-U1442A-11R-1 through 43R-1 to be analyzed for major and trace element concentrations by ICP-AES. In addition, H_2O and CO_2 concentrations were determined for any samples with LOI >2%. The rock surfaces of 167 archive-half pieces were analyzed by pXRF for chemostratigraphic purposes.

The igneous rocks analyzed from Hole U1442A are primarily boninites and their differentiates. The samples have SiO_2 contents of 52.5–63.4 wt%, total alkali (Na_2O + K_2O) contents of 1.44–4.74 wt%, and MgO contents of 2.6–17.0 wt%. Primitive magmas from Sites U1439 and U1442 have wide-ranging major and trace element compositions allowing basaltic boninite, low-Si boninite, and high-Si boninite series with different genetic histories to be distinguished. We were able to track the differentiates for each series based on mineral abundances and variations in the concentrations of SiO_2, MgO, and TiO_2 (see **"Preliminary scientific assessment"**). Site U1442 extends to less high-alkali abundances compared to Site U1439, reflecting the greater degree of alteration in the latter.

Structural geology

Bedding planes are subhorizontal in the sedimentary units above 75 mbsf, with dips generally <10°. Between 75 and 155 mbsf, the bedding planes dip ~35° on average. This change in dip angle defines an angular discordance at ~27–32 Ma based on biostratigraphic ages. In the igneous units, magmatic structures include contacts between distinct rock types, laminations, flow banding structures, alignments of elongated vesicles, and magmatic breccias. In general, magmatic minerals exhibit relatively weak to moderate alignment. Tectonic structures in the basement include shear fractures, cataclastic shear bands, cataclastic shear zones, veins, slickensides, and breccias. Three main fault zones occur at 238.2–267.5, 432.8–444.8, and 490.9–502.2 mbsf. The uppermost fault zone comprises fault gouge rich in talc and zeolites, including phillipsite. Slickensides dominantly indicate reverse dip-slip motion, although normal and oblique sense of shear is also observed.

Physical properties

In the sediments, *P*-wave velocity, magnetic susceptibility, and GRA density values increase across the boundary between lithologic Subunit IIIB and Unit IV at 62 mbsf. This depth corresponds to a strong reflector in the seismic profile across the site. NGR values decrease from the seafloor to the base of Unit IV, with the exception of higher values in Subunit IIIB (clay layer).

In the igneous basement, magnetic susceptibility values are low in igneous Unit 1 (boninite hyaloclastite) and increase abruptly at 260 mbsf near the top of Unit 2 (evolved boninite lavas). NGR values decrease gradually from the top of Unit 1 (83 mbsf) to the base of Unit 4 (523 mbsf). *P*-wave velocities are high and porosities are low in discrete samples taken from 83–170 and 305–480 mbsf. Thermal conductivity values are relatively constant in Unit 1 and Subunit 2A, increase in Subunit 2B, and decrease in Units 3 and 4.

Paleomagnetism

Sediment Cores 352-U1442A-2R through 9R were measured with the pass-through cryogenic magnetometer. However a discontinuous record, poor recovery, and drilling-related deformation makes it impossible to interpret the magnetic stratigraphy reliably.

Paleomagnetic samples from the igneous units give paleoinclinations mostly near zero. Low negative inclinations predominate in the upper part of Hole U1442A above 400 mbsf, whereas low positive inclinations are seen below 440 mbsf. These shallow inclinations are consistent with the low paleolatitude of the Izu-Bonin arc at the time of its formation. Transitions between positive and negative inclinations above 400 mbsf are most likely the result of secular variation at low latitudes. The shift to positive inclinations in the lower part of the hole may indicate a magnetic reversal or simply eruption of igneous Units 3 and 4 in a short interval, during which there was little secular variation. Interestingly, the Hole U1439C igneous section shows mainly low positive magnetic inclinations, whereas that of Hole U1442A mostly shows low negative inclinations. This difference may represent a change in magnetic polarity.

Downhole logging

Hole U1442A was logged with the triple combo-MSS and FMS-sonic tool strings. The borehole diameter was within the limits needed for the tools to function properly but the borehole conditions deteriorated during the first tool string deployment, with the hole filling in ~84 m by the time the second tool string was deployed. Weather

conditions and sea state were excellent, with peak-to-peak heave <1 m. NGR, bulk density, resistivity, magnetic susceptibility, sonic velocity measurements, and microresistivity images were acquired.

Overall, increases in density, resistivity, *P*-wave velocity, and magnetic susceptibility values are observed with depth, whereas NGR values decrease. Eight logging units are defined on the basis of distinguishing features and trends in the various logs. Logging Unit 1 (~95–120 mbsf) is characterized by decreasing NGR and velocity values, coupled with increasing resistivity and magnetic susceptibility values downhole. Unit 2 (~120–188 mbsf) is differentiated from the overlying unit by elevated NGR and resistivity values and consistently low magnetic susceptibility values. There is increased borehole rugosity in Unit 3 (~188–204 mbsf), which may account for the significant variability across the logging data sets, distinguishing it from the units above and below. Unit 4 (~204–232 mbsf) has lower variability in the NGR and density logs and magnetic susceptibility values decrease with depth. Low magnetic susceptibility values, punctuated by 3 significant peaks, is the defining feature of Unit 5 (~232–258 mbsf) in combination with high variability in NGR values. Unit 6 (~258–282 mbsf) is characterized by decreasing downward trends in both resistivity and density values, which is counter to the overall trend in Hole U1442A. The character of the NGR, density, and resistivity logs is markedly different in Unit 7 (~282–326 mbsf) compared to the overlying unit. Finally, Unit 8 (>326 mbsf) does not have full data coverage but is differentiated from Unit 7 by a relatively constant NGR profile and a less variable resistivity profile. Oriented microresistivity borehole images indicate a range of textures and structural features, including veins, fractures, and vesicles.

The downhole logging data share similarities with the corresponding core physical properties and geochemical data. However, the logging unit boundaries that are defined on the basis of petrophysical properties do not correlate directly with the petrological boundaries. Postcruise core-log interpretation will focus on fully integrating the downhole and core data sets.

Preliminary scientific assessment

Expedition 352 successfully cored ~1.22 km of igneous basement created immediately following subduction initiation in the Bonin fore arc, together with 461 m of overlying sediment (Table T2). The original plan was to drill 2 sites to 750 m each. Drilling conditions limited depths of penetration at both sites and, if the original planned

casing strategy had been used, little time would have been left for additional drilling at alternative sites. The decision to drill in the casing at both original sites saved ~10 days, which provided the time for drilling 2 additional sites (U1441 and U1442). This marks only the second time a casing string was drilled in since ODP Leg 196, and the first time a complete reentry system was deployed this way.

The basement core provides diverse, stratigraphically controlled suites of lavas and shallow intrusive equivalents of our target rock types: FAB and boninite related to seafloor spreading and earliest arc development. FAB were recovered at the two deeper sites (U1440 and U1441) and boninites at the two shallower sites (U1439 and U1442). Although recovery averaged ~21% for the igneous sections drilled (see **"Principal results"** for details), this recovery was sufficient to provide an excellent suite of samples for documenting the petrology, geochemistry, volcanology, and structure of the four basement sites. Onboard observations and data collection have already produced a significantly clearer understanding of both the development of the crustal architecture of the Bonin fore arc and the variations in sources and melting mechanisms through time for this region. The sediment core provides a record of the depth-time evolution of the fore-arc basement following subduction initiation and, through study of the interspersed ash layers, contributes to our understanding of the overall volcanic evolution of the region.

The overarching goal of Expedition 352 was to characterize the volcanic products of subduction initiation and early arc development and to use the results to understand better the subduction initiation process and its relevance to on-land geology. The objectives related to this goal and stated in the *Scientific Prospectus* for this expedition are listed below, accompanied by our assessment about how these objectives were addressed and the resulting discoveries. We conclude with a statement listing discoveries that went beyond those directly addressing the original objectives.

1. *Obtain a high-fidelity record of magmatic evolution during subduction initiation by coring volcanic rocks down to underlying intrusive rocks, including radiometric and biostratigraphic ages.*

One major achievement of Expedition 352 was the recovery of 4 lava sequences that provide evidence for the temporal evolution of volcanic activity during the nascent development of the IBM volcanic arc. These sequences cluster into 2 groups (Figure **F19**). The first group (Sites U1440 and U1441) addressed the chemostratigraphy and petrological evolution of FAB, and the second group (Sites U1439 and U1442) did the same for boninite-series igneous rocks. Defining the petrological/geochemical units and formulating ideas about sources and melting processes needed to generate these

lavas onboard the ship was made possible by the analysis of cut rock surfaces using a Thermal Niton pXRF instrument. Expedition 352 is the first instance in which pXRF measurements have been successfully used to distinguish rock units chemically while core is being described. These real-time data also proved useful in targeting intervals for shipboard ICP-AES analyses on cores as they were recovered. The collaboration between the shipboard geochemists and petrologists emphasizes the importance of close coordination between different areas of expertise during core description and analysis, here resulting in the establishment of a new tool for use during basement coring. The targeted ICP-AES data collected onboard allowed us to generally classify the rocks based on major element data and provided important additional trace elements.

The formal naming of the volcanic rocks was carried out using modified IUGS protocols based on the three major element oxides, TiO_2, SiO_2, and MgO. This allowed us to identify parental boninites based on the IUGS criteria (Le Bas et al., 2000) of <0.5 wt% TiO_2, >52 wt% SiO_2, and >8 wt% MgO (Figure **F20**). Criteria based on those in Pearce and Robinson (2010) were used to extend the classification of parental magmas to boninite series. As Figure **F20** shows and as is documented in the individual site chapters, these 2 diagrams provide the basis for the conclusion that the deeper sites (U1440 and U1441) predominantly recovered tholeiitic (FAB) lavas and dikes whereas the shallower sites (U1439 and U1442) predominantly recovered boninitic lavas and dikes.

In addition, lava compositions varied enough in the boninites to compel division into three series. We defined a basaltic boninite series to include lower SiO_2 concentrations for parental magmas than those allowed by the IUGS classification. The boninite field on the MgO versus SiO_2 diagram itself was divided into low-Si and high-Si boninite series following the concept of Kanayama et al. (2013). This subclassification reveals some important variations. Most importantly, relatively primitive high-Si boninites form the upper units of both boninite holes. Another significant finding is the abundance of evolved members of the boninite series (high-Mg andesites) in igneous Unit 2 of Hole U1442A and at the base of the lava sequence in Hole U1439C. Only one series was made for the FAB rocks based on their uniformly basaltic parent magma compositions. Nevertheless, FAB lavas have ranges in TiO_2 concentrations that require significant variations in parental magma compositions. For example, several rocks plot as basalt in the MgO versus SiO_2 diagram but on the boninite/basalt boundary of the TiO_2 versus SiO_2 diagram. We termed these lavas D-FAB (D for

depleted), to our knowledge the first lavas of this composition to be recovered from in situ oceanic crust.

Note that only ICP-AES data can be classified in this way because SiO_2 and MgO could not be analyzed by pXRF. Moreover, SiO_2 is significantly dependent on alteration. As a result we developed proxy diagrams (Ti versus Cr and Ti/Zr versus Cr) that can informally classify the whole core even for relatively highly altered samples or for those not chosen for ICP-AES analysis. The classifications confirm those made by Figure **F20** and have enabled each unit from each core to be classified in terms of magma type, as shown in the stratigraphic summary of Figure **F19.**

FAB Sites U1440 and U1441

The chemical compositions and mineral abundances of the lavas and dikes cored at Sites U1440 and U1441 are similar to each other as well as to those for FAB documented during nearby dives (see Ishizuka et al., 2011), as well as for FAB from the Mariana fore arc (Reagan et al., 2010). Lavas from Hole U1440B are underlain by a transition zone and then 40 m of what appears to be a sheeted dike complex, which we take to indicate that we drilled the entire extant FAB lava sequence. In contrast Hole U1441A had significantly less penetration, was capped by a talus deposit, and did not intersect intrusive rocks. Therefore, Hole U1440B has the best reference section for illustrating the chemostratigraphy of the FAB sites.

FAB lavas and dikes from Sites U1440 and U1441 are seen in Figure **F20** to be tholeiitic rather than boninitic, and the total alkali-silica (TAS) plot of LaBas et al. (1986) shows them to be predominantly basalts. Exceptions are a few basaltic andesites with 52–53 wt% silica, and the highly differentiated andesite that makes up igneous Unit 6 at Site U1440 (see **"Site U1440 summary"**). With the exception of the Unit 6 andesites, FAB from our sites and other IBM fore-arc locations are characterized by low Ti/Zr ratios and low abundances of both elements relative to MORB (Figure **F21**), demonstrating that they are generated by higher degrees of melting or from a more depleted mantle than for lavas from mid-ocean ridges.

The concentrations of trace elements and CaO in FAB lavas are relatively diverse because of variations both in parental melt compositions and in degree of differentiation. Below the heterolithic breccia making up Unit 1 at Site U1441 and especially beneath Unit 4 in Hole U1440B, Cr and Mg concentrations generally increase with depth (Figures **F22, F23**), indicating an increase in the degree of differentiation

upward. Nevertheless, these trends have significant overall fine-scale diversity and are punctuated by narrow sections of core with significantly more, or less, differentiated lavas. The andesites from Site U1440 Unit 6 mentioned above represent one such significant compositional excursion. These lavas have the lowest Ti/Zr and Sr/Zr values (Figure **F21**) of any of the FAB-related lavas. We attribute this to extensive plagioclase and titanomagnetite fractionation, perhaps in a small, isolated, and shallow magma reservoir. Other compositional excursions are represented by the high-Cr, and hence less fractionated, lavas in the two cores that make up Unit 3 in Hole U1440B and the D-FAB from Hole U1441A.

Superimposed on these magma chamber effects are variations in incompatible trace element ratios that represent variations in source compositions. Two units from Hole U1440B (Units 4 and 8) and some basal dolerite dikes have Sr/Zr ratios similar to those of average N-MORB (~1.25), indicative of mantle sources with little or no subducted material. Other units have relatively elevated Sr/Zr, but most are still within the range of MORB glasses taken from the laser-ablation inductively coupled plasma–mass spectrometry data set of Jenner and O'Neill (2012) (Figure **F21**), suggesting that any subduction influence was small, at least in terms of Sr input, throughout the genesis of most lavas from this site. A small set of samples do, however, plot clearly above the field of MORB glasses. This includes the aforementioned D-FAB samples from Hole U1441A, where the ultradepleted source may have made the subduction component more evident. Sr is, of course, mobile during alteration. Nevertheless, the consistency of Sr/Zr within most units likely reflects interbedding of lavas derived from mantle sources with different subduction inputs. The D-FAB unit, as noted above, has exceedingly low incompatible trace element abundances, the highest Ti/Zr (Figure **F21**), and the highest CaO concentrations of any uncalcified lava collected during the expedition. This lava was generated by the highest degree of melting, or from the most depleted source, of all FAB, and we tentatively interpret its high Ti/Zr and high CaO to reflect melting of its mantle source to near the point of clinopyroxene exhaustion.

Boninite Sites U1439 and U1442

The compositions of boninite group lavas drilled at Sites U1439 and U1442 are chemically distinct from FAB. In contrast to FAB Sites U1440 and U1441, lavas in both of the boninite sites have compositions that become more primitive upward. Irrespective of degree of differentiation, TiO_2 concentrations generally decrease and SiO_2 concentrations generally increase upward in lavas from both boninite sites. Based on these compositional variations, the lowermost lavas classified as basaltic boninites

and low-Si boninites, and the capping lavas as high-Si boninites resembling those that form the base of the lava sequence at Chichijima. Nevertheless, differences in the thicknesses of chemostratigraphic units are surprisingly great considering that the sites were only ~1.3 km apart (Figure **F24**).

Our best correlation between the stratigraphic records at the two sites places differentiated basaltic boninite to low-Si boninite series lavas at the base of both sites. The uniformly low Cr and MgO concentrations in these lavas suggest they represent magmas that fractionated in a magma chamber that persisted during the eruption of this unit. The thickness of this basal sequence appears to change from ~20 to ~200 m from Site U1439 east to Site U1442. Overlying the basal sequence at both sites are lavas of the low-Si boninite series that change in thickness from ~230 m at Site U1439 to 80 m at Site U1442. These lavas have higher and more variable Ti/Zr ratios than the underlying lavas (Figure **F21**), indicating that they were tapped from variably depleted mantle by variably high degrees of melting.

Mingling between magmas with high and low Cr concentrations is common in this unit. This demonstrates that some magmas ponded for long enough in the crust to undergo significant crystal fractionation and erupt, whereas others rose to the surface essentially unfractionated, and that these 2 magmas commonly mingled and erupted before significant mixing could occur. Unit 5 in Hole U1439C represents a compositional excursion to basaltic boninite-series lavas. These lavas differ from equivalent series lavas from deeper in this hole in that they have relatively high Cr concentrations in keeping with the more primitive compositions of lavas from adjacent depths in this hole. The high-Si boninites atop both holes have similar compositions. Although a few significantly differentiated lavas are present in these upper boninites, most are relatively primitive with Cr concentrations of 200–1600 ppm and MgO of 9–17 wt%. The extreme depletion of the mantle sources and degrees of melting for these lavas is reflected in the low TiO_2 concentrations, which are typically <0.3 wt%, and in low Ti/Zr ratios, which are <60.

Although coring in Hole U1442A ended in boninite-group lavas, Hole U1439C drilled ~50 m into a sequence of dolerites, with compositions spanning the range of Ti/Zr ratios of overlying lavas but with overall lower Cr concentrations. Our inference is that genetically related dikes underlie the boninitic-group lavas. We found no evidence for the presence of FAB resembling those drilled at Sites U1440 and U1441 beneath the boninite-group lavas.

DSDP Sites 458 and 459

Selected archive cores from Site 458 were onboard the *JOIDES Resolution* for training purposes during Expedition 352. We used this opportunity to analyze these cores using the pXRF instrument so that their compositions could be directly compared with those from our drill sites. The results show that the rocks from DSDP Site 458 are generally more differentiated than those drilled at Sites U1439 and U1442, with Cr concentrations ranging from 275 ppm to below detection limits. Site 458 Cores 28, 39, and 43 have TiO_2 and Zr concentrations resembling those of the low-Si boninites from the lower to middle sections of Holes U1439C and U1442A, whereas Core 47 has compositions similar to the andesite from Hole U1440A (Figure **F21**). The original geochemical data for DSDP sites (Wood et al., 1982; Meijer et al., 1981) demonstrate that Cores 43–45 from Site 458 and Cores 60–64 from Site 459 have compositions that are intermediate between those of our FAB and boninite sites. Our Cr and MgO concentrations and those published in Wood et al. (1982) indicate that the Site 458 and 459 lavas are typically highly fractionated. This further supports the existence of a magma chamber during the eruption of these transitional lavas.

2. *Use the results of Objective 1 to test the hypothesis that fore-arc basalt lies beneath boninites and to understand chemical gradients within these units and across their transitions.*

We expected FAB to be present at the base of the Bonin fore-arc volcanic succession and a sequence of boninite-series lavas to be present atop these FAB. Our pre-expedition drilling strategy, in fact, was to drill a single section from boninite through to FAB dikes. We did not, however, encounter this stratigraphy at any of the drill sites. Instead, the presence of dikes at the base of the sections at Sites U1439 and U1440 provides evidence that these lavas are underlain by their own conduit systems and that FAB and boninite group lavas are likely offset more horizontally than vertically.

The separation of compositions for the FAB and boninite sites is best seen on the plot of Zr versus TiO_2 concentrations (Figure **F21**). On this plot, the trenchward FAB sites (U1440 and U1441) have high Ti/Zr ratios that completely separate them from the low Ti/Zr ratios, and low absolute values of Ti and Zr, of the boninite sites (U1439 and U1442). This gap appears to be filled by the compositions of lavas from Sites 458 and 459, providing some evidence that we drilled the 2 end-members of a FAB–boninite spectrum, but there is a continuity of compositions within which transitional members do exist. The implication is that FAB erupted closer to the trench than boninite,

and we speculate that lavas of transitional compositions may have erupted at an intermediate distance from the trench.

3. *Use drilling results to understand how mantle melting processes evolve during and after subduction initiation.*

The results summarized in the assessment of Objective 2 are best explained by temporal evolution, not just of the mantle melting process itself, but also of location of that melting and of the nature of the plumbing system taking the melts from the mantle to the surface. Although the compositions of FAB lavas erupted at Sites U1440 and U1441 vary through time in terms of the amount of slab fluid involved in their genesis and their extent of differentiation, all are relatively evolved, with most Mg concentrations lying within the range 5–8 wt%. These lavas could have been fed from magma chambers that persisted throughout the eruptive history of FAB.

In the boninitic section, the lowermost lavas at Sites U1439 and U1442 also are relatively differentiated, with a thickness that increases to the east (i.e., from Site U1439 to U1442). Stratigraphically higher lavas at both sites are both differentiated and primitive in composition, with mingling common between the two. Primitive high-Si lavas derived from the most depleted mantle cap the stratigraphy at both sites. The changes in composition support a model in which a persistent magma chamber system was present early during genesis of boninite group lavas, especially at eastern Site U1442. This persistent chamber system disappeared by the time high-Si boninites erupted at both sites. If the lower boninites formed at a ridge axis, these high-Si boninites could represent off-axis magmatism, perhaps the start of a proto-arc.

Overall, the evidence supports the presence of at least a small subduction contribution to the genesis of FAB lavas and dikes. As noted above, the Sr/Zr ratio is equivocal for all but a small set of FAB lavas, including the most depleted where the subduction component is most visible. However, the drilled FAB (Figure **F21**), as well as those previously sampled from the IBM region (Figure **F4**), plot in the island arc field on a V-Ti plot, likely reflecting water-enhanced melting resulting in higher oxygen fugacity and a greater degree of melting (or melting of more depleted sources) than is normally prevalent at mid-ocean ridges (Shervais, 1982).

Boninites all were generated after the addition of a more significant flux of water-rich fluid, and perhaps a melt, from the subducting slab. The degree of depletion of TiO_2 (Figure **F21**), as well as CaO, increases upsection, implying that the overall depletion of the mantle continues from the FAB group through into the boninite group lavas.

These results indicate that seafloor spreading related to subduction initiation and eruption of FAB, having begun at ~52 Ma (Ishizuka et al., 2011; Reagan et al., 2013), also migrated from east to west. We believe, on the basis of the consistently evolved lower lavas and dikes, that spreading was rapid and, like fast-spreading centers (e.g., the East Pacific Rise; Langmuir et al., 1986), an axial magma chamber was present. Melting was largely decompressional during this period, but subducted fluids significantly affected at least some of the melting. Relatively fast spreading continued migrating to the west of the subduction zone through the eruption of the differentiated basaltic boninites. One plausible hypothesis is that the spreading rate had by that time declined such that a persistent magma chamber could no longer be maintained, allowing progressively more primitive lavas to erupt (cf. slow-spreading ocean ridges, Dick et al., 1989; Langmuir et al., 1992). The high-Si boninite at the top of the lava sequence might then represent the final magmatic phase of such a ridge when most erupting lavas were primitive. Alternatively, the high-Si boninites could represent off-axis eruptions resulting from continued melting of depleted mantle trenchward of the westward migrating ridge axis.

The initial extreme depletion of the sources for all boninite group lavas was likely related to FAB generation. This depletion resulted in melting of harzburgite by the time the high-Si boninites were generated. Melting of such mantle to the point of clinopyroxene exhaustion resulted from a strong influx of a subduction component from the subducting plate.

4. *Test the hypothesis that the fore-arc lithosphere created during subduction initiation is the birthplace of supra-subduction zone ophiolites.*

By recovering the first sections of in situ subduction initiation oceanic crust, Expedition 352 successfully demonstrated that fore-arc lithosphere created during subduction initiation could be a potential birthplace of suprasubduction zone ophiolites. This was another major achievement of this expedition.

Specifically, Expedition 352 drilled the end-members of the suprasubduction zone ophiolitic spectrum: oceanic lithosphere created from FAB magma (Sites U1440 and U1441) and oceanic lithosphere created from boninite magma (Sites U1439 and U1442). Although we do not have the complete crustal sections, the fact that two sites rooted in dikes following penetration of oceanic volcanic rocks is consistent with such an interpretation. Moreover the recovery of gabbros and peridotites by dredging and submersible from the deeper parts of the fore arc supports the likelihood that at least the deeper section has an ophiolitic structure.

The relative ages of the 2 sets of sites is critical for any interpretation and will be an important part of the follow-up work. Although they have not yet been dated, comparable rocks recovered from the fore arc prior to the expedition leads us to expect that the age of the FAB section lies between 51 and 52 Ma (Ishizuka et al., 2011; Reagan et al., 2013), whereas the age of the boninite section is somewhat younger (low-Si boninite from Site 458 is ~49 Ma, the oldest high-Si boninite from Chichijima is 48 Ma; Cosca et al., 1998; Ishizuka et al., 2006).

There are ophiolites that have full lava sequences based on only one magma type and, for these, the Expedition 352 sites could provide good analog sections. Some well-preserved examples of ophiolitic upper crust derived entirely from FAB magma include the Western Mirdita complex (Dilek et al., 2008) and the Coto Block of the Zambales ophiolite (Yumul, 1996), which only have FAB lavas (using FAB in the broadest sense of any tholeiitic basalt formed by spreading and located in a fore-arc setting). Examples of ophiolitic crust derived entirely from boninitic magma include Betts Cove in Newfoundland (Bédard et al., 1998) and the Acoje Block of the Zambales ophiolite (Yumul, 1996). In their study of Betts Cove, Bédard et al. (1998) inferred that this entirely boninitic ophiolite formed in a fore-arc setting, a conclusion supported by the core from Sites U1439 and U1442.

However, we are aware that the sequence of events in which fore-arc basalts are overlain by boninites is also common in many ophiolites. Well-documented examples include the Troodos, Oman, Eastern Mirdita, and the Pindos/Vourinos ophiolites (see review by Dilek and Flower, 2003). Here, volcanic rocks of FAB compositions (again, in broad sense) are overlain by lavas, or intruded by dikes, of boninitic composition. Compositionally composite sequences such as these are not comparable with our drilled sections, although the magmatic sequence of FAB followed by boninite in these ophiolites is consistent with our inference that FAB magmas predated boninite magmas in the Bonin fore arc. It is possible, indeed likely, that such composite lithosphere is located between our 2 sets of sites, where there was insufficient sediment for us to drill. However, we are fortunate that deep-sea drilling in the Mariana fore arc (at Sites 458 and 459, our alternate site) did recover lavas of both boninite and FAB composition, as well as lavas transitional between the two, within the same drilled section.

Thus, between our Bonin fore-arc drill sections and those of DSDP in the Mariana fore arc, we usefully cover much of the compositional spectrum of the world's SSZ ophiolites. We note that the IBM fore arc may not be an exact analog for all SSZ ophiolites.

Nevertheless, the general concept of increasing mantle depletion and subduction flux in a highly extensional subduction initiation setting could be a viable general model for their evolution.

Additional results

Sedimentology and biostratigraphy

Eocene to recent deep-sea sediment was recovered from above the Izu-Bonin fore-arc basalts and boninites (the upper part of a putative SSZ ophiolite complex). The sedimentary record provides an excellent reference for modern and ancient sedimentation in an intermediate-latitude, intraoceanic fore-arc setting. Three of the drill sites (Sites U1439–U1441) are located in fault-controlled sediment ponds up to several hundred meters thick, whereas one site (U1442) was positioned on thin sediment overlying a fault-controlled basement high (Figure **F25**).

The overall sediment sequence reflects the interplay of 5 main types of control:

1. Local basement erosion and redeposition (e.g., altered extrusive igneous rocks),
2. Regionally controlled volcanism (arc or back arc),
3. Paleoceanography (e.g., calcite compensation depth and currents),
4. Eolian input (widely dispersed ash and/or Asia-derived continental dust), and
5. Diagenesis (e.g., carbonate, zeolite, and manganese).

The basal sediment, typically overlying a manganese crust (Eocene–Oligocene), is pelagic carbonate mixed with detritus that was eroded from underlying, variably altered igneous crust. Above the basement, pelagic carbonate predominates in the Oligocene to earliest Miocene and also in the late Pliocene to Pleistocene. In contrast, relatively noncalcareous, radiolarian-rich silty clays dominated during the early Miocene. In addition, volcaniclastic sediment is relatively abundant during the early Oligocene to Eocene and also in the middle Miocene to lower Pliocene.

Three phases of highly explosive volcanism (latest Pliocene to Pleistocene, late Miocene to earliest Pliocene, and Oligocene) are represented by 132 graded air fall tephra layers, which are likely to be correlative between the 4 drill sites (Figure **F26**). Felsic ash layers (tephra) appear to be relatively abundant at Sites U1439 and U1440 (larger sediment ponds) compared to more mafic ash layers at Sites U1441 and U1442 (smaller basins).

The switch to mixed clastic and siliceous ooze sedimentation (with well-preserved radiolarian and siliceous sponge spicules) during the Miocene reflects a relative rise in the CCD, which could have been either tectonically or paleoceanographically controlled. The carbonate-poor interval is more extensive in the deeper water sites (U1440 and U1441) compared to the shallower sites (U1439 and U1442).

At Sites U1440 and U1441, sediment was affected, to different extents, by local gravity redeposition and current reworking, which was probably tectonically triggered. Pumice-rich volcaniclastic sediment was reworked from the fault-controlled margins of the sediment ponds, especially at Sites U1440 and U1441. There is evidence of tectonic tilting, both prior to and during sediment accumulation (e.g., Site U1439). Postdepositional tilting of Oligocene sediment and associated fracturing was locally exploited by fluid flow and manganese oxide precipitation (Site U1442). Diagenetic effects include carbonate recrystallization, zeolite growth, and upward mobilization of manganese from the igneous crust into the sediment column.

Finally, the probable difference in age between the oldest sediment recovered (Eocene; ~35 Ma), and the igneous basement based on comparisons with comparable well-dated fore-arc basalts and boninites in the region, indicates that a 7–15 My hiatus may exist between cessation of volcanism and covering of the seafloor by pelagic carbonates in different areas. The likely explanation of such a hiatus is that the outer part of the fore arc that encompasses the four drill sites existed as a submerged bathymetric high that remained free of sediment accumulation until the tectonically controlled formation of the sediment ponds that still remain today.

Structures

Postmagmatic extension of the outer IBM fore arc resulted in the formation of asymmetric sedimentary basins such as, for example, the half-grabens at Sites U1439 and U1442. Along their eastern margins, these basins are bounded by westward-dipping normal faults. Sedimentation was mainly syntectonic. The lowermost sequence of the sedimentary units was tilted eastward by ~20°. These tilted bedding planes were subsequently covered by subhorizontally deposited sedimentary beds. Based on biostratigraphic constraints, the minimum age of the oldest sediments is ~35 Ma; the timing of the sedimentary unconformities lies between ~27 and 32 Ma.

At Sites U1440 and U1441, postmagmatic deformation resulted mainly in strike-slip faults possibly bounding the sedimentary basins. The sedimentary units within these

basins were not significantly affected by postsedimentary tectonic tilting. Based on biostratigraphic ages, the minimum age of the basement-cover contact lies between ~29.5 and 32 Ma.

Overall, the postmagmatic tectonic structures observed during Expedition 352 reveal a multiphase tectonic evolution of the outer IBM fore arc. At Sites U1439 and U1442, shear with dominant reverse to oblique reverse displacement was localized along distinct subhorizontal cataclastic shear zones as well as steeply dipping slickensides and shear fractures. These structures, forming within a contractional tectonic regime, were either reactivated as or cross-cut by normal faults as well as strike-slip faults. Extension was also accommodated by steeply dipping to subvertical mineralized veins and extensional fractures. Faults observed at Sites U1440 and U1441 show mainly a strike slip sense of motion.

Physical properties and logging

Basement rock *P*-wave velocities of 2.5–4.0 km/s are observed in the sonic logs in Holes U1439C and U1440B. These velocities are ~1.5 km/s slower than observed logging velocities of normal ocean crust sites such as Holes 504B and 1256D (Becker et al., 1989; Swift et al., 2008). In contrast, porosities of the IBM and ocean crust sites are similar. Postcruise research will investigate these results, and the implications for IBM fore-arc crust and SSZ ophiolites as analogs for oceanic crust.

Outreach

Education and outreach activities reached the public through social media sites using high-quality imagery, video, and sounds and through interactions that were designed to explain the science, drilling mechanics, and all aspects of shipboard life. Our three social media outlets saw a noticeable increase in followers, reaching 5000 “likes” on Facebook. Scientists contributed expedition updates via their own blogs and the **joidesresolution.org** site. News coverage was provided through two Michigan print-media outlets (MEA Today and Midland Daily News), and through articles hosted on National Geographic’s blog site as well as AGU’s Geoscience Blogosphere. Audio interviews helped produce a podcast for a radio outlet, audio for a former outreach officer, and audio for a future magazine piece about the expedition’s findings. Video footage was developed for conference use, Japanese television station NHK, and a video focused on IODP technicians. We conducted 43 live broadcast events (5 of

which were broadcast to multiple locations) that reached 45 geographic locations, including Egypt, Israel, Japan, Sweden, the United Kingdom, and the U.S. (Table **T3**). Ten broadcast sites were colleges or universities, 4 were public venues, 1 was a School of Rock event, and the rest were kindergarten through twelfth grade schools. Over 50% of the live broadcasts were recorded by the host sites to be used for future educational purposes by the host institutions. Curriculum-related activities were developed in conjunction with shore-based educators to cover topics for math, cultural studies, engineering, and geoscience classes. These will be further developed postexpedition. Expedition materials were collected to share with some of the broadcast sites during postexpedition outreach events. Finally, an expedition crossover document was created to streamline the educational activities for future outreach teams.

References

Alabaster, T., Pearce, J.A., and Malpas, J., 1982. The volcanic stratigraphy and petrogenesis of the Oman ophiolite complex. *Contributions to Mineralogy and Petrology,* 81(3):168–183. **http://dx.doi.org/10.1007/BF00371294**

Becker, K., Sakai, H., Adamson, A.C., Alexandrovich, J., Alt, J.C., Anderson, R.N., Bideau, D., Gable, R., Herzig, P.M., Houghton, S., Ishizuka, H., Kawahata, H., Kinoshita, H., Langseth, M.G., Lovell, M.A., Malpas, J., Masuda, H., Merrill, R.B., Morin, R.H., Mottl., M.J., Pariso, J.E., Pezard, P., Phillips, J., Sparks, J., and Uhlig, S., 1989. Drilling deep into young oceanic crust, Hole 504B, Costa Rica Rift. *Reviews of Geophysics,* 27(1):79–102. **http://dx.doi.org/10.1029/RG027i001p00079**

Bédard, J.H., Lauzière, K., Tremblay, A., and Sangster, A., 1998. Evidence for forearc seafloor-spreading from the Betts Cove ophiolite, Newfoundland: oceanic crust of boninitic affinity. *Tectonophysics*, 284(3–4):233–245.**http://dx.doi.org/10.1016/S0040-1951(97)00182-0**

Bloomer, S.H., Taylor, B., MacLeod, C.J., Stern, R.J., Fryer, P., Hawkins, J.W., and Johnson, L., 1995. Early arc volcanism and the ophiolite problem: a perspective from drilling in the western Pacific. *In* Taylor, B., and Natland, J. (Eds.), *Active Margins and Marginal Basins of the Western Pacific*. Geophysical Monograph, 88:1–30. **http://dx.doi.org/10.1029/GM088p0001**

Cosca, M.A., Arculus, R.J., Pearce, J.A., and Mitchell, J.G., 1998. $^{40}Ar/^{39}Ar$ and K-Ar geochronological age constraints for the inception and early evolution of the Izu-Bonin-Mariana arc system. *Island Arc,* 7(3):579–595. **http://dx.doi.org/10.1111/j.1440-1738.1998.00211.x**

Crawford, A.J., Falloon, T.J., and Green, D.H., 1989. Classification, petrogenesis and tectonic setting of boninites. *In* Crawford, A.J. (Ed.), *Boninites and Related Rocks:* London (Unwin Hyman), 1–49.

DeBari, S.M., Taylor, B., Spencer, K., and Fujioka, K., 1999. A trapped Philippine Sea plate origin for MORB from the inner slope of the Izu-Bonin Trench. *Earth and Planetary Science Letters,* 174(1–2):183–197. **http://dx.doi.org/10.1016/S0012-821X(99)00252-6**

Dick, H.J.B., 1989. Abyssal peridotites, very slow spreading ridges and ocean ridge magmatism. *In* Saunders, A.D., and Norry, M.J. (Eds.), *Magmatism in the Ocean Basins*. Geological Society Special Publication, 42(1):71–105. **http://dx.doi.org/10.1144/GSL.SP.1989.042.01.06**

Dilek, Y., and Flower, M.F.J., 2003. Arc-trench rollback and forearc accretion, 2. A model template for ophiolites in Albania, Cyprus, and Oman. *In* Dilek, Y., and Robinson, R.T. (Eds.), *Ophiolites in Earth History.* Geological Society Special Publication, 218:43–68. **http://dx.doi.org/10.1144/GSL.SP.2003.218.01.04**

Dilek, Y., Furnes, H., and Shallo, M., 2008. Geochemistry of the Jurassic Mirdita Ophiolite (Albania) and the MORB to SSZ evolution of a marginal basin oceanic crust. *Lithos,* 100(1–4): 174–209. **http://dx.doi.org/10.1016/j.lithos.2007.06.026**

Hall, C.E., Gurnis, M., Sdrolias, M., Lavier, L.L., and Dietmar Müller, R., 2003. Catastrophic initiation of subduction following forced convergence across fracture zones. *Earth and Planetary Science Letters,* 212(1–2):15–30. **http://dx.doi.org/10.1016/S0012-821X(03)00242-5**

Ishikawa, T., Nagaishi, K., and Umino, S., 2002. Boninitic volcanism in the Oman ophiolite: implications for thermal condition during transition from spreading ridge to arc. *Geology,* 30(10):899–902. **http://dx.doi.org/10.1130/0091-7613(2002)030<0899:BVITOO>2.0.CO;2**

Ishizuka, O., Kimura, J.-I., Li, Y.B., Stern, R.J., Reagan, M.K., Taylor, R.N., Ohara, Y., Bloomer, S.H., Ishii, T., Hargrove, U.S., III, and Haraguchi, S., 2006. Early stages in the evolution of Izu-Bonin arc volcanism: new age, chemical, and isotopic constraints. *Earth and Planetary Science Letters,* 250(1–2):385–401. **http://dx.doi.org/10.1016/j.epsl.2006.08.007**

Ishizuka, O., Tani, K., Reagan, M.K., Kanayama, K., Umino, S., Harigane, Y., Sakamoto, I., Miyajima, Y., Yuasa, M., and Dunkley, D.J., 2011. The timescales of subduction initiation and subsequent evolution of an oceanic island arc. *Earth and Planetary Science Letters,* 306(3–4):229–240. **http://dx.doi.org/10.1016/j.epsl.2011.04.006**

Jenner, F.E., and O'Neill, H.St.C., 2012. Analysis of 60 elements in 616 ocean floor basaltic glasses. *Geochemistry, Geophysics, Geosystems,* 13(2):Q02005. **http://dx.doi.org/10.1029/2011GC004009**

Johnson, L.E., and Fryer, P., 1990. The first evidence for MORB-like lavas from the outer Mariana forearc: geochemistry, petrography and tectonic implications. *Earth and Planetary Science Letters,* 100(1–3):304–316. **http://dx.doi.org/10.1016/0012-821X(90)90193-2**

Kamimura, A., Kasahara, J., Shinohara, M., Hino, R., Shiobara, H., Fujie, G., and Kanazawa, T., 2002. Crustal structure study at the Izu-Bonin subduction zone around 31°N: implications of serpentinized materials along the subduction plate boundary. *Physics of the Earth and Planetary Interiors,* 132(1–3):105–129. **http://dx.doi.org/10.1016/S0031-9201(02)00047-X**

Kaneoka, I., Isshiki, N., and Zashu, S., 1970. K-Ar ages of the Izu-Bonin Islands. *Geochemical Journal,* 4(2):53–60. **http://dx.doi.org/10.2343/geochemj.4.53**

Kanayama, K., Kitamura, K., and Umino, S., 2013. New geochemical classification of global boninites. *IAVCEI 2013 Scientific Assembly Abstracts*. (Poster 4W_1B-P13)

Kodaira, S., Noguchi, N., Takahashi, N., Ishizuka, O., and Kaneda, Y., 2010. Evolution from fore-arc oceanic crust to island arc crust: a seismic study along the Izu-Bonin fore arc. *Journal of Geophysical Research: Solid Earth,* 115(B9):B09102. **http://dx.doi.org/10.1029/2009JB006968**

Le Bas, M.J., 2000. IUGS reclassification of the high-Mg and picritic volcanic rocks. *Journal of Petrology,* 41(10):1467–1470. **http://dx.doi.org/10.1093/petrology/41.10.1467**

Le Bas, M.J., Le Maitre, R.W., Streckeisen, A., Zanettin, B., and IUGS Subcommission on the Systematics of Igneous Rocks, 1986. A chemical classification of volcanic rocks based on the total alkali-silica diagram. *Journal of Petrology,* 27(3):745–750. **http://dx.doi.org/10.1093/petrology/27.3.745**

Langmuir, C.H., Bender, J.F., and Batiza, R., 1986. Petrological and tectonic segmentation of the East Pacific Rise, 5°30′N–14°30′N. *Nature,* 322(6078):422–429. **http://dx.doi.org/10.1038/322422a0**

Langmuir, C.H., Klein, E.M., and Plank, T., 1992. Petrological systematics of mid-ocean ridge basalts: constraints on melt generation beneath ocean ridges. *In* Morgan, J., Blackman, D., and Sinton, J. (Eds.), *Mantle Flow and Melt Generation at Mid-Ocean Ridges*. Geophysical Monograph, 71:183–280. **http://dx.doi.org/10.1029/GM071p0183**

Meijer, A., Anthony, E., and Reagan, M., 1982. Petrology of volcanic rocks from the fore-arc sites. *In* Hussong, D.M., and Uyeda, S., *Init. Repts. DSDP,* 60: Washington, DC (U.S. Govt. Printing Office), 709–729. **http://dx.doi.org/10.2973/dsdp.proc.60.138.1982**

Meijer, A., Reagan, M., Ellis, H., Shafiqullah, M., Sutter, J., Damon, P., and Kling, J., 1983. Chronology of volcanic events in the eastern Philippine Sea. *In* Hayes, D.E. (Ed.), *The Tectonic and Geologic Evolution of Southeast Asian Seas and Islands* (Pt. 2). Geophysical Monograph, 27:349–359. **http://dx.doi.org/10.1029/GM027p0349**

Parkinson, I.J., Hawkesworth, C.J., and Cohen, A.S., 1998. Ancient mantle in a modern arc: osmium isotopes in Izu-Bonin-Mariana forearc peridotites. *Science,* 281(5385):2011–2013. **http://dx.doi.org/10.1126/science.281.5385.2011**

Pearce, J.A., Kempton, P.D., Nowell, G.M., and Noble, S.R., 1999. Hf-Nd element and isotope perspective on the nature and provenance of mantle and subduction components in western Pacific arc-basin systems. *Journal of Petrology,* 40(11):1579–1611. **http://dx.doi.org/10.1093/petroj/40.11.1579**

Pearce, J.A., Lippard, S.J., and Roberts, S., 1984. Characteristics and tectonic significance of supra-subduction zone ophiolites. *In* Kokelaar, B.P., and Howells, M.F. (Eds.), *Marginal Basin Geology: Volcanic and Associated Sedimentary and Tectonic Processes in Modern and Ancient Marginal Basins*. Geological Society Special Publication, 16(1):77–94. **http://dx.doi.org/10.1144/GSL.SP.1984.016.01.06**

Pearce, J.A. and Robinson, P.T., 2010. The Troodos ophiolitic complex probably formed in a subduction initiation, slab edge setting. *Gondwana Research,* 18(1):60–81. **http://dx.doi.org/10.1016/j.gr.2009.12.003**

Pearce, J.A., van der Laan, S.R., Arculus, R.J., Murton, B.J., Ishii, T., Peate, D.W., and Parkinson, I.J., 1992. Boninite and harzburgite from Leg 125 (Bonin-Mariana forearc): a case study of magma genesis during the initial stages of subduction. *In* Fryer, P., Pearce, J.A., Stokking, L.B., et al., *Proceedings of the Ocean Drilling Program, Scientific Results,* 125: College Station, TX (Ocean Drilling Program), 623–659. **http://dx.doi.org/10.2973/odp.proc.sr.125.172.1992**

Reagan, M.K., Hanan, B.B., Heizler, M.T., Hartman, B.S., and Hickey-Vargas, R., 2008. Petrogenesis of volcanic rocks from Saipan and Rota, Mariana Islands, and implications for the evolution of nascent island arcs. *Journal of Petrology,* 49(3):441–464. **http://dx.doi.org/10.1093/petrology/egm087**

Reagan, M.K., Ishizuka, O., Stern, R.J., Kelley, K.A., Ohara, Y., Blichert-Toft, J., Bloomer, S.H., Cash, J., Fryer, P., Hanan, B.B., Hickey-Vargas, R., Ishii, T., Kimura, J.-I., Peate, D.W., Rowe, M.C., and Woods, M., 2010. Fore-arc basalts and subduction initiation in the Izu-Bonin-Mariana system. *Geochemistry, Geophysics, Geosystems,* 11(3):Q03X12. **http://dx.doi.org/10.1029/2009GC002871**

Reagan, M.K., McClelland, W.C., Girard, G., Goff, K.R., Peate, D.W., Ohara, Y., and Stern, R.J., 2013. The geology of the southern Mariana fore-arc crust: implications for the scale of Eocene volcanism in the western Pacific. *Earth and Planetary Science Letters,* 380:41–51. **http://dx.doi.org/10.1016/j.epsl.2013.08.013**

Rudnick, R.L., 1995. Making continental crust. *Nature,* 378(6557):571–578. **http://dx.doi.org/10.1038/378571a0**

Shervais, J.W., 1982. Ti–V plots and the petrogenesis of modern and ophiolitic lavas. *Earth and Planetary Science Letters,* 59(1):101–118. **http://dx.doi.org/10.1016/0012-821X(82)90120-0**

Stern, R.J., 2004. Subduction initiation: spontaneous and induced. *Earth and Planetary Science Letters,* 226(3–4):275–292. **http://dx.doi.org/10.1016/j.epsl.2004.08.007**

Stern, R.J., and Bloomer, S.H., 1992. Subduction zone infancy: examples from the Eocene Izu-Bonin-Mariana and Jurassic California arcs. *Geological Society of America Bulletin,* 104(12):1621–1636. **http://dx.doi.org/10.1130/0016-7606(1992)104<1621:SZIEFT>2.3.CO;2**

Stern, R.J., Fouch, M.J., and Klemperer, S.L., 2003. An overview of the Izu-Bonin-Mariana subduction factory. *In* Eiler, J. (Ed.), *Inside the Subduction Factory.* Geophysical Monograph, 138:175–222. **http://dx.doi.org/10.1029/138GM10**

Stern, R.J., Reagan, M., Ishizuka, O., Ohara, Y., and Whattam, S., 2012. To understand subduction initiation, study forearc crust: to understand forearc crust, study ophiolites. *Lithosphere,* 4(6):469–483. **http://dx.doi.org/10.1130/L183.1**

Swift, S., Reichow, M., Tikku, A., Tominaga, M., and Gilbert, L., 2008. Velocity structure of upper ocean crust at Ocean Drilling Program Site 1256. *Geochemistry, Geophysics., Geosystems,* 9(10):Q10O13. **http://dx.doi.org/10.1029/2008GC002188**

Tatsumi, Y., and Stern, R.J., 2006. Manufacturing continental crust in the subduction factory. *Oceanography,* 19(4):104–112.**http://dx.doi.org/10.5670/oceanog.2006.09**

Taylor, R.N., and Nesbitt, R.W., 1994. Arc volcanism in an extensional regime at the initiation of subduction: a geochemical study of Hahajima, Bonin Islands, Japan. *In* Smellie, J.L. (Ed.), *Volcanism Associated with Extension at Consuming Plate Margins.* Geological Society Special Publication, 81:115–134. **http://dx.doi.org/10.1144/GSL.SP.1994.081.01.07**

Wood, D.A., Marsh, N.G., Tarney, J., Joron, J.-L., Fryer, P., and Treuil, M., 1982. Geochemistry of igneous rocks recovered from a transect across the Mariana Trough, arc, fore-arc, and trench, Sites 453 through 461, Deep Sea Drilling Project Leg 60. *In* Hussong, D.M., Uyeda, S., et al., *Initial Reports of the Deep Sea Drilling Project,* Vol. 60: Washington (U.S. Government Printing Office), 611–645. **http://dx.doi.org/10.2973/dsdp.proc.60.133.1982**

Yumul, G.P., 1996. Varying mantle sources of supra-subduction zone ophiolites: REE evidence from the Zambales Ophiolite Complex, Luzon, Philippines. *Tectonophysics*, 262(1–4):243–262. **http://dx.doi.org/10.1016/0040-1951(96)00013-3**

Table T1. Operations summary, Expedition 352.

Hole	Latitude	Longitude	Water depth (m)	Total penetration (m)	Drilled interval (m)	Cored interval (m)	Core recovered (m)	Recovery (%)	Total cores (*N*)	APC cores (*N*)	XCB cores (*N*)	RCB cores (*N*)	Ghost cores (*N*)	Start		End		Time on hole (days)
														Date (2014)	Time UTC (h)	Date (2014)	Time UTC (h)	
U1439A	28°24.4487′N	142°36.5120′E	3128.1	199.4	—	199.4	170.7	86	23	10	13	0	0	5 Aug	1824	8 Aug	0620	2.5
U1439B	28°24.4478′N	142°36.5244′E	3128.2	42.2	42.2	—	—	—	—	—	—	—	—	8 Aug	0620	8 Aug	1135	0.2
U1439C	28°24.4491′N	142°36.5368′E	3129.2	544.3	182.0	362.3	107.8	30	42	0	0	42	3	26 Aug	0310	11 Sep	0205	16.0
		Site U1439 totals:		785.9	224.2	561.7	278.5	50	65	10	13	42	3					18.7
U1440A	28°26.9890′N	142°45.2243′E	4775.2	106.1	—	106.1	96.6	91	14	12	2	0	0	8 Aug	2130	10 Aug	2235	2.1
U1440B	28°26.9976′N	142°45.2244′E	4775.2	383.6	102.3	281.3	34.7	12	36	0	0	36	1	10 Aug	2235	26 Aug	0310	15.2
		Site U1440 totals:		489.7	102.3	387.4	131.3	34	50	12	2	36	1					17.3
U1441A	28°25.6379′N	142°43.5390′E	4446.9	205.7	—	205.7	50.7	25	22	0	0	22	0	11 Sep	0205	14 Sep	0550	3.2
		Site U1441 totals:		205.7	—	205.7	50.7	25	22	0	0	22	0					3.2
U1442A	28°24.5784′N	142°37.3368′E	3162.0	529.8	—	529.8	100.7	19	57	0	0	57	0	14 Sep	0550	24 Sep	0130	9.8
		Site U1442 totals:		529.8	—	529.8	100.7	19	57	0	0	57	0					9.8
		Expedition 352 totals:	—	2011.1	326.5	1684.6	561.2	33	194	22	15	157	4					49.0

APC = advanced piston corer, XCB = extended core barrel, RCB = rotary core barrel. — = no data.

Table T2. Sediment and basement cored intervals, Expedition 352.

Hole	Sediment (mbsf)	Basement (mbsf)
U1439A	0–178.5	178.5–199.4
U1439C	—	182.0–544.3
U1440A	0–103.5	103.5–106.1
U1440B	102.3–115.3	115.3–383.6
U1441A	0–83.0	83.0–205.7
U1442A	0–83.1	83.1–529.8
Total (m):	461.1	1223.5

Table T3. Live outreach events, Expedition 352.

Date (2014)	Institution	Level	Students (*N*)	Location
11 Aug	School of Rock	Adult Educators	20	Delaware
20 Aug	St. Ursula Academy	11th–12th grade	25	Toledo, Ohio
20 Aug	Uto High School	16–18 years old	8	Kumamoto, Japan
20 Aug	University of South Florida (Main and Marine Campuses)	Adult	25	Tampa, Florida
21 Aug	Kittredge Magnet School	6th grade	40	Atlanta, Georgia
23 Aug	National Museum of Nature and Science	General Public	100	Tokyo, Japan
27 Aug	University of South Florida	Undergraduate	45	Tampa, Florida
28 Aug	Unity Point School	6th grade	30	Carbondale, Illinois
30 Aug	Meiho Junior High School	13–15 years old	85	Oita, Japan
2 Sep	Pound Middle School	7th grade	62	Lincoln, Nebraska
3 Sep	Pound Middle School	7th grade	23	Lincoln, Nebraska
4 Sep	Pound Middle School	7th grade	61	Lincoln, Nebraska
6 Sep	Pound Middle School	7th grade	35	Lincoln, Nebraska
7 Sep	Long Beach Aquarium*	General Public	6	Long Beach, California
8 Sep	Whitehall Middle School	8th grade	100	Montague, Michigan
9 Sep	Exeter High School	11th & 12th	25	Exeter, New Hampshire
10 Sep	University of South Florida	Undergraduate	45	Tampa, Florida
11 Sep	St. Bruno Catholic School	5th grade	25	Pinckneyville, Illinois
12 Sep	Colorado State University	Undergraduate	350	Ft. Collins, Colorado
13 Sep	Our Lady of Providence Junior/Senior High School	8th grade	20	Clarksville, Indiana
15 Sep	Adams Elementary School	3rd–4th grade	100	Midland, Michigan
15–18 Sep	Midland and Dow High Schools (6 broadcasts)	10th–12th grade	360	Midland, Michigan
17 Sep	University of South Florida	Undergraduate	45	Tampa, Florida
18 Sep	University of Edinburgh	Undergraduate	65	Edinburgh, Scotland
18 Sep	Modesto Junior College	Undergraduate	30	Modesto, California
18 Sep	College of Charleston	Undergraduate	30	Charleston, South Carolina
19 Sep	University of Haifa	General Public	65	Haifa, Israel
19 Sep	Austin Community College	Undergraduate	20	Austin, Texas
19 Sep	Eastern Mennonite School (2 broadcasts)	9th grade	50	Harrisonburg, Virgina
20 Sep	St. Anne School	7th grade	23	Orange County, California
21 Sep	Science Factory	General Public	30	Eugene, Oregon
21 Sep	French School of Alexandria	12th grade	20	Alexandria, Egypt
23 Sep	All Saints Episcopal School	6th grade	20	Tyler, Texas
24 Sep	Uppsala University	Undergraduate (2nd year)	25	Uppsala, Sweden
24 Sep	All Saints Episcopal School	6th grade	20	Tyler, Texas
24 Sep	Indian Lake Elementary (dual broadcast w/ All Saints)	5th grade	75	Vicksburg, Michigan
24 Sep	Valley View Junior High	8th grade	24	Farmersville, Ohio
25 Sep	All Saints Episcopal School	6th grade	20	Tyler, Texas
		Total:	2152	

* = JR Outreach Network Event.

Figure F1. Regional map of the Izu-Bonin-Mariana (IBM) system showing the location of sites from Expeditions 350, 351, and 352.

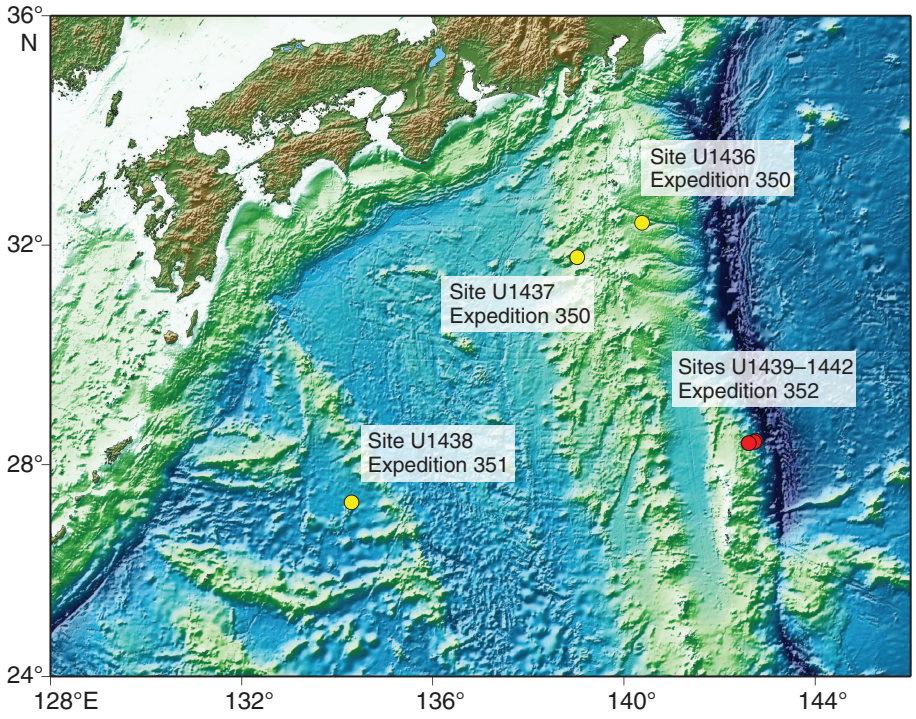

Figure F2. Compilation of $^{40}Ar/^{39}Ar$, K/Ar, and U-Pb zircon dating results for Eocene igneous rocks from the IBM fore arc, modified after Ishizuka et al. (2011). Expedition 352 focuses on the detailed stratigraphy of the 7–8 My period between subduction initiation and the start of "normal" arc volcanism. Data sources: Meijer et al. (1982), Cosca et al. (1998), Reagan et al. (2008), Kaneoka et al. (1970), Ishizuka et al. (2006), Ishizuka et al. (2011), and Reagan et al. (2013).

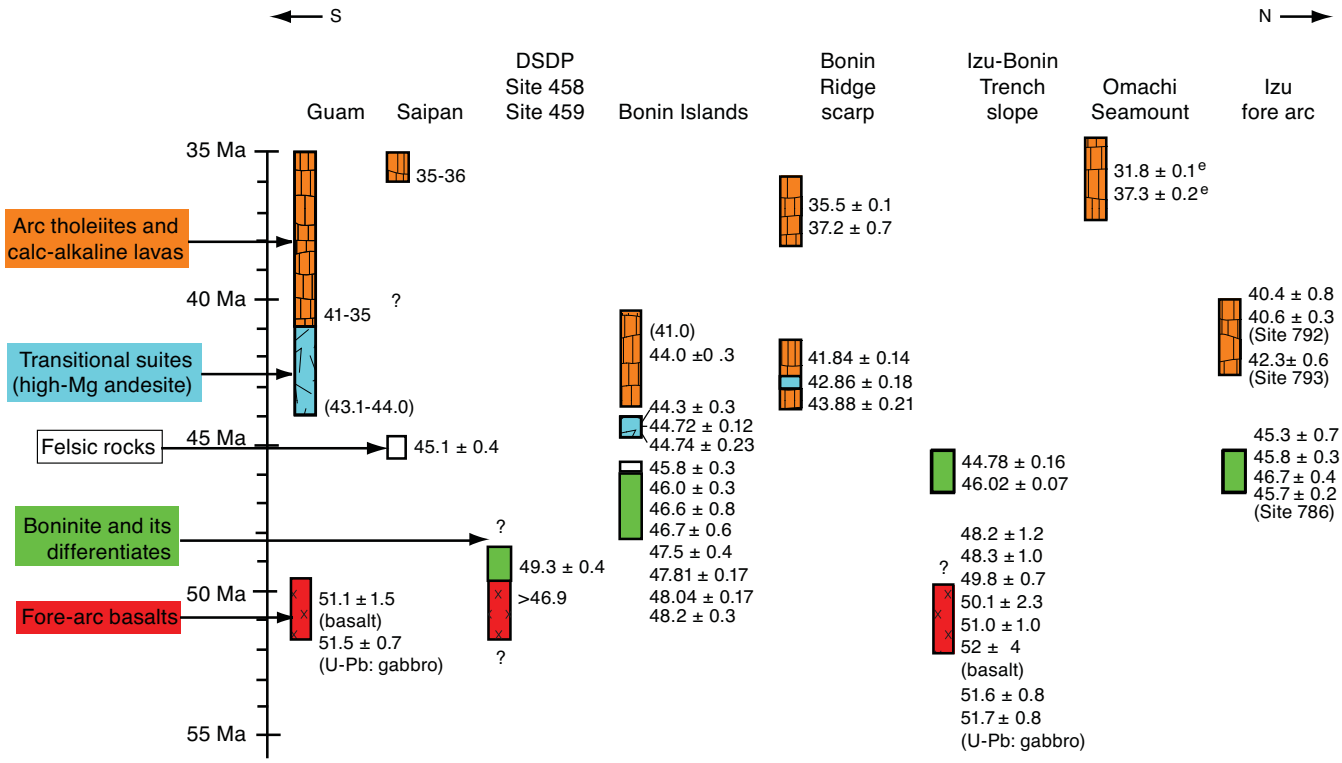

Figure F3. Variations in rare earth element patterns in the Bonin fore arc following subduction initiation. Note the recently discovered MORB-like patterns of the first volcanic products, the fore-arc basalt, and the contrast with the later U-shaped boninite patterns. Expedition 352 research will obtain complete information on gradations within and between these units. Data from Ishizuka et al. (2006, 2011).

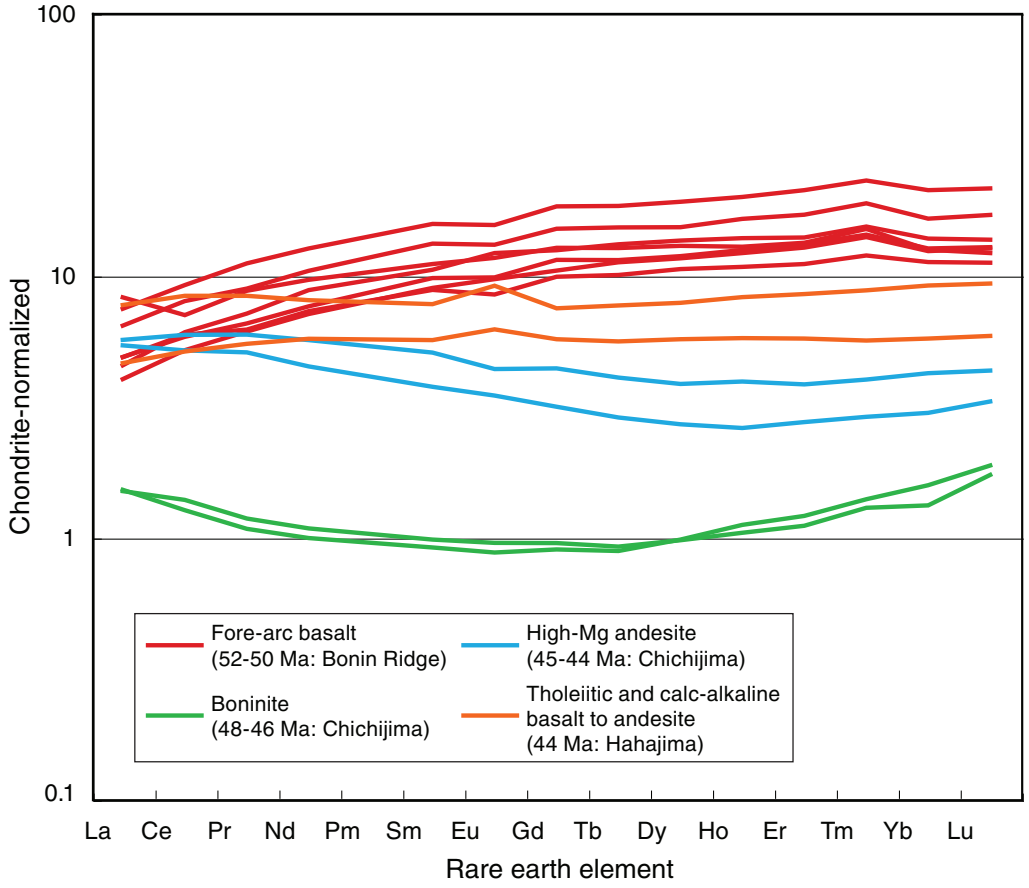

Figure F4. V-Ti systematics (Shervais, 1982) for the lavas erupted following subduction initiation. Note that the earliest lavas to erupt following subduction initiation (the fore-arc basalt [FAB]) are distinct from mid-ocean-ridge basalt (MORB) and from later boninites. These are, however, isolated outcrops. Data from Ishizuka et al. (2006, 2011).

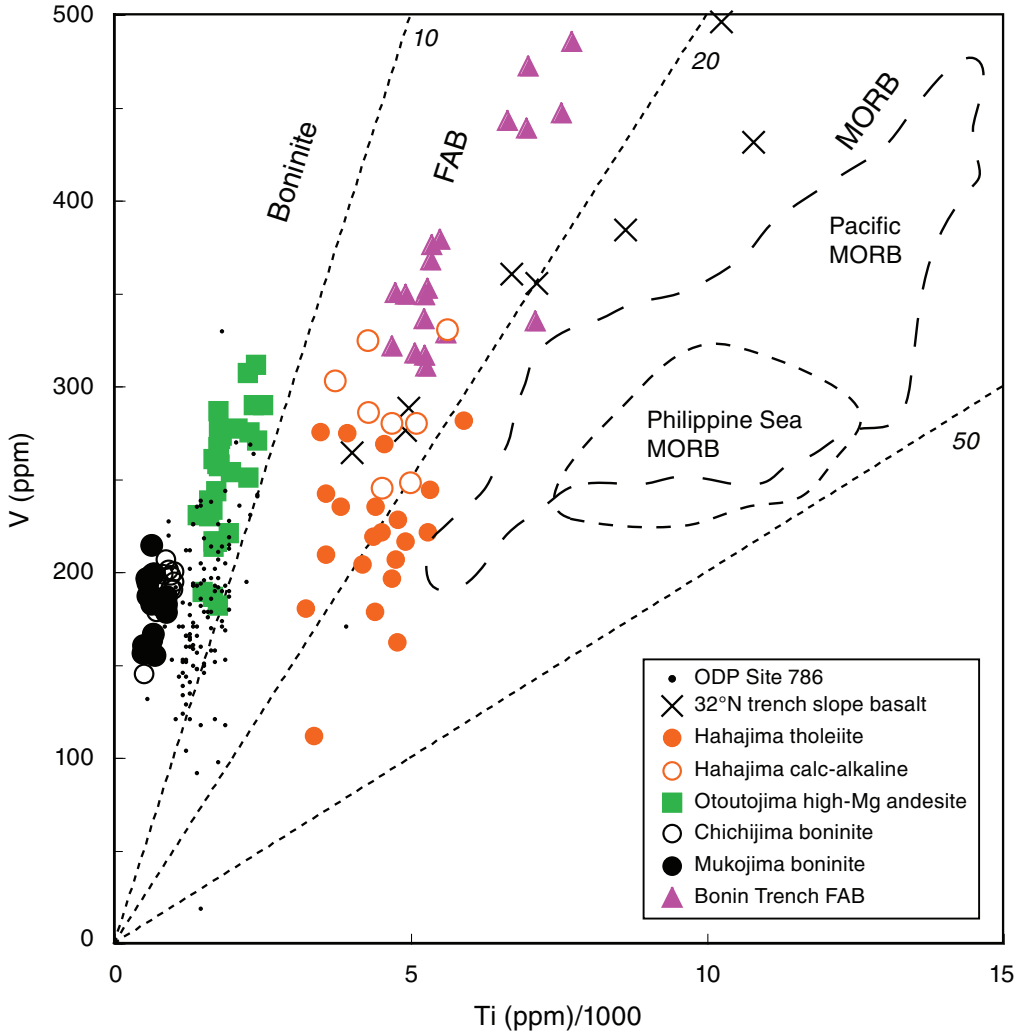

Figure F5. Isotopic compositions highlight the complex variations in lava chemistry following subduction initiation. A complete stratigraphy will enable better interpretation of these data in terms of variations in mantle sources and subduction components following subduction initiation. Data from Ishizuka et al. (2006, 2011). HMA = high-Mg andesites, KPR = Kyushu-Palau Ridge, MORB = mid-ocean-ridge basalt, NHRL = Northern Hemisphere reference line.

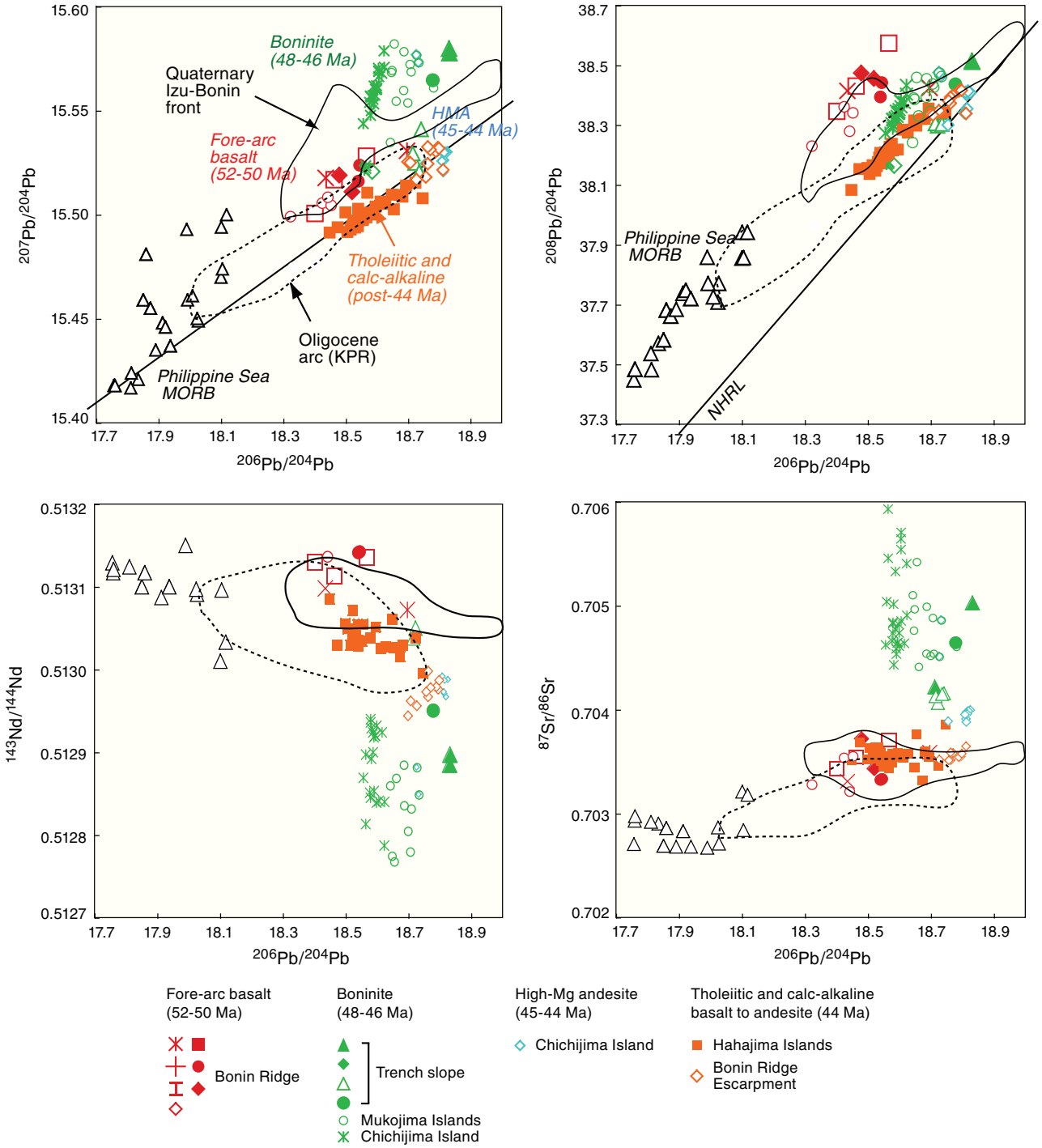

Figure F6. Interpretation of tectonic evolution of the Bonin Ridge in Ishizuka (2006) based on the concept of Stern and Bloomer (1992). According to this model, subduction initiation is followed by sinking of the slab with slab-parallel subduction and hence normal arc volcanism only beginning later. Later discoveries of fore-arc basalt in the Mariana and Bonin fore arcs (Reagan et al., 2010; Ishizuka et al., 2011) have pushed back to 52–45 Ma, the period addressed by this expedition in an attempt to test this model in detail. BRE = Bonin Ridge Escarpment.

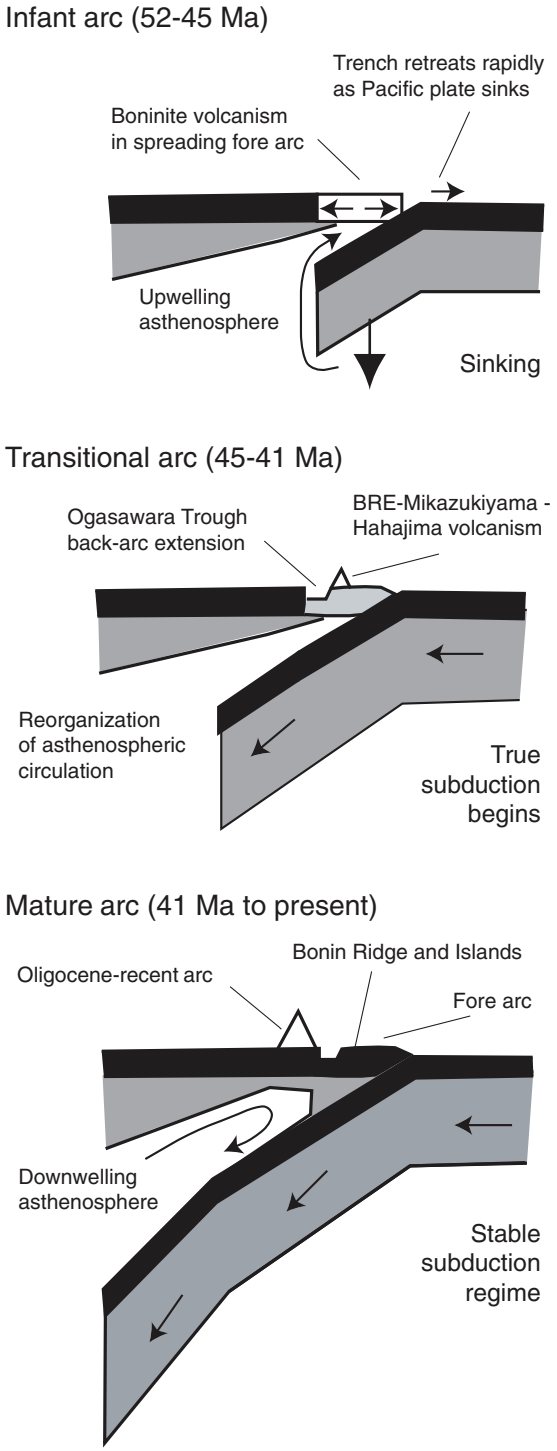

Figure F7. Basaltic vs. boninitic character as a function of the age of the lava following subduction initiation in the Bonin fore arc. Fore-arc basalt (FAB) erupts first and at the end (Hahajima), but otherwise boninites dominate. Boninites are characteristic of subduction initiation, and the full stratigraphy would enable their tectonic significance to be explained better. Data are from Pearce et al. (1999), Reagan et al. (2010), and Ishizuka et al. (2011). MORB = mid-ocean-ridge basalt, IAB = island arc basalt.

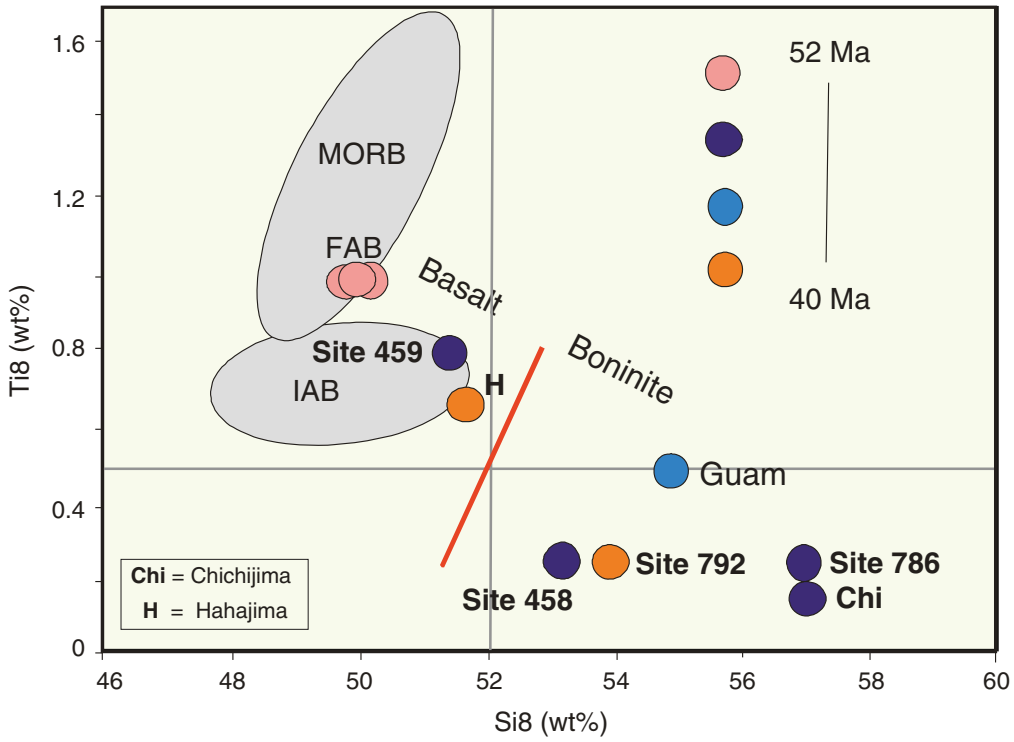

Figure F8. Expedition 352 sites and locations of *Shinkai* 6500 dives discussed in the text.

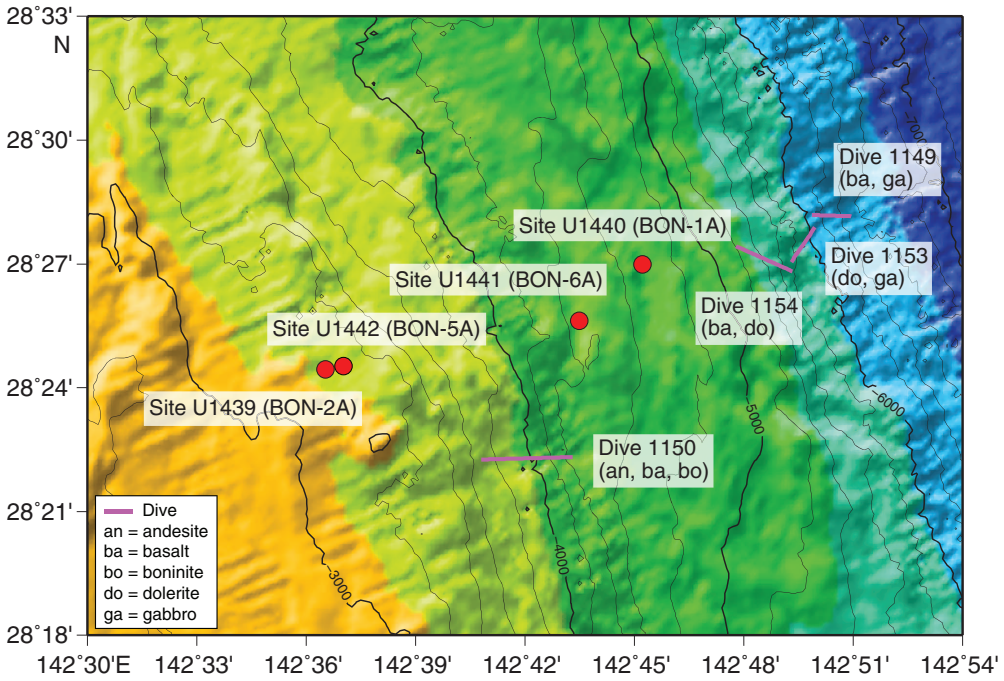

Figure F9. Rock types recovered from dredging and diving expeditions to the Bonin fore arc, showing its ophiolitic structure (after Ishizuka et al., 2011). Sites U1439–U1442 are shown as stars. Boxes depict the areas chosen for more detailed site survey dives.

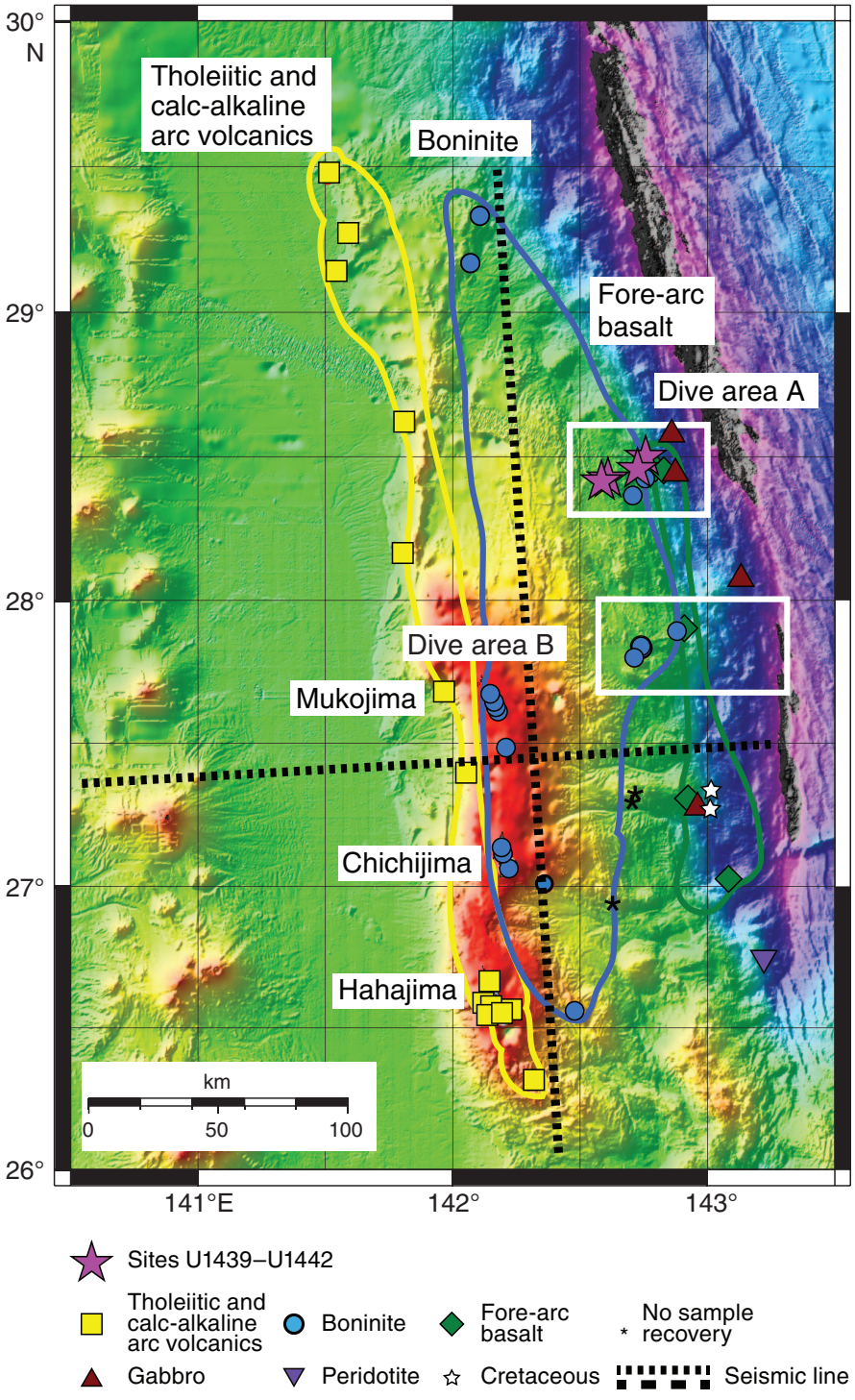

Figure F10. Schematic stratigraphic section (not to scale) for the Bonin fore-arc drill site area. FAB = fore-arc basalt.

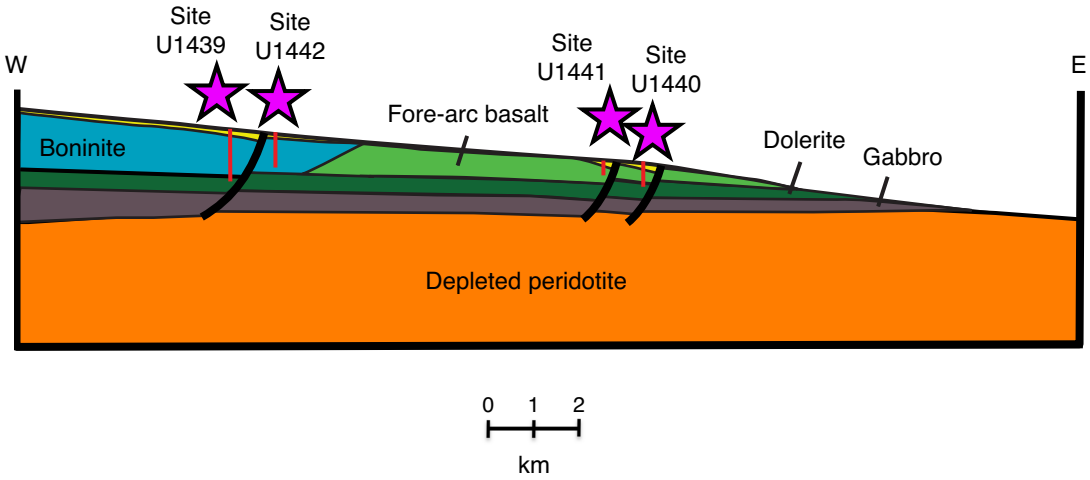

Figure F11. Lithostratigraphic sediment units and ages, Hole U1439A.

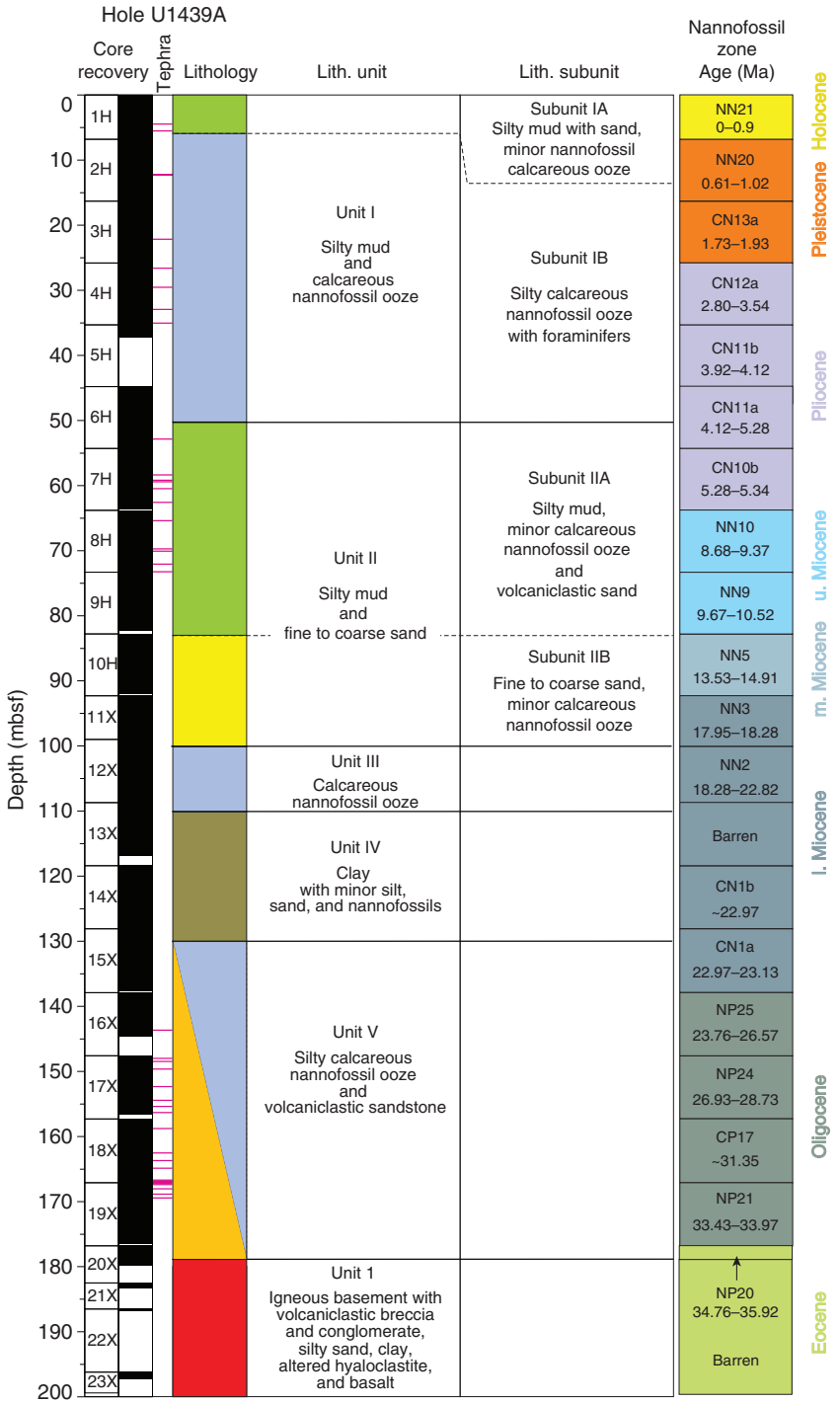

Figure F12. Lithostratigraphic igneous units, Hole U1439C. Red bars adjacent to lithology column represent fault zones.

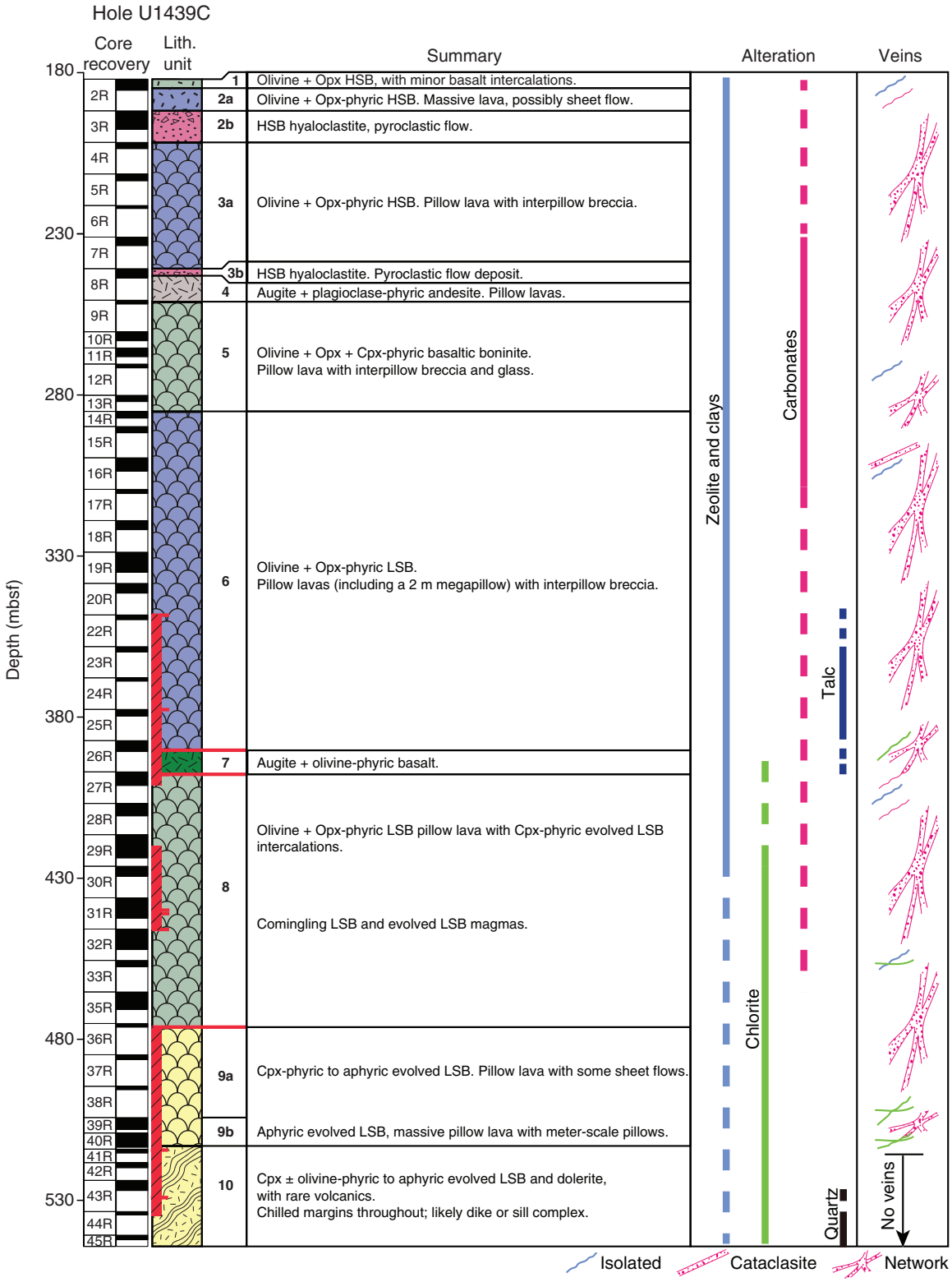

Figure F13. Lithostratigraphic sediment units and ages, Holes U1440A and U1440B.

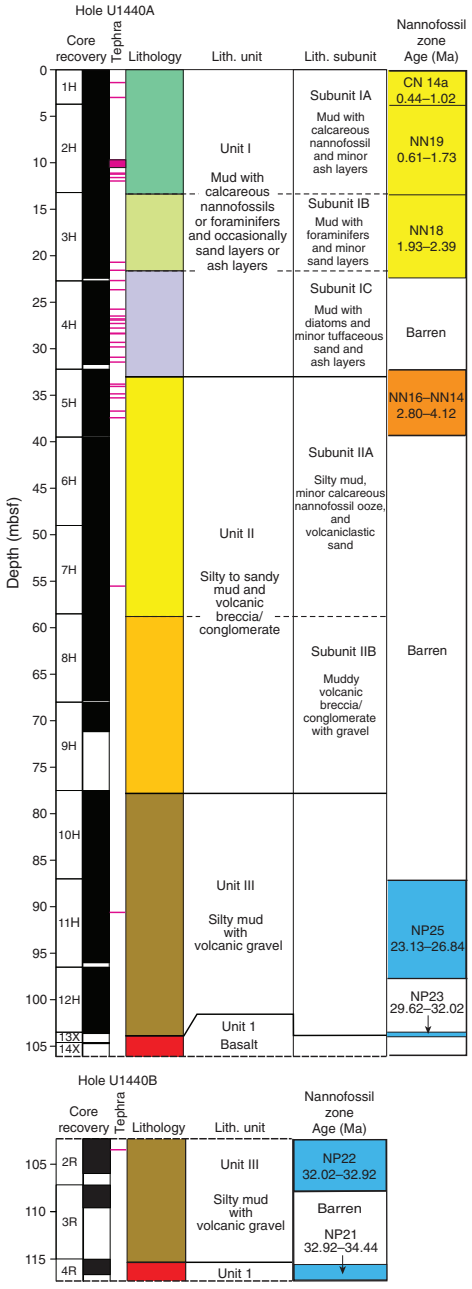

Figure F14. Lithostratigraphic igneous units, Hole U1440B.

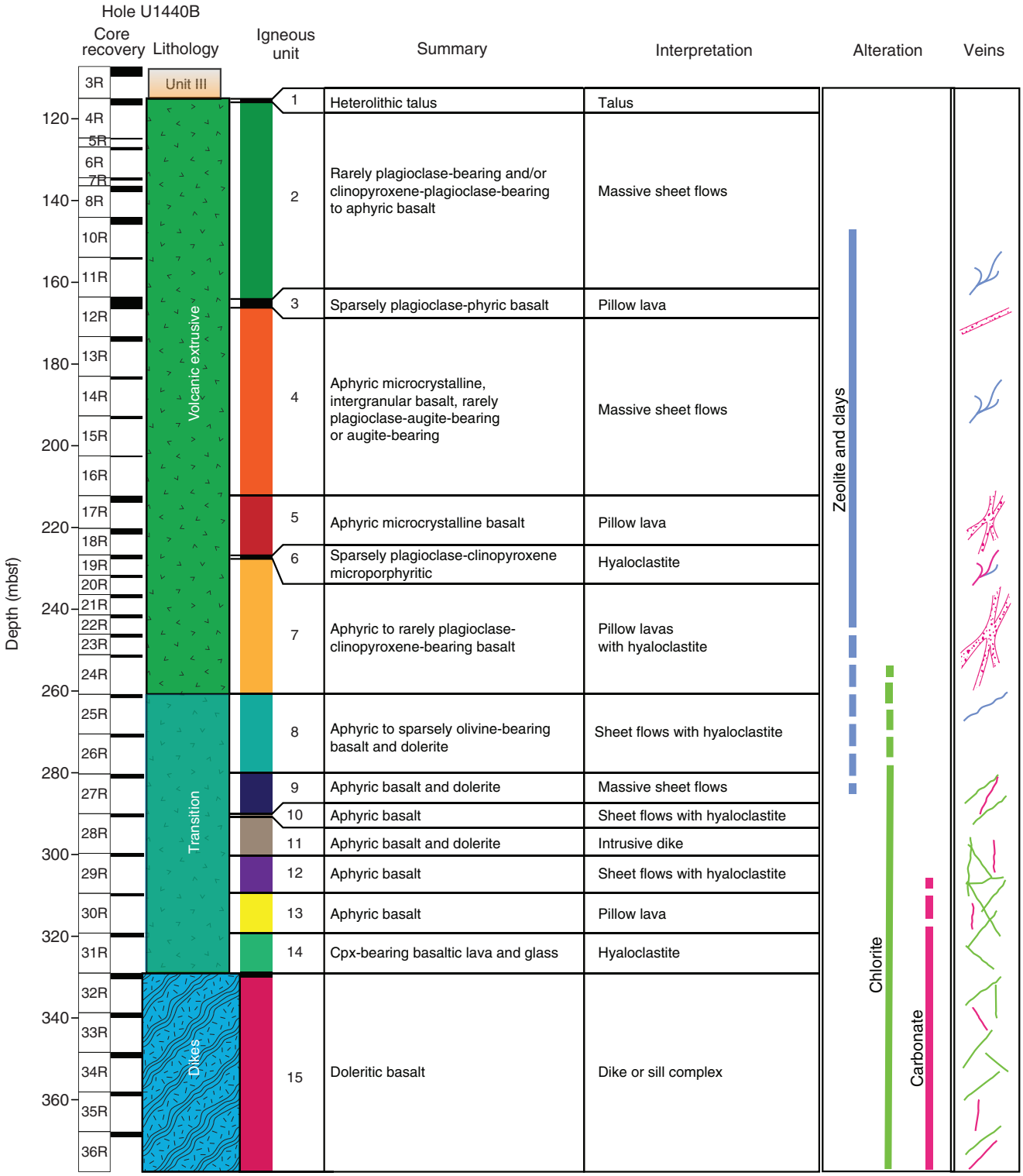

Figure F15. Lithostratigraphic sediment units, Hole U1441A.

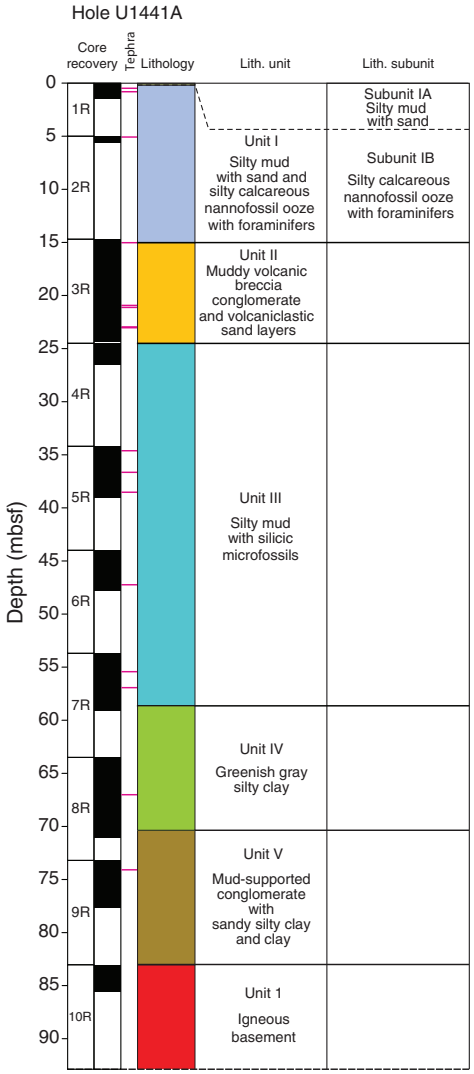

Figure F16. Lithostratigraphic igneous units, Hole U1441A.

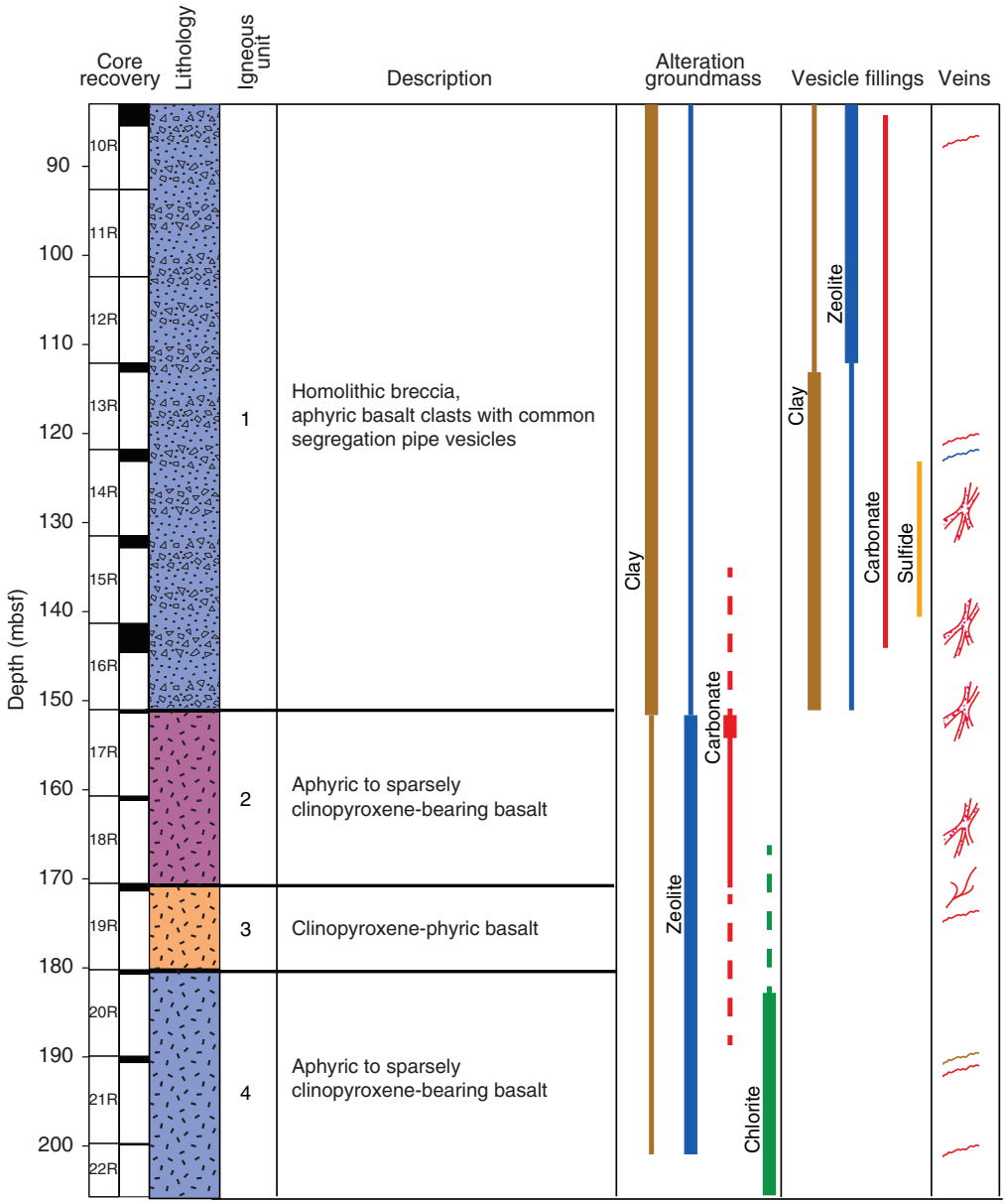

Figure F17. Lithostratigraphic sediment units and ages, Hole U1442A.

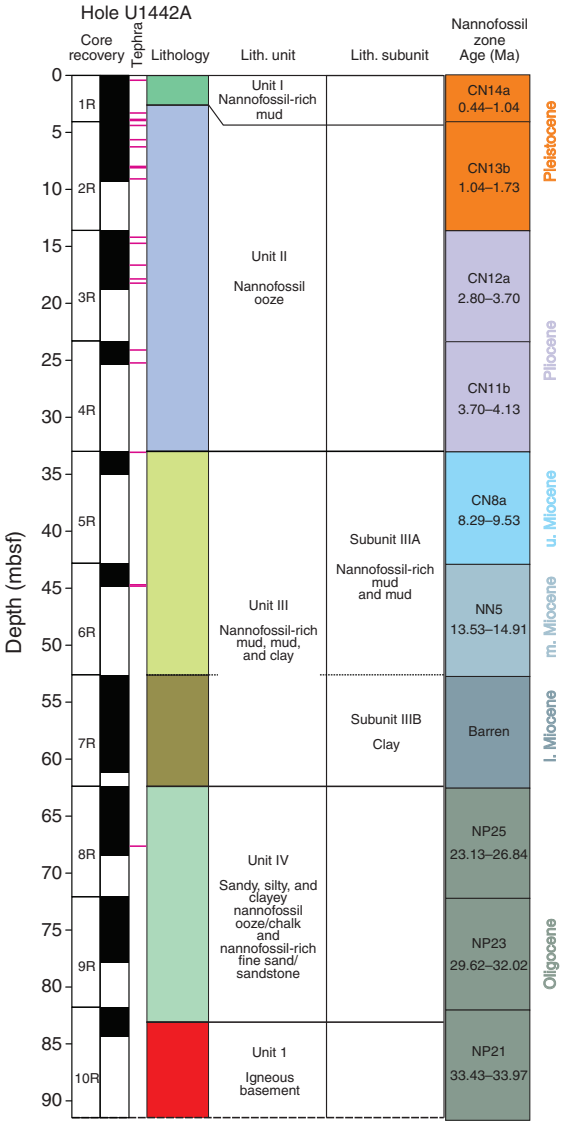

Figure F18. Lithostratigraphic igneous units, Hole U1442A. Red bars adjacent to lithology column represent fault zones.

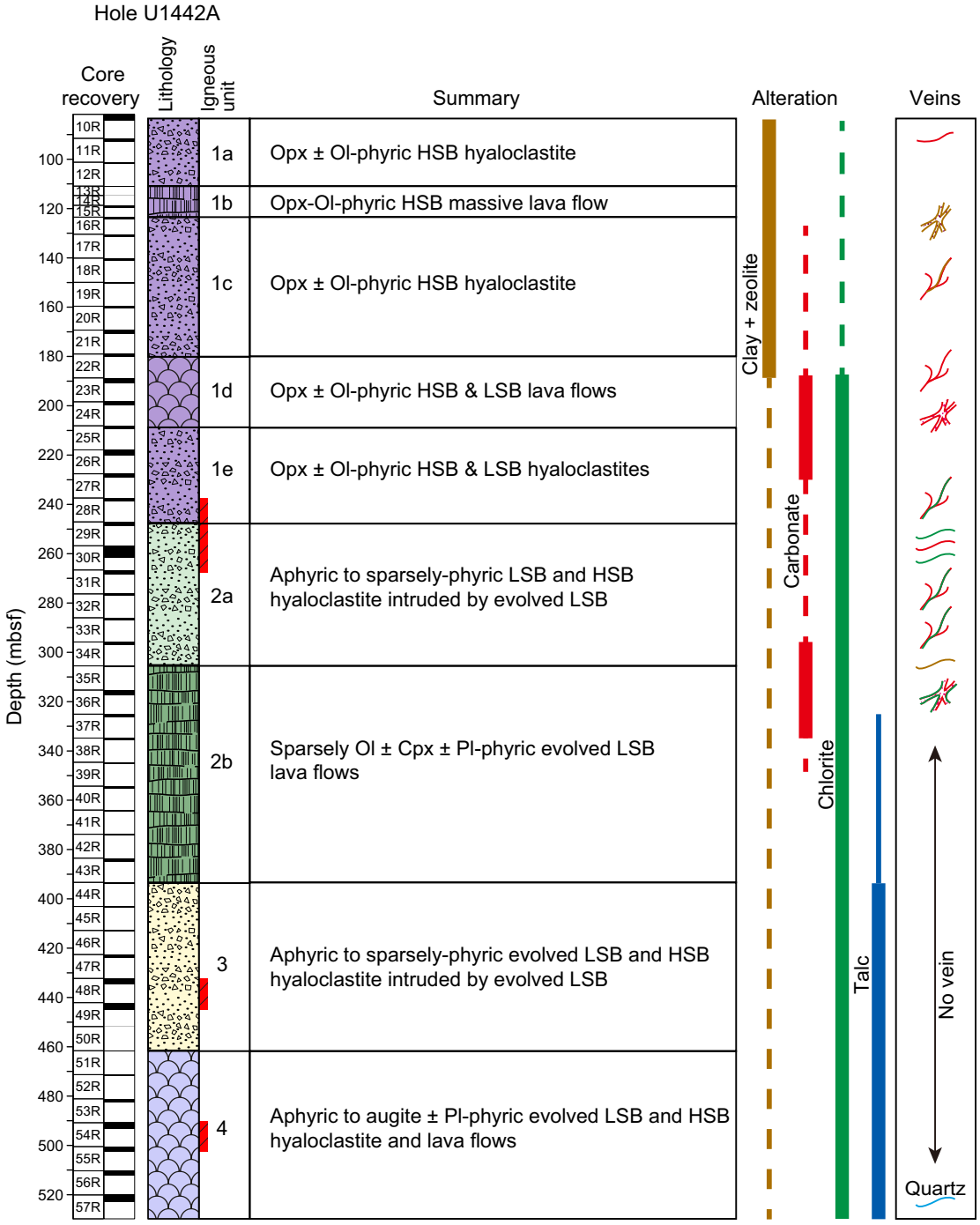

Figure F19. Schematic igneous stratigraphic columns for Expedition 352 drill sites, from west to east. The western sites, U1439 and U1442, consist of boninite group lavas, including high-silica boninite (light green), low-silica boninite (slate blue), basaltic boninite (dark green), and evolved boninite-series lavas (purple). Site U1442 includes a thick section of volcaniclastics (brown with breccia pattern) and consists largely of hyaloclastite breccias with intercalated lava flows. In contrast, Site U1439 comprises lava flows with fewer hyaloclastite horizons. At both boninite sites, the most depleted primary boninites are found at the top of each section. The eastern sites, U1441 and U1440, consist of fore-arc basalts, including lavas (brown), dikes or sills (ochre), and a transition zone of lavas and dikes (red). D-FAB, an ultradepleted variety of FAB with exceptionally low Ti concentrations, was found at Site U1441.

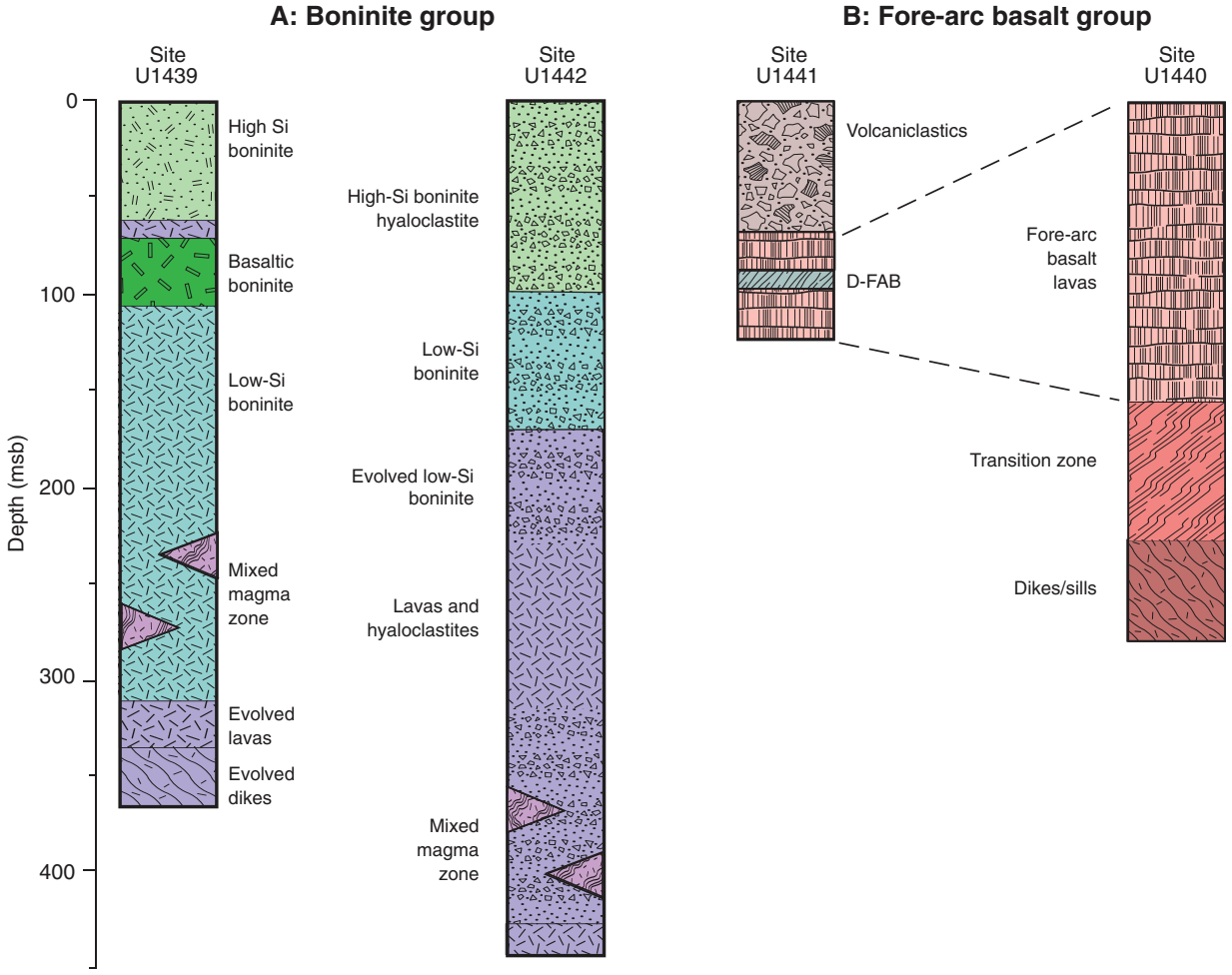

Figure F20. (**A**) MgO vs. SiO_2 and (**B**) TiO_2 vs. MgO diagrams used to classify the volcanic rocks and dikes sampled during Expedition 352. Boninites (sensu stricto) are defined by IUGS (Le Bas, 2000) as having MgO > 8 wt%, TiO_2 < 0.5 wt%, and SiO_2 > 52 wt% and so must plot in the shaded rectangular fields on both diagrams. The dividing line between the boninite and the basalt-andesite-dacite-rhyolite (BADR) series is from Pearce and Robinson (2010) (trans. = transitional). The upper boninite series field has been arbitrarily divided by us into basaltic boninite (B), low-Si boninite (L), and high-silica boninite (H) for use in more precise naming of recovered rocks. Evolved boninite series rocks classify as high-Mg andesites (HMA) and plot in the fields shown.

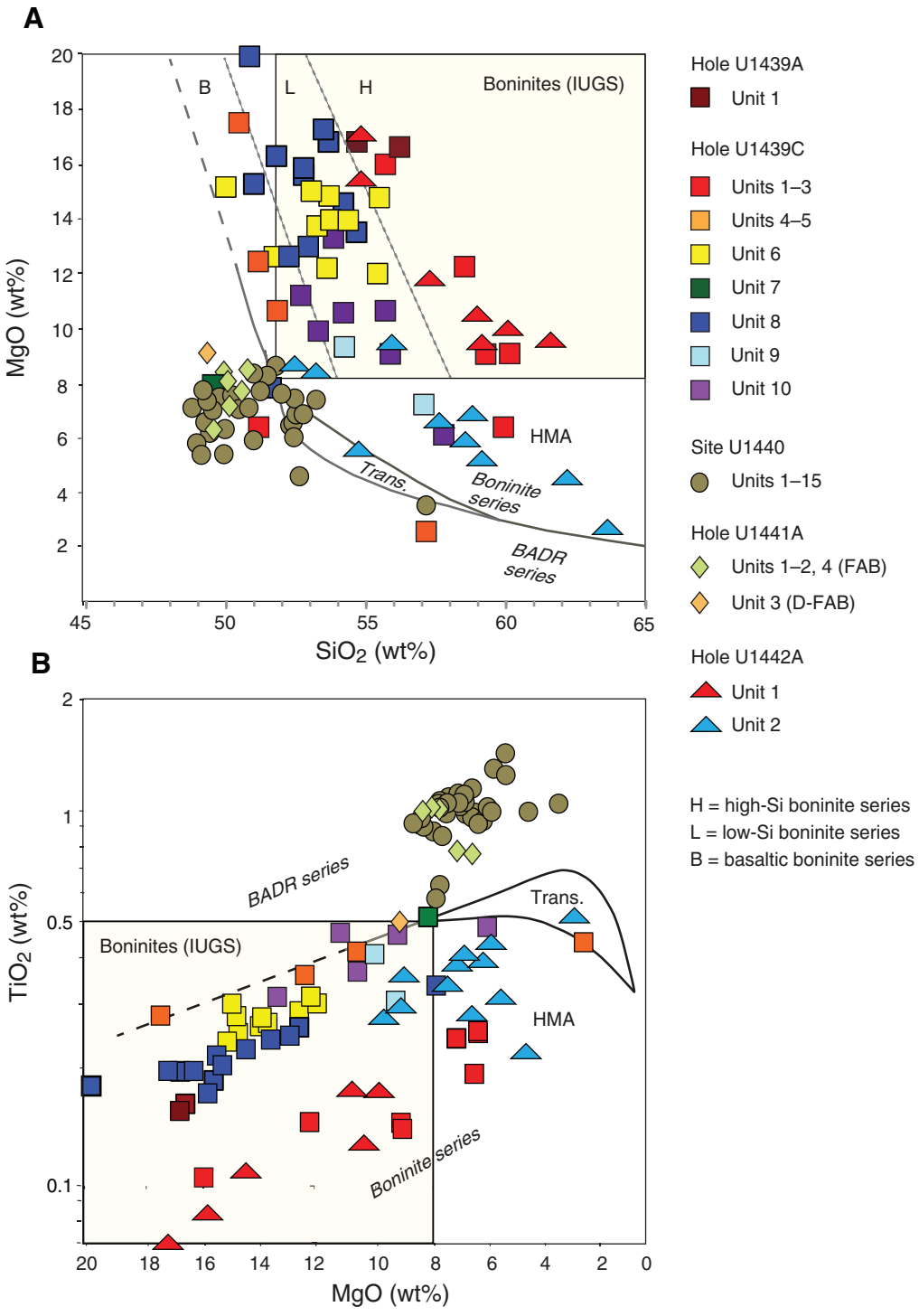

Figure F21. (**A**) Zr vs. TiO_2, (**B**) Sr/Ti vs. Ti/Zr, and (**C**) V vs. TiO_2 for Sites U1439–U1442 and selected cores from DSDP Site 458. Diagonal lines in A illustrate Ti/Zr ratios, and those in C represent Ti/V ratios. The yellow fields illustrate Pacific and Atlantic MORB compositions using the glass analyses of Jenner and O'Neill (2012).

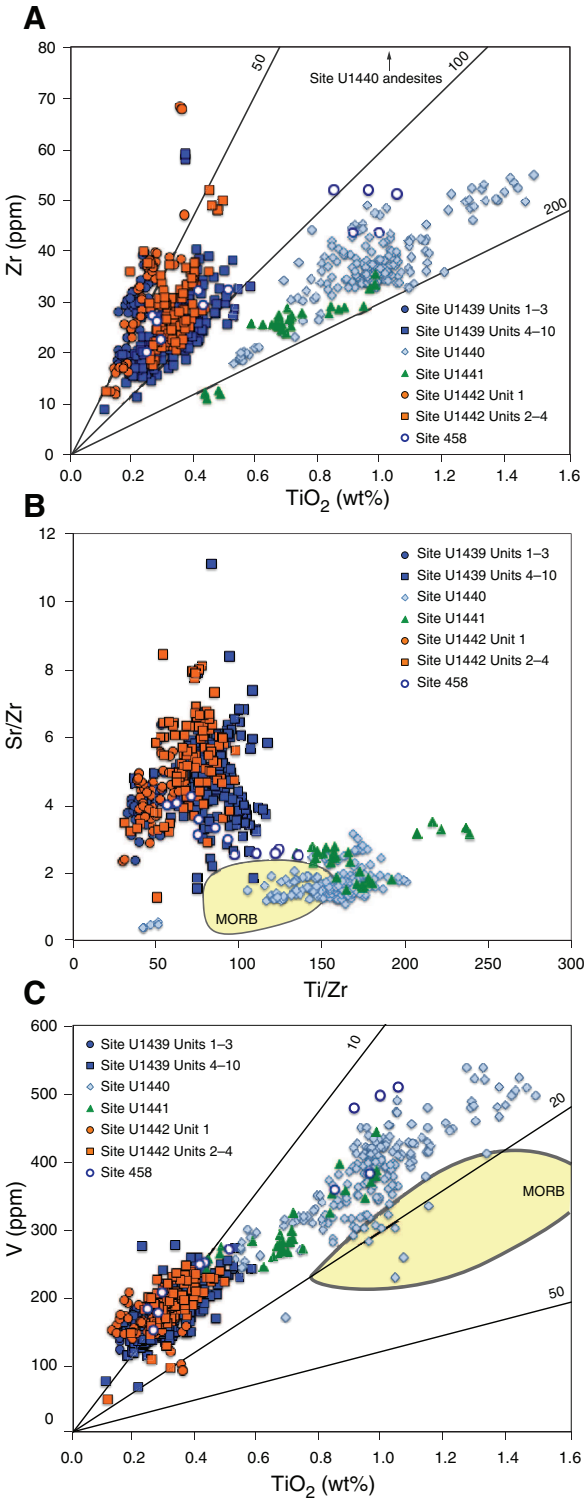

Figure F22. Concentrations of TiO_2 and Cr with depth, Hole U1440B.

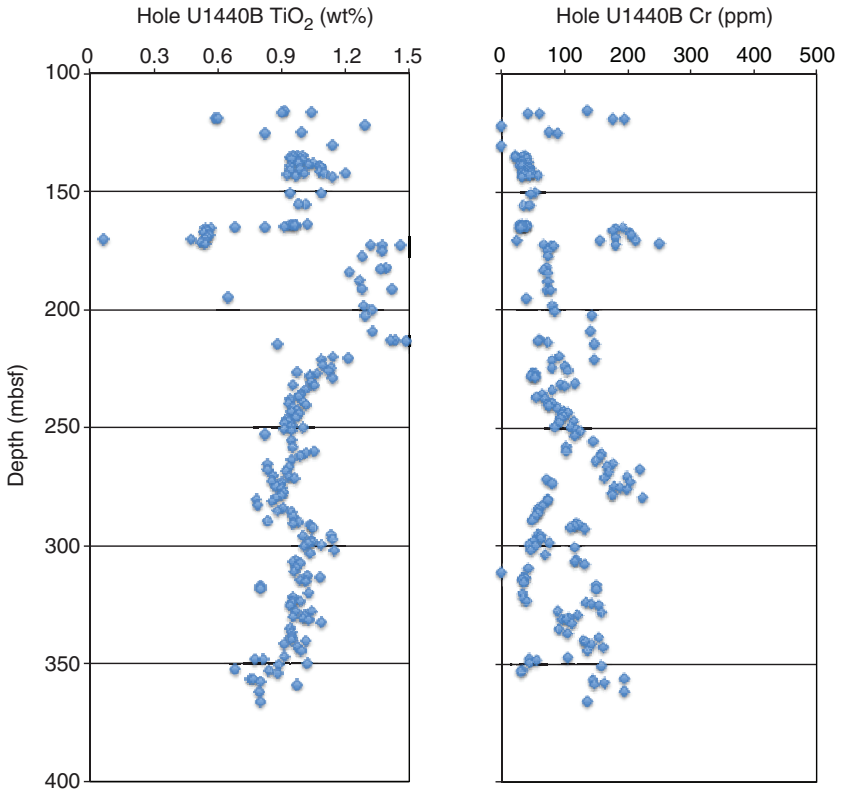

Figure F23. Concentrations of TiO_2 and Cr with depth, Hole U1441A.

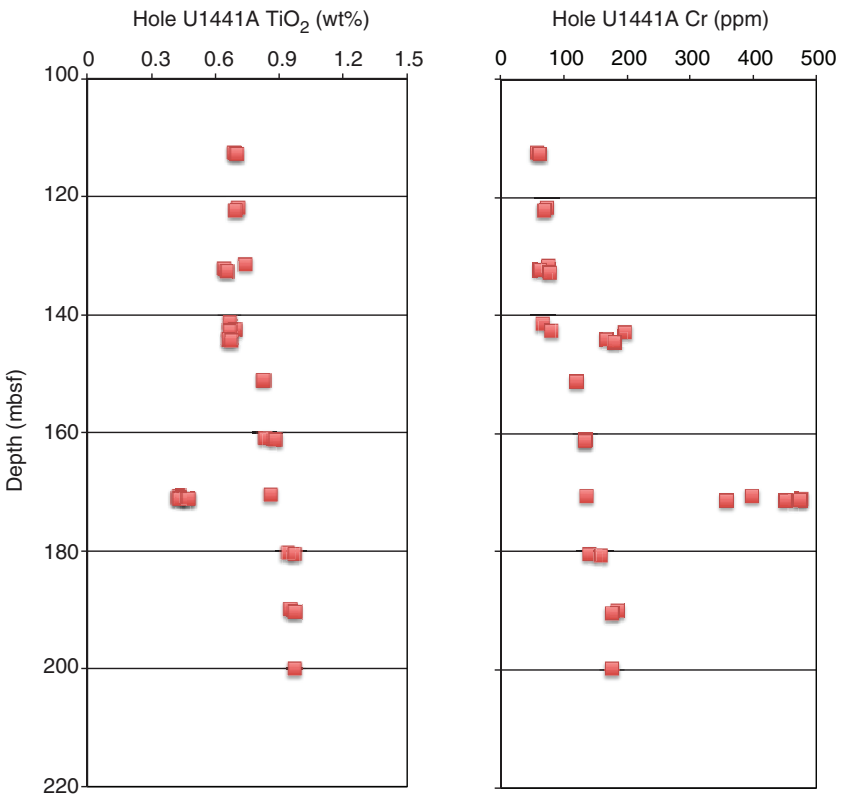

Figure F24. Cr concentrations and Ti/Zr ratios with depth, Holes U1439C and U1442A. The central colored bars represent our stratigraphic correlation between these two holes (see text for further explanation).

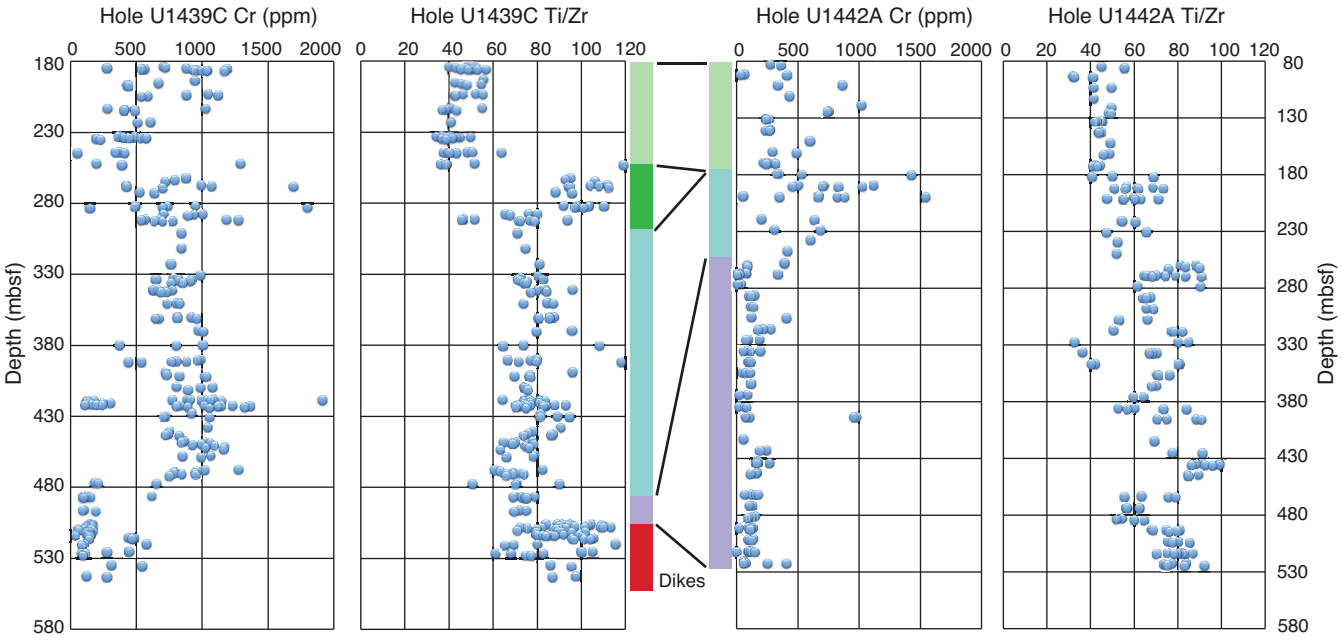

Figure F25. Summary of sedimentary sections, Sites U1439–U1442. Eocene to Holocene sediment shows typical pelagic carbonates. They are variably influenced by local and regional volcanism, leading to the alternating sequences of (volcani)clastic-rich and nannofossil-pure lithologic units.

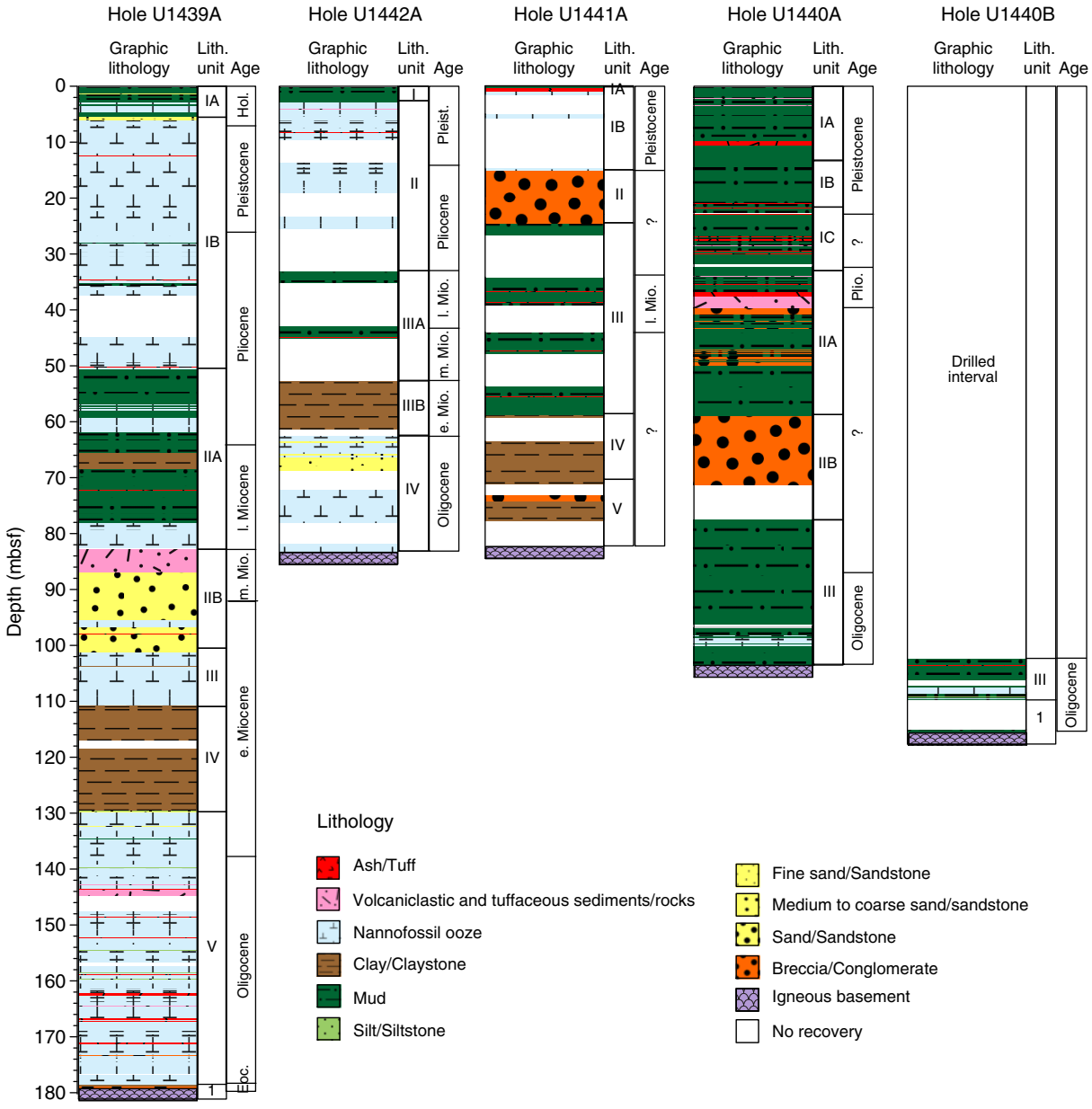

Figure F26. Normalized ash abundance, Sites U1439–U1442. Note different amounts of felsic and mafic ash layers across the slope. Arrows mark the decrease (pink) and increase (green) of felsic and mafic tephras, respectively.